Computer Simulation and Life Cycle Analysis of a Seasonal Thermal Storage System in a
Residential Building

Alexandre Hugo

A Thesis

in

the Department

of

Building, Civil & Environmental Engineering

Presented in the Partial Fulfillment
for the Degree of Master of Applied Science at
Concordia University
Montreal, Quebec, Canada

November 2008

Canada

ABSTRACT

Computer Simulation and Life Cycle Analysis of a Seasonal Thermal Storage System in a Residential Building

Alexandre Hugo

The residential sector represents 17% of Canada's secondary energy use, with more than 78% of this contribution due to space and domestic hot water heating. In that perspective, systems that do not require any auxiliary energy are of a certain interest. Such objective is not easy to accomplish, especially in cold climates, but yet can be reached by both upgrading the buildings overall thermal performance and using efficient renewable energy sources.

An integrated building model is developed into the TRNSYS 16 simulation environment. First, a typical one-storey detached house, located in Montreal is considered as a base case. Conventional electric baseboard heaters and an electric domestic hot water storage tank provide the space heating and domestic hot water requirements. A life cycle performance of the house is performed and results of the life cycle energy use, environmental impacts and life cycle cost are presented.

Second, several design alternatives are proposed to improve the life cycle performance of the base case house. The solution that minimizes the energy demand is finally chosen as a reference building for the study of long-term thermal storage.

Third, the computer simulation of a solar heating system with solar thermal collectors and long-term thermal storage capacity is presented. The system is designed to supply hot water for the radiant floor heating system and domestic hot water. Simulation results show that the system is able to cover a whole year of energy requirements using a minimum of auxiliary

energy. A sensitivity analysis is performed to improve the overall performance. The life cycle energy use and life cycle cost of the system are investigated and results presented in the thesis.

Acknowledgments

I want to express my gratitude to my research supervisors. First, thanks to Dr. Zmeureanu for his great availability, support and always constructive remarks. His enthusiasm and thoroughness in research motivated me to strive for the best and will remain forever an extremely enriching experience. Second, thanks to Dr. Hugues Rivard, Professor at ÉTS in the Department of Construction Engineering, Chair of Canada Research in Computer-Assisted Engineering for Sustainable Building Design for his comments and suggestions

I would like to thank as well the Building Engineering team for creating a pleasant work environment and for providing me with help whenever I needed it. Particularly, I would like to acknowledge Mitchell Leckner for his insightful remarks and his ability to bring new ideas.

During these two demanding years of study, the support of my family and my girlfriend was extremely important. I would like to thank them for their continuous encouragement.

Finally, I would like to thank the members of my defense committee for their insightful comments and suggestions, all of whom made valuable contributions to this thesis.

This thesis is dedicated to my grandmother for her unconditional love and support.

Table of Contents

List of Figures

List of Tables

Nomenclature

A Area [m^2]

a_0 Optical efficiency

a_1 First-order coefficient in collector efficiency equation [W/(m^2·K)]

a_2 Second-order coefficient in collector efficiency equation [W/(m^2·K^2)]

C Cost [$]

C_p Specific heat [J/(kg·°C)]

cap_S Thermal capacitance [GJ/°C]

CO_2 Equivalent carbon dioxide emissions [kg]

COP   Coefficient of performance

E Annual primary energy generated [kWh/yr]

EPT   Energy payback time [years]

EYR   Energy yield ratio

$\mathscr{F}$ Solar fraction

F' Collector efficiency factor

F_R Overall collector heat removal efficiency factor

G	Solar radiation [W/m^2]
h_c	Convective heat transfer coefficient [W/(m$^2\cdot$°C)]
i	Discount rate
i'	Effective interest rate
j	Inflation rate
j_E	Inflation rate of electricity
K	Incidence angle modifier
L	Life span [years]
$\dot{m}$	Mass flow rate [kg/s or kg/h]
N	Number of days in the month, number of years
N_S	Number of identical collectors in series
N_{snow}	Number of days with snow depth greater than 5 cm
$\dot{P}$	Electrical power [W]
PW	Present Worth [$]
Q	Energy [kWh]
r	Correction factor
T	Temperature [°C]
T_F	Freezing temperature [K]
T_{city}	Temperature of cold water from the city line [°C]

U	Internal energy of storage [GJ]
U'_L	Modified first-order collector efficiency [W/(m^2·°C)]
UA	Heat transfer capacity rate [W/°C]
V	Volume [m^3]
v	Wind velocity [m/s]
W	Annual energy output [GJ/yr]

Subscripts

aux	Auxiliary
c	Collector, critical
$calc$	Calculated
$combi$	Combisystem
d	Day
db	Dry-bulb
DHW	Domestic hot water
$ELEC$	Electrical
f	Final
h	Hot
HX	Heat exchanger
i	Inlet, initial

l	Longitudinal
min	Minimum
n	Normal
o	Out, outdoor, outlet
pp	Power plant
R	Room
ret	Return
set	Setpoint
T	On a tilted plane
t	Tank, transversal
TH	Theoretical
u	Useful

Greek symbols

α	Absorptance, tilt angle [°]
α_{1-5}	Equivalent CO_2 emissions due to the generation of electricity [kt CO_2/TWh]
ϵ	Effectiveness
η	Efficiency
γ	Control signal
λ	Thermal conductivity [W/(m·°C)]

μ	Dynamic viscosity [Pa·s]
ρ	Density [kg/m^3]
ρ_{nosnow}	Snow-free albedo of ground
ρ_{snow}	Snow-covered albedo of ground
τ	Transmittance
θ	Incidence angle [°]
ξ	Concentration of propylene-glycol

Chapter 1

Introduction

1.1 Background

Climate change is recognized by many scientists as one of the greatest challenges facing Canada, and the world today. In February 2007, the Intergovernmental Panel on Climate Change released a report supporting the idea that the global warming is - with 90% certainty - caused by human activity (IPCC, 2007). The document forecasts that the average temperature will rise by 1.8 to 4°C by the year 2100 and sea levels will creep up by 17.8 to 58.4 cm by the end of the century. If polar sheets continue to melt, another rise of 9.9 to 19.8 cm is possible.

In Canada, greenhouse gas (GHG) emissions have increased by 25% between 1990 and 2005 (Figure 1.1), from 596 megatons to 747 megatons of carbon dioxide equivalent (Mt CO_2 eq.), the standard of measurement for greenhouse gases (IPCC, 2007). This represents the biggest percentage increase among G8 countries over the same time period, according to a report published by Statistics Canada (2008). The study says the resulting growth in GHG is in part attributable to a number of other changes in the country over the same time period, notably demographic and economic growth.

Canada has about 0.5% of the world's population but, with an average of 23 tons CO_2 eq.
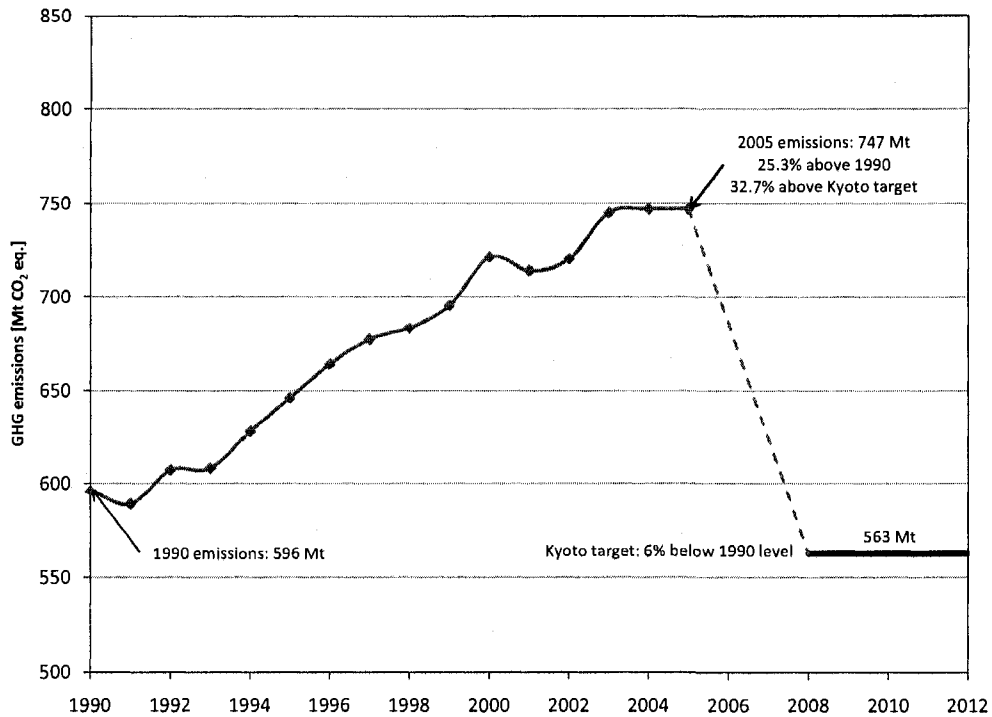
Figure 1.1. Greenhouse gas emissions in Canada from 1990 to 2005 and Kyoto target

per person each year, it contributes more than 2% of the total greenhouse gas emissions. It means that Canadians are among the highest per capita polluters in the world as Canada's per capita greenhouse gas emissions are the third-highest in the world, trailing only Australia (27.7 tons per person) and the United States (24.4 tons) (UNFCCC, 2008).

If current federal and provincial policies on energy and environment remain unchanged, the projected GHG emissions by 2010 will rise to 764 megatons. This number would be 199 megatons above the target established in the Kyoto Protocol ratified by Canada, which requires that by the period 2008-2012, Canada will reduce its GHG emissions to 6% below its 1990 level (IPCC, 2007).

The relationship between buildings and environment is very close. Indeed, the consumption of energy in the residential sector is a significant contributor to Canada's energy GHG

emissions since it is responsible of 17% of secondary energy use (Table 1.1). The space and domestic hot water heating account for 78% of the residential energy use.

Table 1.1. Canada's secondary energy use by sector and residential secondary energy consumption by end-use, 2005. From (NRCan, 2006)

		Energy use by sector				
		Industrial	Transportation	Residential	Commercial	Agriculture
Energy use	[PJ]	3,209	2,502	1,402	1,153	209
Contribution	[%]	38	30	17	14	2
		Residential energy consumption by end-use				
		Space heating	Water heating	Appliances	Lighting	Space cooling
Energy use	[PJ]	846	248	203	68	37
Contribution	[%]	60	18	14	5	3

Based on these facts, it can be concluded that the construction and operation of buildings represent a large quantity of energy and create substantial amounts of harmful pollutants emissions. The way that a building is designed can affect the environment that immediately surrounds us in a severe way. More globally, the reduction of energy consumption by means of energy-saving policies, the use renewable energy resources for substitution of fossil energy sources and the reduction of CO_2 emissions will have to become a priority in near future.

1.2 Research objectives

The proposed research aims to explore ways to lower the energy use and greenhouse gases emissions throughout the life cycle of a typical Canadian house, and evaluate its associated life cycle cost. The purpose is to analyze some practical and effective solutions to minimize the life cycle energy use and emissions in a residential building, and eventually to promote the research results in the engineering and architectural communities.

The focus is made on applications taking full advantage of available renewable energies

for space and water heating. More specifically, the system is intended to reduce the corresponding energy use to a minimum by means of a seasonal storage system.

1.3 Methodology

In order to achieve the stated objectives, the following methodology is proposed:

- A literature survey is conducted to review existing and future projects of low energy and net-zero houses in different parts of the world and deduce successful strategies, as well as key factors to design efficient solar thermal systems for space and water heating;

- Using the simulation program TRNSYS 16, the integrated building model of a single family house in Montreal is developed;

- The life cycle performance of the base case house is carried out by estimating the life cycle energy use, life cycle emissions and life cycle cost;

- Several design alternatives that upgrade the life cycle performance of the base case house are investigated;

- The modelling of a solar combisystem with a long-term thermal storage capacity is presented;

- A sensitivity analysis, based on a certain set of design parameters, is achieved to evaluate the repercussions of those parameters on the overall performance of the system;

- A life cycle analysis is employed to estimate the life cycle cost and life cycle energy

use of the system.

Chapter 2

Literature review

The literature survey conducted for the purpose of this study aims to review the existing and future projects of energy efficient houses in different continents of the world. A review of available and successful technologies is conducted in order to effectively implement the low energy houses concept under the Canadian cold climate.

This chapter focuses as well on solar applications used to provide space or water heating commonly named solar "combisystems". The overview on the worldwide situation of the solar thermal market is given, followed by a summary of some major research results from the recent years. Finally, based on these studies, efficient methods to design a seasonal storage system are presented and used as a starting point for this work.

2.1 Net-zero energy homes

As countries are starting to instigate environmental measures to reduce green house gas emissions to fight global warming, there is an increasing interest in developing strategies and initiatives that encourage the market introduction of what are called low and net-zero energy homes (NZEH).

By definition, such home is not only energy efficient as it also produces its own power (Net-

Zero Energy Home Coalition, 2007). Just like a typical home, a NZEH is connected to, and uses energy from, the local electric utility. But unlike typical homes, at times the NZEH makes enough power to send some back to the utility. Annually, a NZEH produces enough energy to offset the amount purchased from the utility-resulting in a net-zero annual energy bill.

2.2 International projects and initiatives

2.2.1 European Passive House

The term "Passive House" is a standard that refers to buildings in which the space heat requirement is reduced by means of passive measures to the point at which there is no longer any need for a conventional heating system; the air supply system essentially suffices to distribute the remaining heat requirement. It is basically a refinement of the low energy house standard. To permit this, it is crucial that buildings peak heating loads do not exceed 10 W/m^2 (Schnieders and Hermelink, 2006), which corresponds roughly to average energy consumptions of 15 $kWh/(m^2 \cdot year)$ (under Central Europe climatic conditions). In addition, efficient technologies are also used to decrease the other sources of consumptions, like electricity for household appliances.

CEPHEUS (Cost Efficient Passive Houses as EUropean Standards) was a project within the THERMIE-Programme of the European Commission (CEPHEUS, 2007). Started in 1998, this demonstration project served to examine and prove the sustainability of the Passive House concept in Europe. Fourteen inexpensive Passive Houses with a total of 221 residential units were built in five different countries. All houses have occupants and

were evaluated via similar measurement procedures. The target of the CEPHEUS project was to keep the total primary energy requirement for space heating, domestic hot water and household appliances below 120 kWh/(m^2·year). At this time, this was dividing by a factor of 2 to 4 the specific consumption levels of new buildings designed to the standards applicable across Europe (CEPHEUS, 2001). All this had the following goals:

- To demonstrate technical feasibility of achieving the targeted energy performance indexes at low extra cost for an array of different buildings;

- To give development impulses for the further design of energy- and cost-efficient buildings and for the further development and accelerated market introduction of innovative technologies compliant with Passive House standards;

- To facilitate the broad market introduction of cost-efficient Passive Houses.

Measurement data presented by Schnieders and Hermelink indicate average space heating savings of 80% compared to the reference consumption of conventional new buildings. In the same way, final and primary energy were reduced by more than 50%. These results show that the Passive House standard is clearly a great achievement as it enhances the principle of low energy buildings by fulfilling fully its commitments.

2.2.2 IEA SHC tasks

The International Energy Agency was established in 1974 as an independent agency within the framework of the Economic Cooperation and Development (OECD) to achieve a comprehensive program of energy cooperation among its 25 member countries and the Commission of the European Communities (IEA, 2007). A significant part of the Agency's program involves collaboration in the research, development and demonstration of new

energy technologies to reduce reliance on imported oil, increase long-term energy security and reduce greenhouse gas emissions of its member's. Research is carried out through different implementing agreements. The Solar Heating and Cooling (SHC) Program was one of the first implementing agreements to be established. Since 1977, its 21 members have been cooperating to develop active solar, passive solar and photovoltaic technologies and their application in buildings.

A total of 42 Research Tasks have been initiated and 34 have been completed so far. Three of them that are mainly focused on the development of low energy buildings will be elaborated here:

- Task 13: Advance Solar Low Energy Buildings (1989-1994)

- Task 28: Solar Sustainable Housing (2000-2005)

- Task 40: Towards Net Zero Energy Solar Buildings (2008-2013)

Task 13

Over the last two decades, significant progress has been made in reducing the energy consumption for space heating. Researches have resulted in promising concepts and products. In 1989, Task 13 was initiated to analyze, test and develop new technologies for the purpose of integrating them in whole building concepts (Hestnes et al., 2003). The main purpose was the application of passive and/or active solar technologies for space heating of single and multi-family residential buildings. The use of passive and active solar concepts for cooling, ventilation, and lighting was also addressed, as well as advanced energy conservation measures to reduce heating and cooling loads while maintaining a good indoor climate. Since the emphasis was principally on innovation and long-term cost-effectiveness, the materials,

components, concepts, and systems considered were not expected to be feasible, economical, or on the mass market.

The design strategies were implemented in 15 experimental houses, located in different climates. There was a monitoring over time to provide information about the various materials and components of the buildings, as well as complete systems performances. This section will outline the main concepts from a selection of projects.

A remarkable project was the German Zero-Heating Energy House in Berlin, Germany. Indeed, by reducing the transmission losses and by combined active and passive solar strategies, the house did not require any auxiliary space heating energy. The housing estate was built in the form of a right angle. In the top of this angle, the zero-heating energy house was situated ideally facing south. While the north side of this building was limited to a minimal surface area, the living space widely opened up from southeast to southwest. An array of 54 m^2 of high-efficiency collectors was integrated in the south side facade. The collectors supplied a 350 l water tank and two 300 l tanks of nearby houses in summer. Surrounded by circular stairs in the center of the house, a 20 m^3 seasonal storage water tank was heated by the additional solar energy.

A mandatory condition for the function of the zero-heating energy house was its extremely low heating demand. For instance, the outer walls, the roof and the basement ceiling were heavily insulated and triple-glazed xenon filled windows with two low-e coatings were selected. As a result, with the help of the long-term water storage, it was possible to transfer the excess supply of solar energy from summer to the cold and sunless winter months and heat the house without fossil fuel all year long.
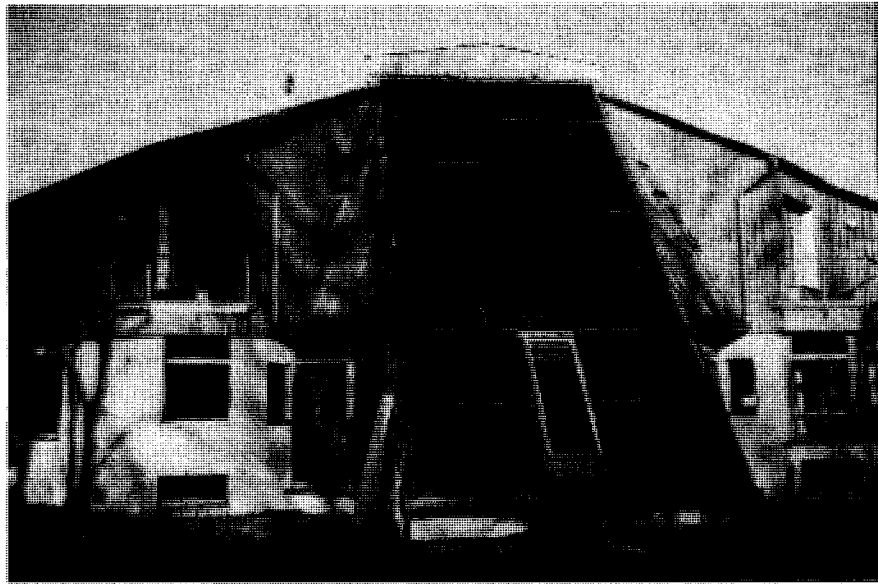
Figure 2.1. Zero-Heating Energy House, Berlin, Germany (Technischen Universität Berlin, 2007)

In their paper, Thomsen et al. (2005) illustrate the results from measurements and experiences gained from interviews on 12 solar low energy houses. According to the authors, Task 13 projects can be considered as successful as the daring original target of 75% energy saving of the energy consumption of typical houses was nearly attained with measured results of 60%. This difference is explained by the lower performance of some building components compared to what was assumed, like the airtightness of the envelope, and by an energy consumption of the occupants higher than expected, due to higher indoor air temperatures and higher electricity use for household appliances. Moreover, Thomsen et al. point out that it is important to prevent overheating in our northern latitudes thanks notably to thermal mass, solar shading devices and efficient ventilation systems.

Task 28

High performance dwellings are primarily achieved by reducing heat losses. While the number of buildings using this concept has grown in recent years, a complementary approach

like the increase of energy gains in very well insulated housing needed to be studied. So, starting in 2000, Task 28 was implemented to address cost optimization of the panel of concepts reducing energy losses, increasing available solar gains and efficiently providing backup in order to achieve the same high performance (Charron, 2005). As a consequence, twenty-two projects have been built in 11 different countries with a space-heating target of 15-25 kWh/m^2. The information can be found on the IEA SHC website.

An interesting project was the 20-terrace house complex in Gothenburg, Sweden. The goal was to show that it was possible to build passive solar houses with very low energy use and at reasonable prices in a Scandinavian climate, corresponding to some regions of Canada Charron (2005). The design strategy was to minimize transmission and ventilation losses and the building envelope is therefore highly insulated. Also, a special care was taken to neutralize thermal bridges and to ensure the airtightness of the buildings. A mechanical ventilation system with an efficiency of 80%, an electric resistance of 900 W for the heating supply and 5 m^2 of solar thermal collectors for the domestic hot water supply were used. The resulting monitored energy demand was about 68 kWh/m^2 (Wall, 2006).

Some other projects were located in cold climate regions. So, to confirm all the potential of buildings energy efficiency in such regions, Smeds and Wall (2007) studied six key design characteristics of high performance houses fulfilling IEA Task 28 targets. These important features were the area to volume ratio, the thermal insulation, the airtightness of the building envelope, the ventilation system, the windows areas and the shading devices. In their paper, the authors asserted that they are absolutely all mandatory to get environmental friendly dwellings with a comfortable indoor climate and low energy consumptions. Using the computer software DEROB-LTH for dynamic simulations, they

compared conventional buildings using typical construction and system designs with: (i) high performance buildings like Task 28 houses, and (ii) with constructions and systems that maximize the utilization of renewable energy. Their results indicated that it was possible to reduce the heating loads by up to 83% and the total energy demand (space heating, domestic hot water, electricity) by up to 92% for single-family houses.

Task 40

The objective of Task 40, expected to start by October 2008, will be to investigate current net-zero, near net-zero and very low energy buildings and to develop a common knowledge, a methodology, tools, innovative solutions and industry guidelines. The idea is to broaden the NZEH concept into practical reality in the marketplace. A database of realistic case studies will be presented, with the aim to lower industry resistance to acceptance of these concepts.

2.2.3   BedZED & Eco-Village development

The Beddington Zero Energy Development (BedZED) is a development of 100 eco-homes and workspaces in south London (UK), addressing every area of sustainable living. Residents have been living there since March 2002. All construction materials used were carefully selected from sustainable sources. 15% were reclaimed, for instance the timber used in studwork, or recycled, an example being the crushed concrete used as road sub-base. Preference was given to materials sourced within a 50 km radius thus reducing transportation, cutting fossil fuel consumption, reducing the contribution to global warming and improving air quality. Embodied energy was also reduced in this way and the regional economy saw benefits too.

Key features of BedZED included active and passive solar design strategies, high insulation levels, high efficiency windows and a combined heat & power plant fuelled by woodchips from waste timber that provides electricity and hot water. In addition, a green transport plan that promotes walking, cycling and the use of good local public transport links was established. During the first year of occupation, a monitoring of building performance and transport patterns was realized. Table 2.1 shows substantial reduction of energy consumption with the UK average for space heating and hot water. Such a comprehensive project with coherent examples of sustainable living should be a source of inspiration for implementing this in other countries.

Table 2.1. Monitoring results of BedZED & Eco-Village Development (BedZED & Eco-Village Development, 2007)

	Monitored reduction	Targeted reduction
Space heating	88% (73%)[a]	90%
Hot water	57% (44%)[a]	33%
Electricity	25%	33%
Pipes water	50%	33%
Car mileage[a]	65%	50%

[a] New homes built after year 2000 UK Building regulations
[b] Fossil fuel consumption

2.3 Canadian initiatives

2.3.1 Advanced House program

In 1992, with the vision to develop sustainable and energy efficient housing, Natural Resources Canada (NRCan) launched the Advanced Houses program to study innovative methods that decrease energy consumptions, provide better indoor environments and reduce

the environmental impact of houses (Gerbasi, 2000). Ten houses were built across the country, with technical requirements beyond the R-2000 standard (NRCan, 2005) as they also considered the total purchased energy. The objective was to use the half of a typical R-2000 home's energy, or one quarter of the energy and half the water of a typical Canadian home. There were also individual targets for space heating, cooling, water heating, lighting, and appliances (including motors for fans and pumps). The Advanced Houses had to meet minimum requirements for airtightness, ventilation rates, and lighting energy per floor area.

As illustrated in Table 2.2, 75% of the energy reductions were achieved compared to the average yearly energy use of typical buildings at this time of 39,000 kWh annually. These impressive numbers were obtained without a major use of renewable energy as only half the ten Advanced Houses projects included solar thermal technologies and only two used PV panels. Indeed, considering the local climate, the NOVTEC house in Montreal had the lowest energy consumption rating without using any active solar systems since it was equipped with a prototype ground-source heat pump. Hence, such solutions was highly recommended by Gerbasi.

The differences between the predicted and the actual energy consumptions can be the result of the precision of simulations programs or by the lower performances than expected of the original equipments used in the designs. Since the technology has largely evolved since that time, both active and passive solar technologies should not be an obstacle anymore for the broad integration of highly efficient buildings in Canada.

15

Table 2.2. Overview of the Advanced Houses program (NRCan, 2007)

Project	City	Predicted energy consumption (kWh/yr)	Actual energy consumption (kWh/yr)	Energy intensity (kWh/(m²·yr))	PV capacity	Solar thermal
BC Advanced House	Surrey	14,486	12,266	45.4		
SK Advanced House	Saskatoon	20,514	31,322	91.9	1.92 kW	Yes
MB Advanced House	Winnipeg	17,685	20,463	110.0		
Waterloo Green Home	Waterloo	14,026	14,987	65.0	Water pump	Yes
Hamilton Neat Home	Hamilton	13,911	19,834	49.0		
Innova House	Ottawa	16,649	18,053	N/A	2.6 kW	
Maison NOVTEC House	Montreal	11,422	13,227	59.6		
Maison Performante	Laval	11,067	12,055	63.8		Yes
PEI Advanced House	Charlottetown	13,997	N/A	-	Water pump	Yes
The Envirohome	Bedford	17,390	N/A	-	Water pump	Yes

2.3.2 Net-Zero Energy Coalition

In 2004, a group of home builders and investors started the Net-Zero Energy Home Coalition (Net-Zero Energy Home Coalition, 2007). This group of forward looking people considered how residential energy could be supplied in a sustainable way that minimizes greenhouse gas emission. They proposed a multiphase approach that included pilot projects in major urban centers across Canada and a national plan that combines R-2000/Energy Star or higher energy efficiency standards, with a minimum 3 kW photovoltaic rooftop array or equivalent renewable energy generation source. Their goal was to have all new residential buildings designed by 2030 to meet a net-zero energy standard.

2.3.3 Solar Building Research Network

The Solar Buildings Research Network (SBRN) was launched in 2006 by the Natural Sciences and Engineering Research Council (NSERC) through its Research Network Grant Program (SBRN, 2007). Led by Concordia University, top Canadian researchers in the solar technology coming from Canadian universities, Natural Resources Canada (NRCan), the Canada Housing and Mortgage Corporation (CMHC) and Hydro Quebec joined forces to develop the solar-optimized homes and commercial buildings of the future. Its vision is the realization of the solar building operating in Canada as an integrated advanced technological system that approaches the zero-energy target. Consequently, the Network leads to the development of innovative solar utilization building systems, load management techniques and software tools that support solar building design.

2.3.4   EQuilibrium Housing

Initiated by the CMHC with the collaboration of some major stakeholders, EQuilibrium Housing is a pilot initiative that demonstrates a new approach to housing in Canada. It addresses five key principles for sustainable design such as health, energy, resources, environment and affordability (EQuilibrium Housing, 2007). The goal is to design a highly energy-efficient house that provides healthy indoor living for its occupants, and produces as much power as it consumes on a yearly basis with no environmental impact on land, water and air. Connected to the electricity grid, these homes are expected to draw power only as needed and to return excess power back into the system. In February 2007, 12 winning teams of the sustainable housing competition were awarded 50,000 $ each. This money will help them to build energy-efficient healthy demonstration homes across Canada. Such development is expected to contribute largely to the advancement of net-zero energy homes.

2.4   Successful strategies

To translate these successful initiatives into winning strategies for future Canadians homebuilders, a database taking over the useful information on low energy residential buildings would constitute a major asset. Yet, such analogous task has already been investigated by Hamada et al. (2003) with the purpose of the collecting information on passive and active techniques. Indeed, the authors studied 66 homes built from 1988 to 1997 and allocated in 17 different countries. Seven main categories were considered: the design guidelines, housing data, environmental data, cost data, energy data, system efficiency and other data. Details like the performance of the building envelope, solar systems and energy use were included within the categories. Results showed that four key features (passive

solar design, super thermal insulation, high performance windows and airtightness of the building envelope) were the most frequent strategies to achieve low energy homes. Yet, the spectrum of energy consumptions varied substantially depending on the design strategies and the climate. Indeed, annual energy fluctuated from a ratio of one to twenty-five.

In order to eliminate the differing environmental conditions making comparisons difficult, an interesting method was proposed by Charron (2005). The author rated a design as a comparison to other typical dwellings built in nearby locations. Results are illustrated in Table 2.3 and present very useful informations about the accurate design strategies for low energy residential buildings. They show the remarkable value of the thermal insulation and the airtightness of the building envelope, as the energy consumption can be reduced by 31% compared to a typical home. Yet, the addition of passive solar strategies does not raise that number drastically. However, it must be considered that a suitable utilization of thermal mass to decrease temperature swings as well as shading control devices still imply a rise of thermal comfort feelings (Athienitis and Santamouris, 2002). However, the best compromise seems to be the Category E when PV panels and solar collectors are added, as the average energy reduction soars to 75%. Finally, this illustrates very well that it is certainly conceivable to achieve net-zero energy homes if passive solar elements and heating system strategies are adequately chosen and assessed.

2.5   Solar water heating systems

Using the sun's energy to heat water is not a new idea. More than one hundred years ago, in 1891, Clarence Kemp patented and commercialized the world's first solar water

Table 2.3. Average energy reduction based on different strategies (Charron, 2005)

	Strategies used to reduce energy consumptions	Number of houses	Average reduction compared with typical home
A	Super insulation + airtight construction	4	31%
B	Category A + passive solar design	3	33%
C	Category A + solar collectors	6	59%
D	Category A + PV panels	3	45%
E	Category A + PV airtight construction	9	75%
F	Category A + other strategies	4	61%

heater (DOE, 2008). Since then, the solar water heating technology has greatly improved and becomes more and more popular every year.

Solar water heating systems (SWHS) are classified as direct or indirect systems (Duffie and Beckman, 2006). In a direct SWHS system, the thermal collector absorbs solar radiation energy and transfers this energy to a circulating fluid. The circulating fluid then transfers the collected energy to a storage device thanks to an internal heat exchanger or, in some applications like swimming pool heating, to the load directly. In an indirect SWHS system, there are two separate fluid loops; one collector loop and one tank loop. The energy is transferred from the collector loop to the tank loop through an external heat exchanger.

2.5.1 Situation of the solar thermal market

Solar thermal applications can be very different in terms of their design (glazed collectors that include flat-plate and evacuated tube collectors, unglazed collectors for heating swimming pool water, air collectors, etc.), solar yields and costs. At the end of the year 2006, the solar thermal collector capacity in operation worldwide was equal to 127.8 GW,

corresponding to 182.5 million square metres. Of this, 102.1 GW were accounted for by flat-plate and evacuated tube collectors and 24.5 GW for unglazed plastic collectors. Air collector capacity was installed to an extent of 1.2 GW (Weiss et al., 2008). Based on data collected from detailed country reports, the jobs created by the production, installation and maintenance of solar thermal plants is estimated to be 150,000 worldwide.

However, it is observed that the market penetration of solar thermal energy varies greatly depending on the location in the world (Table 2.4)). Indeed, there is a huge gap between the European countries and Canada. Climatic conditions are obviously different, but a country like Austria shows that it is quite possible to reach a much higher level of solar thermal energy contribution, despite being located in the cold environment of central Europe. The fact is that the adoption of solar thermal applications has been stronger in countries where there are both national and local long-term policies and support measures. For example, to counter a slowdown of the solar thermal collector industry in 2002, the German Government raised the incentives for solar water heating systems from 92 to 125 EUR per m^2 of collector area in February 2003 and thus contributed to improving the market. Locally, city regulations that require the installation of solar thermal collectors to supply hot water for buildings have stimulated a rapid growth of such installations, as in the case of the city of Barcelona in Spain (Aitken, 2003) and (Wiedemann, 2004).

So the question is: Does Canada really have an interest in solar thermal applications? The answer is not as clear since the huge dependency of the European countries on fossil fuel makes much more attractive the use of alternative energy sources to decrease the grade of dependency (Kjärstad and Johnsson, 2007). On the opposite, the hydroelectric energy is the main source of electricity in Canada, representing nearly two-thirds of all

Table 2.4. Market development of flat-plate and evacuated tubular collectors in some countries; installed capacity per year from 1999 until 2006, total capacity in operation in 2006 (absolute and per inhabitant) and the corresponding heat production and CO_2 reduction per year (Weiss et al., 2008)

		AUT	S	CH	GER	DK	F	CAN	USA
Inhabitants	[millions]	8.2	9.0	7.3	82.7	5.4	62.3	32.3	298.2
		Installed capacity of flat-plate and evacuated tubular collectors							
1999	[MW_{th}/yr]	99	7	21	294	11	17	0	27
2000	[MW_{th}/yr]	107	13	18	434	9	24	1	26
2001	[MW_{th}/yr]	112	15	16	630	18	27	1	17
2002	[MW_{th}/yr]	107	11	16	378	11	49	1	35
2003	[MW_{th}/yr]	117	14	15	504	6	59	1	36
2004	[MW_{th}/yr]	128	14	22	525	8	78	1	33
2005	[MW_{th}/yr]	163	16	20	665	15	92	2	53
2006	[MW_{th}/yr]	207	5	27	982	32	170	1	80
Total$_{2006}$	[MW_{th}]	1,898	165	285	5,638	262	746	58	1,634
Total$_{2006}$	[W_{th}/inhabitant]	231	18	39	68	48	12	2	5
		CO_2 emissions avoided by solar plants							
Total$_{2006}$	[GW/yr][1]	1,102	115	178	3,159	132	388	179	8,697
$CO_{2\ red}$	[kt/yr][2]	452	36	70	1,247	51	192	80	4,073
$CO_{2\ red}$	[kg/inhabitant]	54.9	3.9	9.7	15.1	9.4	3.1	2.5	13.7

[1] Calculated collector production and corresponding CO_2 reduction of all solar thermal systems (hot water, space heating and swimming pool heating).

[2] CO2 emissions avoided by solar plants are estimated from the energy savings (oil equivalent). The emission factor of 2.73 kg CO2 per litre of oil is used.

electricity produced (NRCan, 2008). Consequently, thanks to abundant water resources, electric utilities are able to produce low-cost energy (BC Hydro, 2003), which has a perverse effect on the general adoption of solar thermal energy in buildings.

Differences between Europe and North American countries are also very well marked in Table 2.5 as in some countries like Austria (81.9%), Sweden (78.9%) and Germany (91.5%), solar plants mainly use flat-plate and evacuated tube collectors to prepare hot water and to provide space heating, while in the United States (7.9%) and Canada (11.7%), swimming pool heating is the dominant application with cheaper unglazed plastic collectors.

Table 2.5. Distribution of different solar collector by country in operation at the end of 2006 (Weiss et al., 2008)

		AUT	S	CH	GER	DK	F	CAN	USA
Unglazed	[%]	18.1	21.1	34.3	8.5	5.3	8.2	88.3	92.1
Flat-plate	[%]	80.7	72.1	61.7	82.4	94.0	90.4	11.3	6.0
Evacuated tube	[%]	1.2	6.7	4.0	9.1	0.8	1.4	0.3	1.9

2.5.2 Energy storage

Storage of thermal energy is critically important in many engineering applications. The problem is particularly true for solar applications since most of the energy is required when the solar availability is minimum, typically in winter. Therefore, to insure the continuity of a thermal process, technologies have to able to collect and store the excess heat during periods of bright sunshine for a later distribution during phases of high energy demand. Yet, even today, this concept remains technically challenging even after years of research and development.

For storing the energy, three techniques have been considered over the years for solar thermal applications. These are (i) the *sensible heat storage* (where a change of temperature occurs), (ii) *latent heat storage* (where a change of phase occurs), and (iii) *thermochemical storage* (where a reversible chemical reaction takes place) (Hasnain, 1998).

The most popular and well-developed technology is definitively the sensible heat storage (SHS) as it is conceptually the simplest form of storing thermal energy. A SHS consists of a storage medium, a container and input/output devices. The container must retain storage material for a future use while limiting heat losses to the environment. The amount of energy stored is proportional to the difference between the storage input and output (Dincer et al., 1997).

Unfortunately, the sensible heat storage is the least efficient method for energy storage because of low heat storage capacity per unit volume of the storage medium (Beasley and Clark, 1984). Latent heat storage (LHS) systems using phase change material (PCM) as storage medium offer advantages such as high heat storage capacity, small unit sizes and isothermal behavior during charging and discharging processes (Nallusamy et al., 2007). However, these types of systems are still in the development process and are not in commercial use as much as SHS.

2.5.3 Seasonal storage

A storage system collecting from hot summer to use in the winter is called a seasonal storage. The objective is to increase the *solar fraction*, defined as the fraction of heating needs that can be covered by solar, as high as possible (Duffie and Beckman, 2006). In Europe, for single family home applications, solutions have been found and are available on the market since the 1990's (Thomsen et al., 2005). Indeed, configurations for seasonal storage are essentially the same as those considered for short-term storage (overnight). The main difference between the two types of systems are in the relatives and absolute sizes of the water tanks and the solar collectors, as the storage capacity for a seasonal system must be able to store a maximum part of the energy collected during summer months. Consequently, the ratio of storage to collector area is always much higher for seasonal storage systems (Braun et al., 1981). For instance, in a low energy building and depending on the insulation level and the climatic conditions, a water tank with a volume ranging from 3 to 30 m^3 is used to store enough energy to achieve a 100% solar fraction (Hadorn, 2005).

For solar water heating systems with a seasonal storage capacity, some design alternatives

are recommended such as: (i) use of an external heat exchanger for domestic hot water preparation is necessary to avoid legionella problems Krause and Jaehnig; (ii) select the optimum tilt angle equal to the latitude (Braun et al., 1981).

2.5.4   Stratification in storage tanks

The hotter the water, the lower the density of the water. Hot water thus naturally and stably finds its way above layers of cold water. This phenomenon makes it possible to have stratification, with layers of different temperature in one physical store. The degree of thermal stratification in the storage tank is a measure of its performance. High tank performance is achieved by eliminating mixing and when the stratification is maintained (Duffie and Beckman, 2006). Also, due to heat losses from the surface of the storage tank, the temperature of water near the vertical walls is lower, which leads to natural convection currents that affect the temperature of layers (Garg et al., 1985). Therefore, a sufficient thickness of insulation shall be used to maintain the stratification over a long period.

One way to enhance the stratification is to use external heat exchangers. Indeed, as opposed to internal heat exchangers, they avoid to disturb the temperature distribution within the tank (Dayan, 1997). One other way is to use a rigid inlet stratification pipe (stratifier) with several outlets, as illustrated in Figure 2.2. This arrangement allows water to exit the unit at the height with approximately the same temperature in the store, thus maximizing stratification. Such stratifying devices are typically used with both internal and external heat exchangers in the solar circuit and for the return from the space-heating loop. Though, this method requires careful attention since the flow in the tube should be within a limited range, between 5 and 8 kg/min, otherwise the water comes out at an incorrect height (Shah

et al., 2005) and (Andersen et al., 2008).
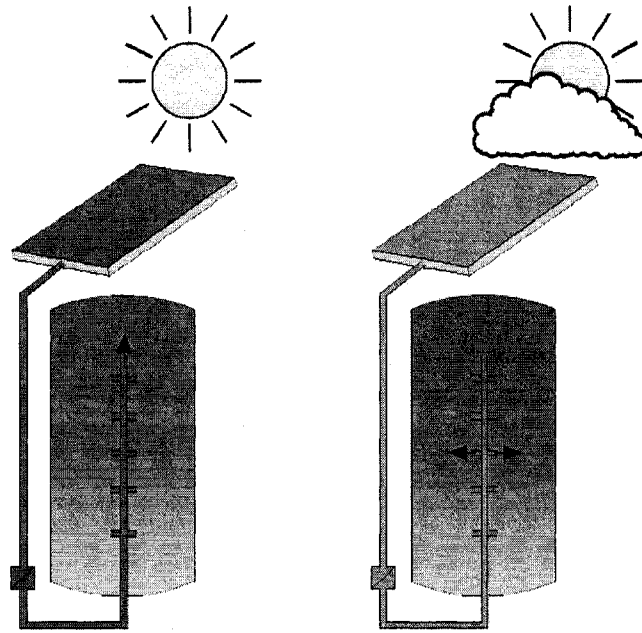
Figure 2.2. Stratifying device for hot water stores (Solvis, 2007)

2.6 Solar combisystems

Since the end of the 1970's, the use of solar collectors for domestic hot water has increased continuously, showing that solar heating systems are both technically reliable and well established. Nowadays, in most countries, the market is still focused on such systems, which are straightforward and have short pay back times, especially due to good subsidies in some countries (Weiss et al., 2008). But so-called "solar combisystems", which supply heat for both domestic hot water and space heating, are still only really noticeable in Austria, Sweden, Switzerland and Germany (Figure 2.6). Reasons for that, beside others, might be not sufficiently attractive energy savings as well as too much effort and risks for installers due to the complexity of many system concepts and products (Thür, 2007).

Also, the building integration of such applications becomes increasingly challenging with the trend towards large contributions like seasonal storage systems. Appropriate surfaces have to be found by the architect for large collector areas and correspondingly large storage volumes, considering both aesthetics and building physics (Weiss, 2003).

Table 2.6. Distribution of different applications by country for the total capacity of flat-plate and evacuated tube collectors in operation at the end of 2006 (Weiss et al., 2008)

		AUT	S	CH	GER	DK	F	CAN	USA
DHW-SFH	[%]	63	65	67	80	86	95	95	100
DHW-MFH and district heating	[%]	9	10	8	8	13	1	5	0
Combisystems	[%]	28	25	25	12	1	4	0	0

DHW: Domestic hot water systems; SFH: Single family house; MFH: Multi-family house.

These combisystems are typically coupled with a biomass boiler. Common systems for a single-family house consist of 15 m^2 up to 30 m^2 of collector area and a 1-3 m^3 storage tank. The share of the heating demand met by solar energy in these systems is between 20-60% (Weiss, 2003). Yet, a variety of systems concept are present on the market. The difference in the systems is partly due to the conditions prevailing in the individual countries. For instance, in the Netherlands, "smallest systems" in terms of collector area and storage volume are more popular and gas or electricity is primarily used as the auxiliary energy source. So, a typical solar combisystem consists of 4-6 m m^2 of solar collector and a 300 l storage tank, and therefore, solar energy meets a relatively smaller share of the heating and hot water demand.

2.6.1 Task 26: Solar Combisytems

The most comprehensive research on solar combisystems was certainly performed in the frame of Task 26 of the IEA Solar Heating and Cooling Programme (IEA SHC,

2007). Between 1998 and 2003, 35 solar experts have collaborated to further study solar combisystems. A system survey and a comparison of 21 different generic combisystem configurations were carried out to understand and support the growing market of solar combisystems in Europe. The ultimate objective was to improve the confidence of the end user in that technology.

The optimization of 9 systems under the same climatic reference conditions was investigated by using a sensitivity analysis based on simulation results from the TRNSYS program. Several design improvements were investigated and some key design strategies were presented (Tepe et al., 2004) such as: (i) select a low temperature space heating system like a radiant floor; (ii) keep heat losses of the storage tank as low as possible by adding an appropriate thickness of insulation; (iii) use energy efficient pumps to decrease the electricity demand; and (iv) use stratifying devices and external heat exchangers to maintain the stratification in the storage tank.

Low-flow systems are recommended since they ensure a better temperature distribution in the storage tank when combined with a stratifier (Frei et al., 2000). So, the mass flow rate of a typical system has to drop from about 50 to 10-15 kg/h per square metre of collector (Kenjo et al., 2003). Besides of that, low-flow systems are capable of reducing equipment and installation costs and they allow equipment to be considerably sized down; piping and pumps are smaller. Cost advantages are in terms of decreased material costs, less parasitic pumping power required from the utility and reduced costs with installing lightweight systems (Dayan, 1997).

2.6.2 ALTENER

A follow up project of the Task 26 was the European project ALTENER "Solar Combisystems" that took place between 2001 and 2003 (Ellehauge, 2003). More than 200 solar combisystems in seven European countries were installed, documented and theoretically evaluated, and 39 of them were also monitored in detail. The goal of this project was to demonstrate the state of the art of solar combisystems in practice and to be able to compare the measured results with the annual calculations performed within Task 26.

2.7 Conclusions

A lot of research has been conducted to develop new technologies for low energy and even net-zero energy buildings, especially in the residential sector. Constructions combining higher level of insulation, air tightness, passive solar design and efficient solar combisystems seem promise to a bright future. In Europe, the increase in the use of solar collectors in recent years for domestic hot water preparation has shown that solar heating systems are a mature and reliable technology. Every day, thousands of systems demonstrate the possibilities of this ecologically harmless energy source. Motivated by the confirmed success of these systems for hot water production, an increasing number of homebuilders are considering solar energy for space heating as well.

Yet, designing a seasonal storage combisystems in a cold climate like Canada seems quite challenging. Indeed, higher standards of thermal insulation are required to allow the heating loads to be met at reasonable size of solar collector area and storage tank volume. Innovative concepts and efficient techniques need to be explored. Therefore, since the heat store is

the heart of a solar combisystem, a particular attention should be paid to improve the thermal stratifications by considering low-flow systems, stratifying devices and external heat exchanger.

Chapter 3

Life cycle performance of a base case house

In this chapter, the integrated building model of a typical single family house in Montreal (Quebec) is developed using the simulation program TRNSYS 16. The life cycle performance of the base case house is carried out by estimating the life cycle energy use, life cycle emissions and life cycle cost. Several design alternatives that upgrade the life cycle performance are investigated.

3.1   Description of the base case house

An existing one-storey detached house located in Montreal and built in the 1990's is used as a base case study house. Its total floor area is about 210 m^2. The house is made in wood-frame structure and brick veneer. Figures 3.1 and 3.2 present the drawings of floors and elevations. Conventional electric baseboard heaters and an electric storage water tank heater provide the space heating and domestic hot water requirements.
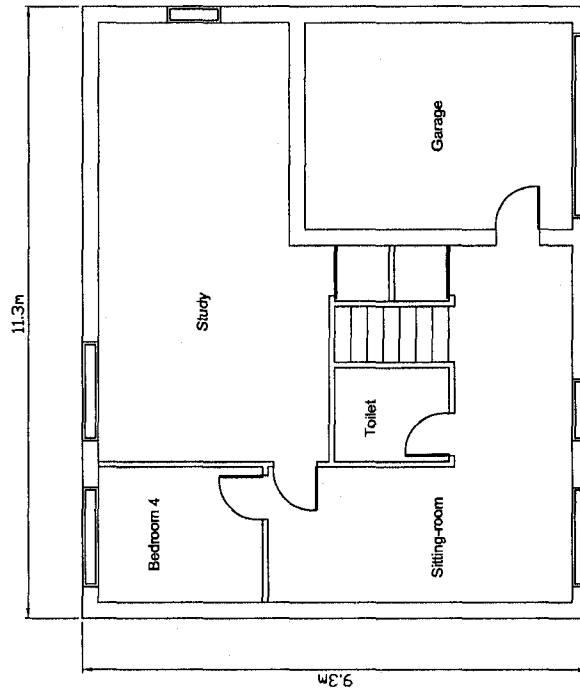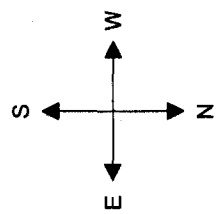
(a) Basement floor
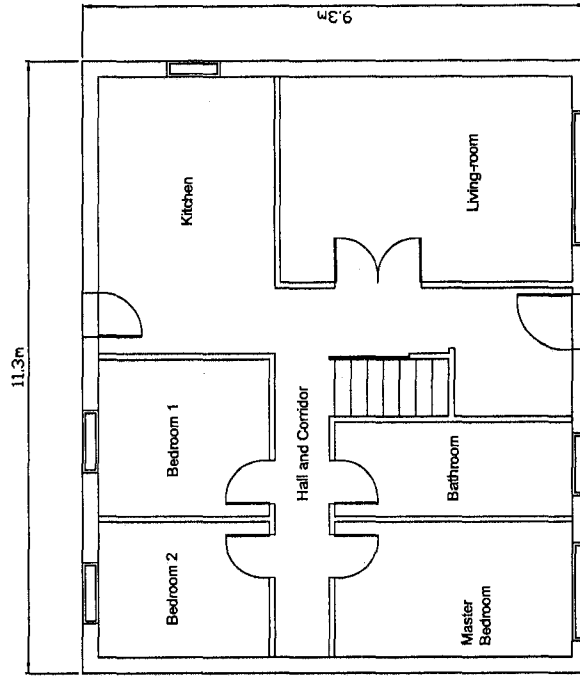
(b) First floor

Figure 3.1. Base case house floors plans
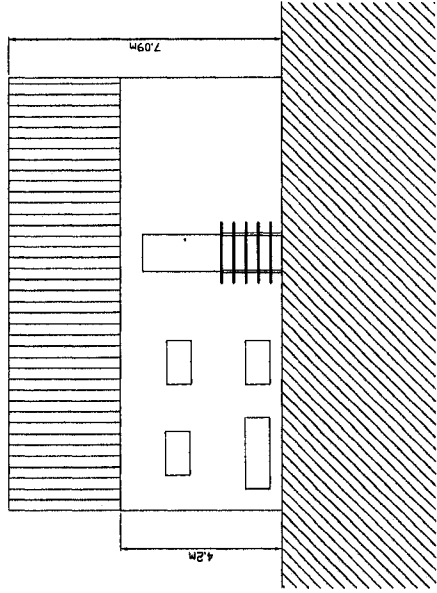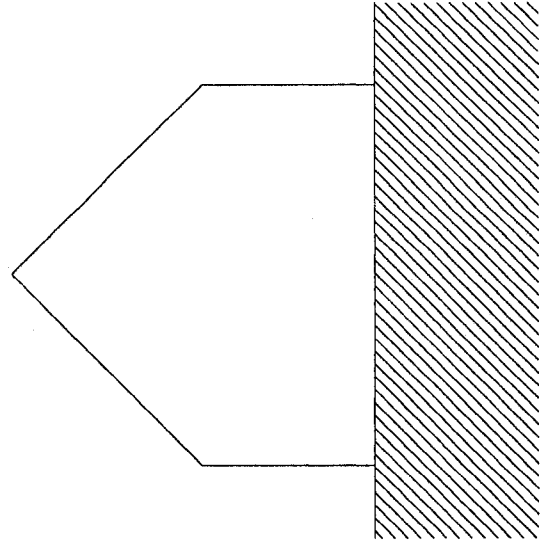
(a) Northern facade   (b) Southern facade

(c) Eastern facade   (d) Western facade
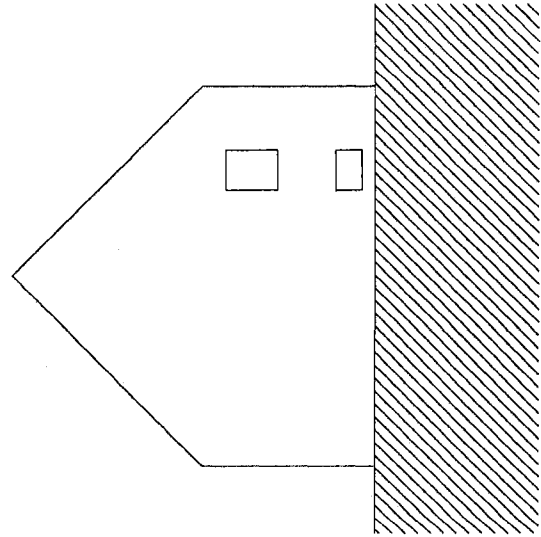
Figure 3.2. Base case house facades plans

3.2 Description of TRNSYS components used for modelling

The assessment of energy use is implemented using the transient system simulation program TRNSYS (SEL, 2007). TRNSYS components are referred to as "Types". They are configured and arranged using the integrated visual interface known as the TRNSYS Simulation Studio, while building input data is entered through a dedicated visual interface (TRNBuild). Due to its modular approach, TRNSYS is widely used for solar and nonsolar modeling applications (DOE, 2008).

Table 3.1 presents TRNSYS standard and TESS libraries (TESS, 2007) components used in the simulation. It is performed for a complete year, with a one-hour time step.

Table 3.1. List of TRNSYS types

Type	Description	Name used in Simulation Studio
2	Differential Controller	Heaton, Coolon, Lightson, Shadingon, Lightson
4	Storage Tank	Tank
9	Data Reader For Generic Data Files	Type9e
11b	Tempering valve	Diverter
11h	Tee piece	Tee piece
16	Solar Radiation Processor	Type16g
25	Printer (output file)	System printer
28	Simulation Summary	Q-total-sum, Q-DHW-sum, Q-HVAC-sum
33	Psychometrics	Type33e
56b	Multi-Zone Building	Type56b
65	Online graphical plotter	Type65d, Type65d-2
69	Effective sky temperature	Type69b
89	TMY2 Data Reader	Type89b
515	Heating and Cooling Season Scheduler	Type515
516	Hourly Forcing Function Scheduler	Type516
518	Monthly Forcing Function Scheduler	Type518
646	Air Diverting Valve	Type646
648	Air Mixing Valve	Type648, Type648-2, Type648-3
701	Basement Conduction	Type701
754	Simple Heating and Humidifying System	Type754f
760	Sensible Air to Air Heat Recovery	Type760a

3.2.1 Type 56: Building envelope

The building is divided in two distinct zones: one zone comprising the basement without the garage and a second zone comprising the main living area. The garage and the attic are unheated and, therefore, temperatures in these spaces are considered as free-floating.

The total heated floor area is 186 m^2, including a basement of 81 m^2. The house has a gable roof with a slope of 45° and a ceiling with a total area of 105 m^2. Joists and rafters of 38×89 mm (2×4 in), spaced by 600 mm (24 in) represent the frame of the roof and the ceiling. Exterior cladding of the sloped part is made of asphalt shingles, while bricks are used for the gable ends. The ceiling includes a total fiberglass insulation of 203 mm (8 in) and a gypsum board of 12.7 mm constitutes the interior finish. The overall thermal resistance of the ceiling is equal to 6.08 (m^2·°C)/W.

The above-ground exterior walls are composed of traditional bricks as cladding, 20 mm of air space, 25.4 mm (1 in) extruded polystyrene (XPS) sheathing boards, wood studs frame spaced at 400 mm (16 in) with 89 mm (4 in) of fiberglass batt insulation, 6 mm polyethylene sheet and 12.7 mm gypsum boards. The resulting thermal resistance is equal to 4.11 (m^2·°C)/W.

Partition walls are composed of wood studs frame spaced at 400 mm (16 in) with two gypsum boards of 12.7 mm on each side as finish. 89 mm (4 in) of XPS insulation batts are considered for the interior wall between the garage and the basement.

Foundation walls are 2.60 m high with a 1 m depth below grade. They are made of 300 mm of cast-in place concrete, with 25.4 mm (1 in) of expanded polystyrene batt insulation (EPS), and 12.7 mm gypsum board as interior finish. The thermal resistance of foundation

walls is equal to 1.09 $(m^2 \cdot {}^\circ C)/W$.

The first floor is composed of wood I-joists, 25.4 mm (1 in) of EPS batt insulation, 15 mm plywood subfloor sheathing, 50 mm of light weight concrete and 20 mm of tile. Gypsum boards of 12.7 mm thick represent the interior finish of the basement ceiling.

The basement floor is made of 100 mm concrete layer, 25.4 mm (1 in) of EPS batt insulation, 50 mm of light weight concrete and 20 mm of tile. The resulting thermal resistance is equal to 0.99 $(m^2 \cdot {}^\circ C)/W$.

Exterior windows have aluminium frame and double glazing with the cavity filled by Argon, which corresponds to a U-Value of 1.4 $W/(m^2 \cdot {}^\circ C)$. The front and rear doors are wooden and the garage door is composed by Polystyrol plastic with a thermal resistance of 1.89 $(m^2 \cdot {}^\circ C)/W$.

Typical thermal properties of building and insulating materials are taken from ASHRAE (2005). Table 3.2 presents a summary of different dimensions and thermal resistances of the building envelope.

For the base case house, only the exterior walls and the ceiling/roof comply with the minimal thermal resistances stipulated in the Quebec regulation for new buildings (Province of Quebec, 1992), since the values need to be superior to 5.3 $(m^2 \cdot {}^\circ C)/W$ for the ceiling/roof, 3.4 $(m^2 \cdot {}^\circ C)/W$ for above-ground walls, 2.2 $(m^2 \cdot {}^\circ C)/W$ for foundation walls, and 1.2 $(m^2 \cdot {}^\circ C)/W$ for the basement floor.

Table 3.2. Base case house characteristics

Dimensions		
Heated floor area	[m²]	186.0
Heated volume	[m³]	483.6
Roof area	[m²]	148.6
Attic volume	[m³]	248
Exterior doors	[m²]	4.5
Garage door	[m²]	7.8
Windows area	[m²]	14.7
North/East/South/West	[m²]	9.1/1.5/4.1/0.0
Thermal resistance of the exterior envelope		
Ceiling/roof	$[(m^2 \cdot °C)/W]$	6.08
Above-ground walls	$[(m^2 \cdot °C)/W]$	4.11
Foundation walls	$[(m^2 \cdot °C)/W]$	1.09
Basement floor	$[(m^2 \cdot °C)/W]$	0.99
Exterior doors (wood)	$[(m^2 \cdot °C)/W]$	0.47
Garage door (Polystyrol)	$[(m^2 \cdot °C)/W]$	1.89
Windows U-value	$[W/(m^2 \cdot °C)]$	1.40
Aluminium frame, double glazing filled by Argon		
Overall thermal resistance	$[(m^2 \cdot °C)/W]$	3.37

3.2.2 Weather input data

The TMY2 (Typical Meteorological Year version 2) weather file for Montreal is selected. It is connected with Types 33 and 16 that define respectively the moist air properties and the solar insolation on all surfaces of the building. Type 69 calculates the effective sky temperature for long-wave radiations. The different components required to assess weather conditions are connected to Type 56, as shown in Figure 3.3.
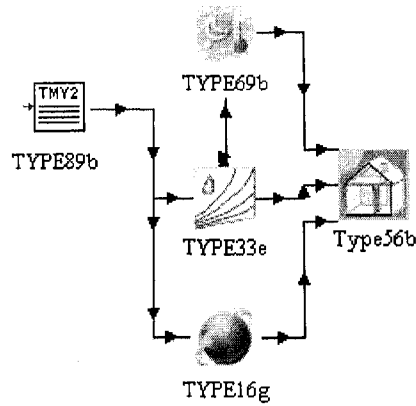
Figure 3.3. Weather data components

Impact of ground reflectance

Using appropriate values of ground reflectance (albedo) during the winter season in cold

climates is an absolute necessity, since the energy use can be influenced by reflection of

solar radiation off the snow (Thevenard and Haddad, 2006). Yet, Type 16 allows only one

constant value to input as parameter. Therefore, a monthly estimation of ground reflectance

is performed using an Equation-Type (calculator) to assess the following expression:

$$\rho_g = \rho_{nosnow} \left(1 - \frac{N_{snow}}{N}\right) + \rho_{snow} \frac{N_{snow}}{N} \tag{3.1}$$

where the snow-free albedo of ground ρ_{nosnow} is equal to 0.2 (green grass), N_{snow} is the

number of days with snow depth greater than 5 cm (Environment Canada, 2007), N is the

number of days in the month, and ρ_{snow} the snow-covered albedo of ground is equal to 0.4

(typical urban site) (Hunn and Calafell, 1977). Table 3.3 presents the results of monthly

ground reflectance computation.

These values are set as input data in the monthly scheduler Type 518, which is connected

Table 3.3. Monthly ground reflectance values

Month	N	N_{snow}	ρ_g
Jan	31	24.3	0.36
Feb	28	22.4	0.36
Mar	31	17.2	0.31
Apr	30	2.4	0.22
May	31	0.0	0.20
Jun	30	0.0	0.20
Jul	31	0.0	0.20
Aug	31	0.0	0.20
Sep	30	0.0	0.20
Oct	31	0.0	0.20
Nov	30	3.3	0.22
Dec	31	17.2	0.31
Year			0.25

to the solar radiation processor Type 16, as shown in Figure 3.4.

TypeS18   TYPE16g   TypeS6b
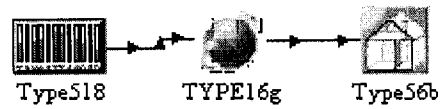
Figure 3.4. Ground reflectance components

3.2.3 Type 701: Basement conduction

A particular effort is made to reproduce accurately the heat transfer from the basement (four walls and the floor) to the soil surrounding the five surfaces of the basement, as Type 701 from TESS libraries is applied. The heat transfer is assumed to be conductive only and moisture effects are not accounted for in the model. The model is based on a 3D finite difference model of the soil and solves the resulting inter-dependent differential equations using an iterative method. The temperature of the zone side surfaces of the floor and walls as well as the U-values are set as input data. Parameters like the soil properties and the conditions outside of the basement (near-field) are presented in Table 3.4. The soil grid geometry is illustrated in Figure 3.5. The initial soil conditions are calculated from the Kasuda correlation (Kasuda and Archenbach, 1965). The surface conditions for the near-field and far-field soil are calculated from an energy balance on the surface plane. The near-field soil temperatures are affected by the heat transfer from the basement. The far-field soil temperatures are only affected by the surface conditions (time of year) and depth.

Table 3.4. Parameters for the basement conduction model

Soil properties		
Soil properties		
Conductivity	$[\text{W}/(\text{m}\cdot{}^\circ\text{C})]$	2.42
Density	$[\text{kg}/\text{m}^3]$	3200
Specific heat	$[\text{kJ}/(\text{kg}\cdot{}^\circ\text{C})]$	0.84
Surface emissivity	-	0.9
Surface absorptance[1]	-	0.75
Conditions outside of the basement (near-field)		
Mean surface temperature[2]	$[{}^\circ\text{C}]$	6.3
Amplitude of the surface temperature	$[{}^\circ\text{C}]$	30.3
Day of minimum surface temperature	[day]	11

[1] The surface absorptance is assumed equal to $1 - \rho_{g,year}$ (from Table 3.3).

[2] The mean (average) surface temperature of undisturbed soil, assumed equal to the annual average temperature.
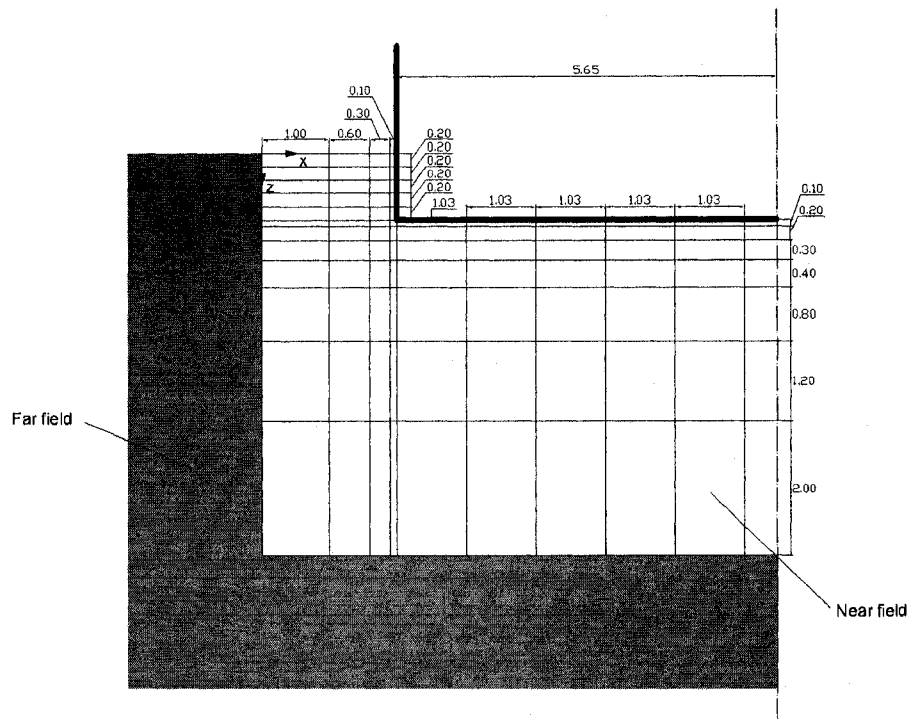
(a) Soil volumes in the x and z directions
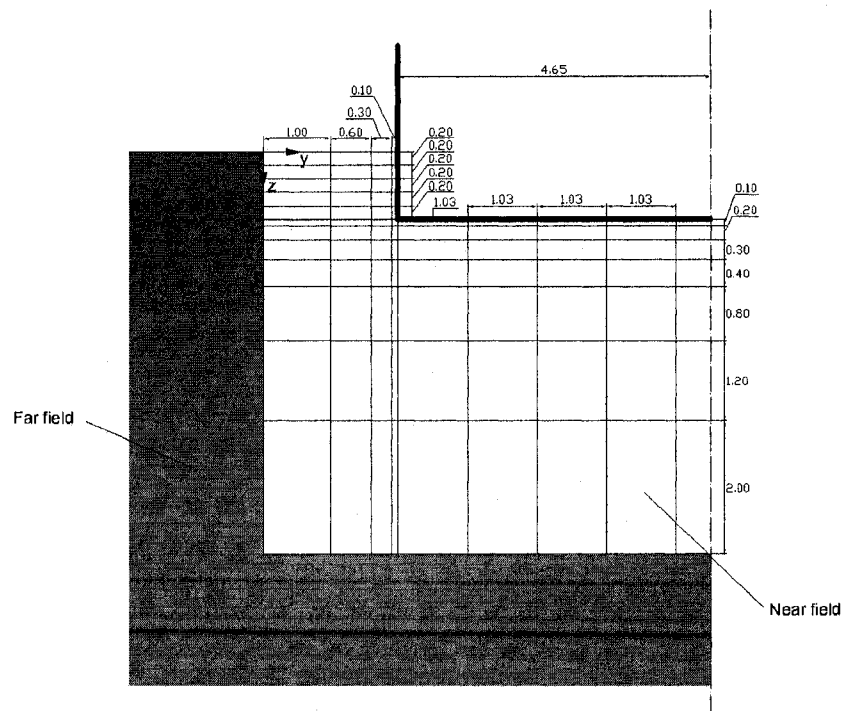
(b) Soil volumes in the y and z directions

Figure 3.5. Representation of basement walls, with near and far-field

Figure 3.6 shows that zone inside surface temperatures for the floor and walls, as well as the U-values are taken from Type 56. Outside surfaces temperatures are then computed by Type 701 and sended back to Type 56 as input.
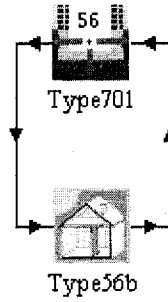
Figure 3.6. Connections between Types 56 and 701

Instead of considering a fixed value for the convective heat transfer coefficient between the soil surface and the outdoor air h_c, its value is computed as a function of wind velocity v using Jürges equation (Duffie and Beckman, 2006):

$$h_c = \begin{cases} 5.8 + 3.9v & \text{if } v < 5 \text{ m/s} \\ 7.1v^{0.78} & \text{if } v \geq 5 \text{ m/s} \end{cases} \qquad (3.2)$$

where:

h_c = convective heat transfer coefficient [W/(m^2·°C)]; and

v = wind velocity [m/s].

3.2.4 Space heating

A system of independent electric baseboard heaters is installed inside the two zones. It maintains the following temperature profile during the winter period (from October 1 to May 15).

- On weekdays:

    - from 00:00 to 06:00, $T_{set} = 19°$C

    - from 06:00 to 10:00, $T_{set} = 21°$C

    - from 10:00 to 16:00, $T_{set} = 19°$C

    - from 16:00 to 23:00, $T_{set} = 21°$C

    - from 23:00 to 00:00, $T_{set} = 19°$C

- On weekends:

    - from 00:00 to 06:00, $T_{set} = 19°$C

    - from 06:00 to 23:00, $T_{set} = 21°$C

    - from 23:00 to 00:00, $T_{set} = 19°$C

During the summer period (from May 15 to October 1), the heating system is turned off. As illustrated in Figure 3.7, these parameters are introduced in Types 515 and 516. The starting of the heating system is then pondered by a ON/OFF differential controller (Type 2), assuming a dead band value of 1°C.
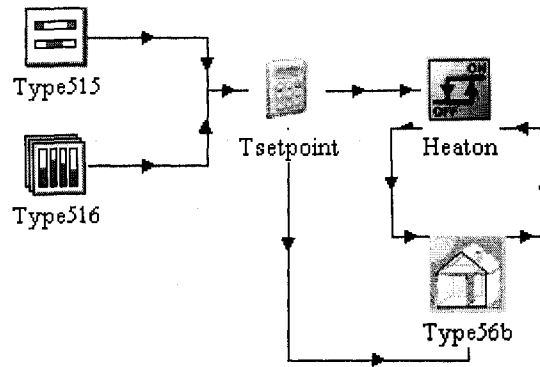
Figure 3.7. Heating system components

3.2.5 Occupancy

A family of four is assumed to occupy the place intermittently. The occupancy parameter is directly related to the previous temperature schedule since its value is equal to 1 (100% of the occupants) when the heating temperature setpoint is 21°C, all year long.

3.2.6 Infiltration

Typically, air infiltration rates for new houses in Quebec range from 3.1 ach_{50} to 3.9 ach_{50} (Zmeureanu et al., 1998b). Therefore, the airtightness of the exterior envelope is assumed to be in the average for new houses in Quebec and is set to a constant value 3.5 ach_{50} in Type 56, for the basement and the first floor.

3.2.7 Space ventilation

A heat-recovery ventilator (HRV) from Venmar (Venmar, 2007) provides the space ventilation (see technical specifications, Appendix A). The total supply air flow rate is fixed at the recommended value of 0.35 ach (ASHRAE, 2001), which corresponds for the house to 169.3 m^3/hr. The sensible heat recovery efficiency of the system is a function

of the outside temperature and the air flow rate. It has a value of 64% if the outdoor air temperature is higher than -13°C and 62% the rest of the time. In the same way, the electrical power varies between 110 W and 114 W.

As presented in Figure 3.8, the system is modeled using Type 760 that calculates the temperature of the mixed outside and exhaust air as well as fans energy consumption. Exterior data are taken from Types 89 and 33. Type 754 calculates the energy use of the electric heater required to heat the supply air to the zone setpoint temperature. Two different types of valves are included, as Type 648 is used to mix the exhaust air from the first floor and the basement, while Type 646 is used to distribute the fresh air to the same rooms. Output data from Type 646 (temperature, air flow rate and RH of the inlet air) are transposed to Type 56 as input.
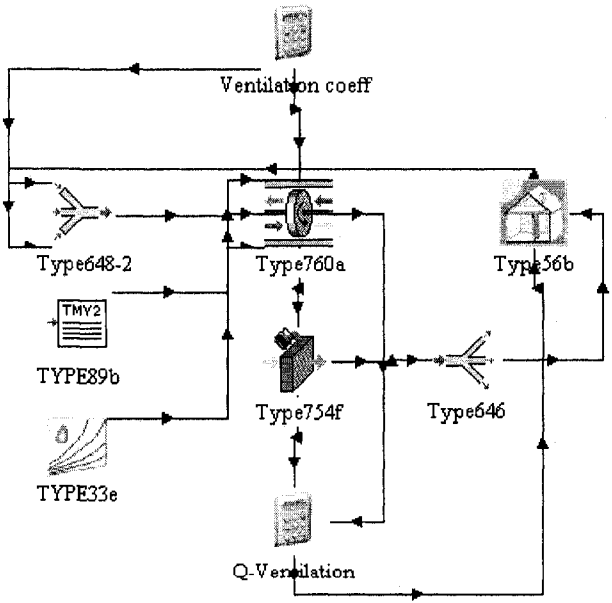
Figure 3.8. Ventilation system components

3.2.8 Space cooling

Two split type air conditioners (wall mounted) from Fujitsu (2007) are selected to provide cooling and dehumidification for the first floor and the basement of the base case house. Each unit has a nominal cooling power of 3.6 kW and a Coefficient Of Performance (COP) of 3.5. An average air flow rate of 550 m^3/h) per unit, blown at a supply temperature of 14°C and 50% RH, is assumed.

As shown in Figure 3.9, two Types 2 (Coolon-1st, Coolon-base) are used to start the cooling units if the zone air temperature exceeds typical design values for indoor conditions of 24°C (ASHRAE, 2005). The dead band is fixed at 1°C. The flow rate coming from the units is then mixed with the air coming from Type 754 (ventilation system) using two Types 648 in order to consider the first floor and the basement separately. Input data (temperature, air flow rate and RH of the inlet air) transposed to Type 56 are taken from Type 648 outputs.
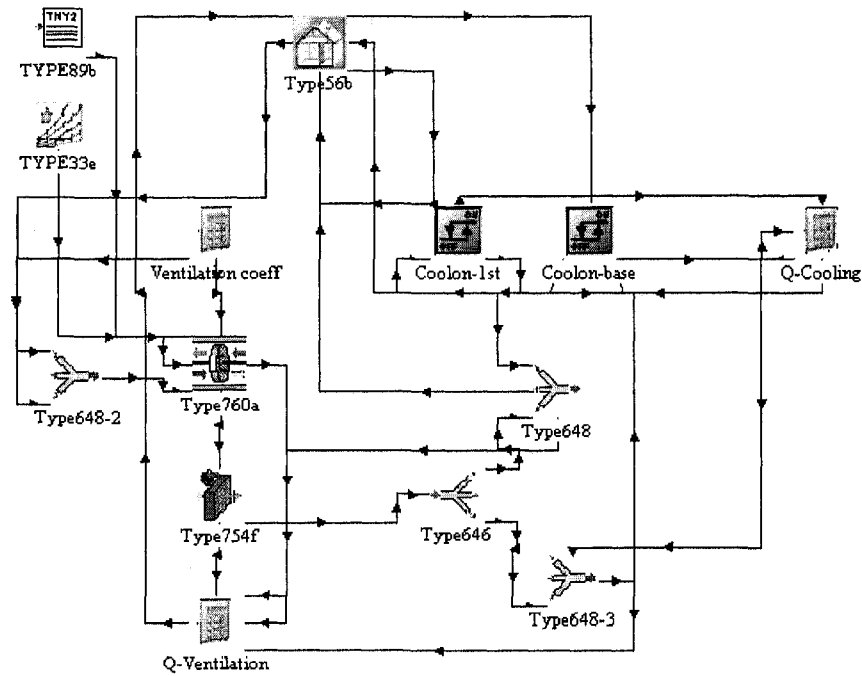
Figure 3.9. Combination of ventilation and cooling system components

3.2.9 Humidification

Using several Types 2 ON/OFF differential controllers (Figure 3.10) and Type 56, an humidifier is modeled to control the relative humidity of air for the basement and the first floor. As recommended by Lstiburek (2002), the lower boundary of the relative humidity in the building has to be limited to 25% in winter. Therefore, when the relative humidity falls below this limit, the system supplies the minimum value of 25% RH. The dead band is assumed at 1%.

3.2.10 Shading devices and artificial lighting

In order to assess shading devices and artificial lighting impacts on energy use, different control strategies as function of exterior solar radiation are assumed.

47
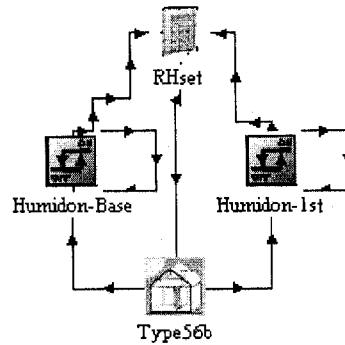
Figure 3.10. Relative humidity control components

Shading devices

In TRNSYS, the modelling of internal devices is detailed including multiple reflection between the window pane and the shading device (Welfonder et al., 2003). Therefore, with the perspective to reduce heat loss during winter and to avoid high temperatures during summer, white opaque curtains are selected. They are located on the inside surface of all exterior windows. The textile is assumed to have an approximate thermal resistance of 0.24 $(m^2 \cdot {}^\circ C)/W$ (Pierce, 2000). Since shades solar-optical properties are taken from ASHRAE (2005), the transmittance is fixed to zero, the reflectance to 0.65 and the absorptance to 0.35. These parameters are considered as input data in Type 56.

Type 2 and Type 16 are used to control the opening and closing of the shading devices. At night, they are considered as always closed. During the day of winter months, they are assumed to be open when the solar radiation on the south facade is superior to 140 W/m^2, and closed when it is inferior to 120 W/m^2. During the day of summer months, the opposite situation occurs since they are closed when the solar radiation on the exterior wall is superior to 140 W/m^2, and open when it is inferior to 120 W/m^2. These boundary values are assumed

from default values proposed in Type 56 and from van Moeseke et al. (2007) study.

Artificial lighting

A similar procedure simulates the artificial lighting inside the house. This time, Type 2 and Type 16 are used to turn the lights on when the total horizontal solar radiation is lower than 120 W/m^2 during daytime, and turn them off when it is higher than 200 W/m^2. These boundary values are assumed from default values proposed in Type 56. Assuming typical incandescent lights, the total electric input is assumed at 250 W for the first floor, and 125 W for the basement.The combination of shading and lighting components is presented in Figure 3.11.
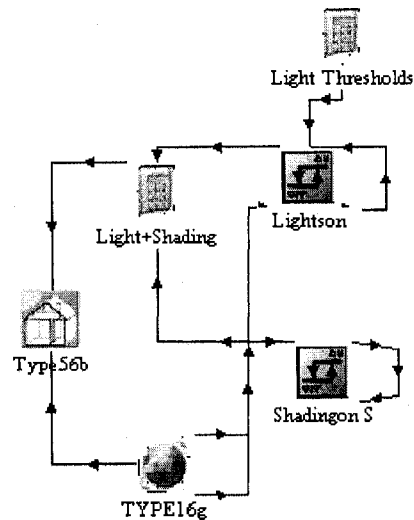
Figure 3.11. Shading devices and lighting components

3.2.11   Internal heat gains

Internal heat gains related to the occupancy parameter, lighting and household appliances are taken into account in the simulation, using Type 56 to specify the different input data.

49

Occupants

Internal heat gains due to occupancy are computed for the first floor and the basement, using different control strategies. Indeed, three people are assumed to be on the first floor and one on the basement when the building is occupied. Heat gains per occupants are specified using the proposed alternatives in Type 56. The option considering people under the "seated, light work, typing" condition is chosen.

Artificial lighting

The total heat gain due to artificial lighting is computed using Type 56, assuming that the total electric input of incandescent lamps is converted to 10% of convective gains (EnergyPlus, 2007).

Household electrical appliances

A 230 W personal computer (with color monitor) the only appliance considered in the calculation. It is assumed to run on the basement level when the occupancy parameter is equal to 1.

3.2.12 Domestic hot water supply

The domestic hot water (DHW) is supplied by an electric water heater of 303 l (80 gallons) located on the basement, with an average tank loss coefficient assumed equal to 0.8 W/(m^2·$^\circ$C). The storage tank, divided in 6 nodes of 10 in (25.4 cm) each, is simulated in TRNSYS using Type 4.

Two heating elements maintain the water to a setpoint temperature of 55°C. The cold water inlet is located in the bottom part of the tank and the hot water outlet at the top. The flow

rates of water entering and leaving the storage tank are set equal to the consumption profile values. Two types of valves, a tempering valve and a tee piece, are used to ensure the mix of cold and hot water. The loss of heat from piping is not considered in the simulation.

DHW consumption profile

The DHW consumption profile is based on a report presented by Jordan and Vajen (2001) that was initially developed within the scope of the International Energy Agency (IEA, Task 26: Solar Combisystems). It consists of values of the DHW flow rates, selected by statistical means, for every hour of the year assuming a mean daily load of 266 l/day (Aguilar et al., 2005). As an example, flow rates from January 10 to January 13 are presented in Figure 3.12.
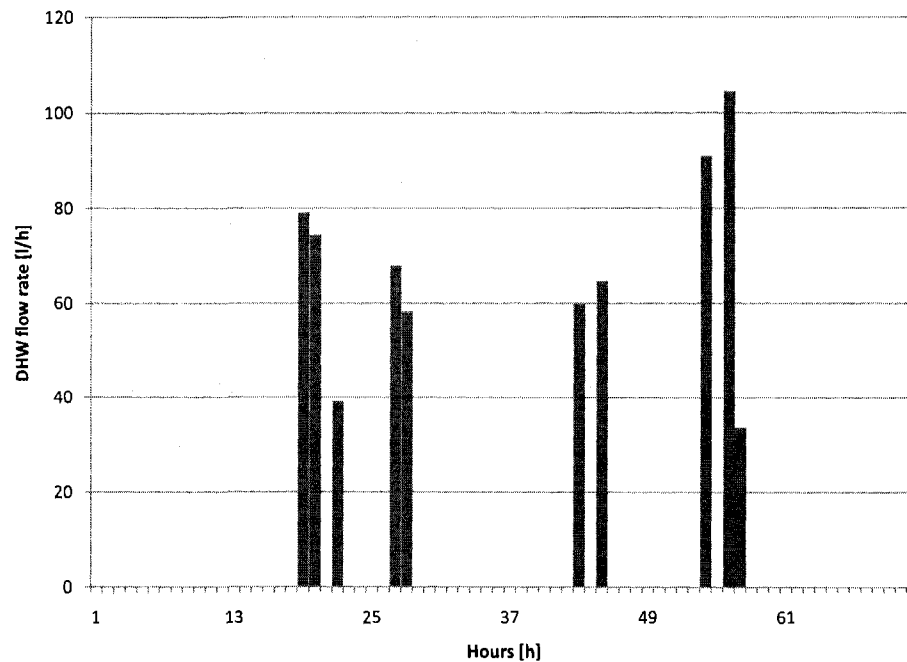
Figure 3.12. Sequence of the DHW profile from January 10 to January 13

City line water temperature

Temperature of cold water from the city line is based on measured data from an aqueduct located in Montreal (ASHRAE Montreal Chapter, 2007), between years 1994 and 2004. These data are correlated using the graphing tool FindGraph (UNIPHIZ Lab, 2007) in order to predict the temperature T_{city} for every hour of the year. The best fit equation (Equation 3.3) proposed by the program is a Fourier series with 17 harmonics. Coefficients used in the equation are presented in Appendix B. Figure 3.13 illustrates measured data and the plot of the best fit equation.

$$T_{city} = a + c_1 \cos(bN) + d_1 \sin(bN) + c_2 \cos(2bN) + d_2 \sin(2bN) + \cdots \qquad (3.3)$$
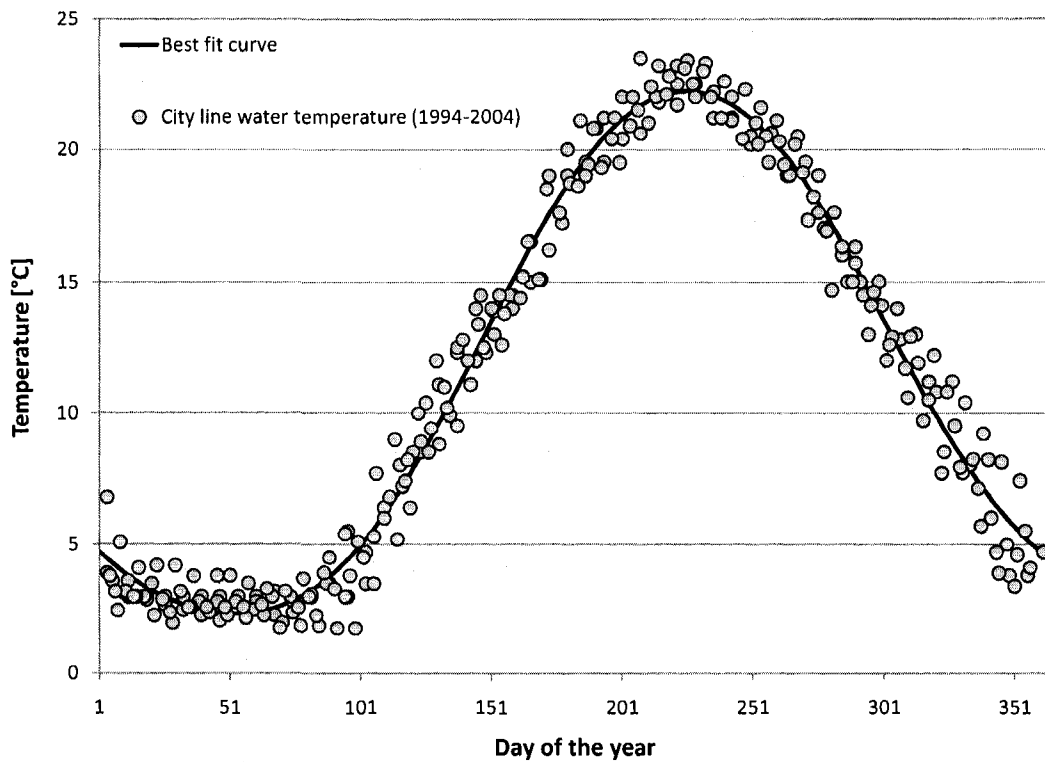
Figure 3.13. Temperature of cold water from the city line

52

Figure 3.14 summarizes the components required to simulate the domestic hot water system. Type 9 is used to read hourly values of DHW profile from an input file, while an Equation-Type computes T_{city} using Equation 3.3.
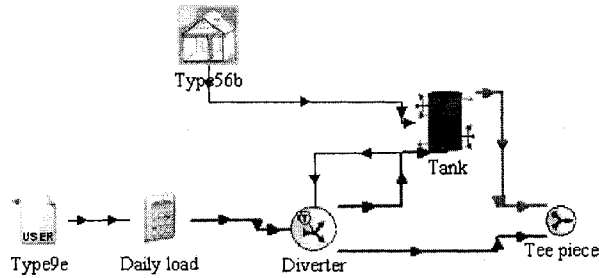
Figure 3.14. Domestic hot water components

3.3 Energy performance results and discussion

The estimated energy consumption for the base case house, imported from the TRNSYS program, is equal to 26,156 kWh (94,163 MJ), corresponding to 140.6 kWh/m^2 (506 MJ/m^2) of heated floor area. These values are comparable with 123.8±29.0 kWh/m^2 of normalized annual energy use monitored by Zmeureanu et al. (1998a), for a sample of 10 houses located in Montreal and built during the 1986-1990 period.

The monthly repartition of energy use during the year as well as its distribution are shown in Table 3.6. With a total of approximately 16,500 kWh, the winter period, which is represented by the months of December, January, February and March, constitutes the highest contribution to the energy consumption since the heating demand remains elevated. From June to September, the energy use is almost constant at an approximative value of 650 kWh/month. This is due mainly to the ventilation system and domestic hot water

preparation.

Table 3.6. Monthly repartition and distribution of energy use

Energy use	Month											
[kWh]	Jan	Feb	Mar	Apr	May	Jun	Jul	Aug	Sep	Oct	Nov	Dec
Heating	3,505	2,594	2,044	1,164	320	-	-	-	-	636	1,369	2,276
Ventilation	717	635	632	495	360	285	294	294	285	466	554	687
DHW	499	443	507	399	298	290	194	182	288	384	352	542
Lighting	136	111	102	88	72	65	67	80	97	126	143	143
Humidification	211	178	122	31	-	-	-	-	-	1	43	169
Cooling	-	-	-	-	-	29	100	45	6	-	-	-
Total	5,068	3,961	3,406	2,178	1,050	668	656	600	677	1,613	2,462	3,817

The annual distribution of energy consumption is detailed in Figure 3.15. The heating system represents the highest contribution to the energy consumption as it counts for 53.2% of the total value, followed by ventilation with 21.8%, domestic hot water with 16.7%, lighting with 4.7% and humidification with 2.9%. The contribution of cooling is insignificant compared to other components.
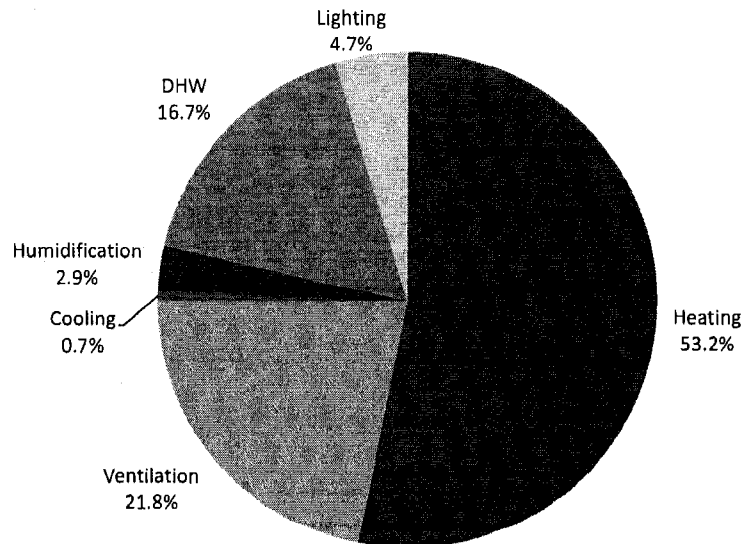
Figure 3.15. Annual distribution of energy use

As illustrated in Figure 3.16, the energy signature of the base case house is estimated by assuming a simple linear regression between the hourly heating energy consumption and the corresponding hourly outdoor dry-bulb temperature:

$$Q_{heating} = a + b \, T_{db} \qquad (3.4)$$

where:

$Q_{heating}$ = energy use for space heating [kWh];

a = y-intercept [kWh];

b = slope [kWh/°C]; and

T_{db} = dry-bulb temperature [°C].

Using data from TRNSYS, the model obtained gives a equal to -0.146 kWh and b equal to 2.467 kWh/°C, with a coefficient of determination R^2 of 0.743.
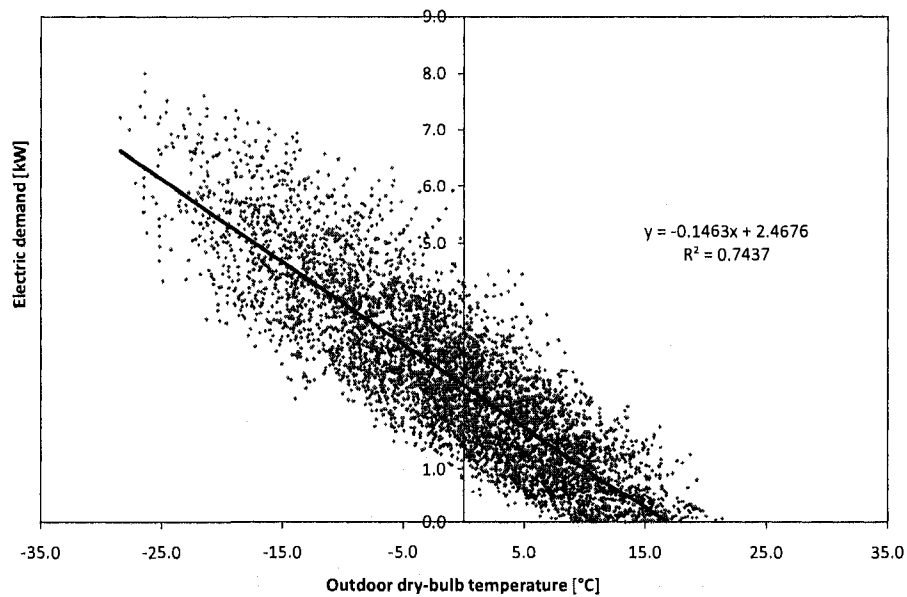
Figure 3.16. Energy signature of the base case house

In order to illustrate interior conditions in the base case house, Figures 3.17 and 3.18 show air temperature and relative humidity profiles coming from TRNSYS, for a period of three days in the beginning of February and July, respectively. In February, temperatures vary as expected between the two setpoint values of 19 and 21°C and the humidification system appears to operate a majority of time, fixing the relative humidity to the design value of 25%. On some occasions during the month of July, the temperature and the relative humidity on the basement are superior to values on the first floor. In a general way, temperatures range between 21 and 24°C, and the relative humidity between 40 to 60%.
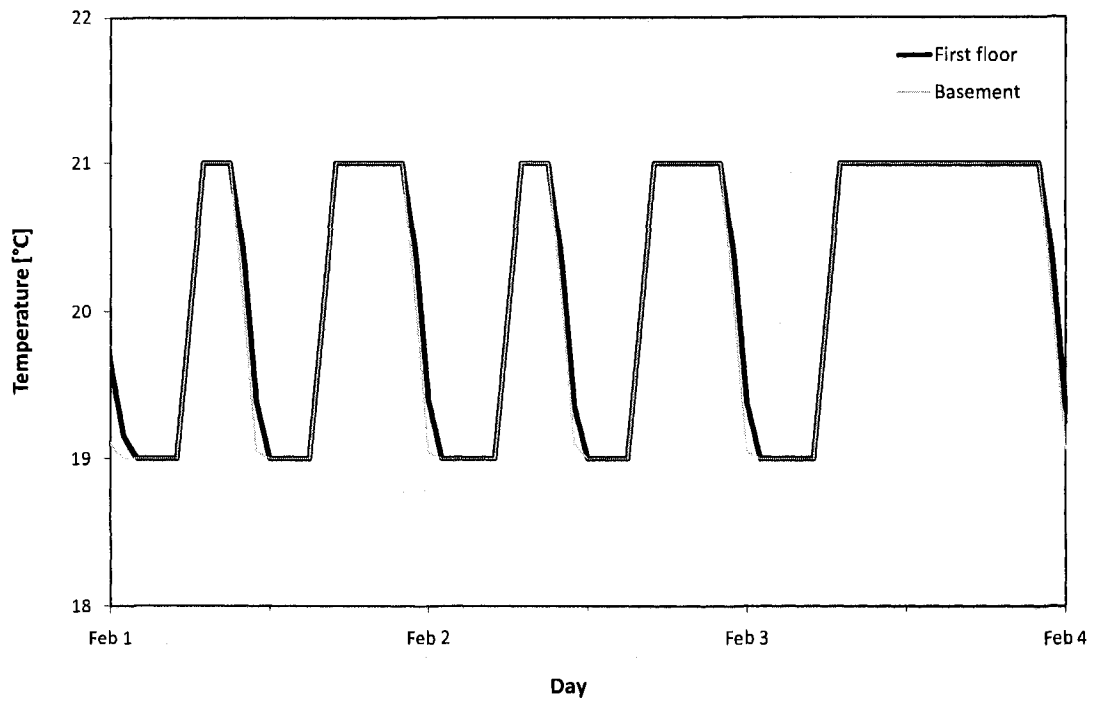
(a) Profiles of temperature
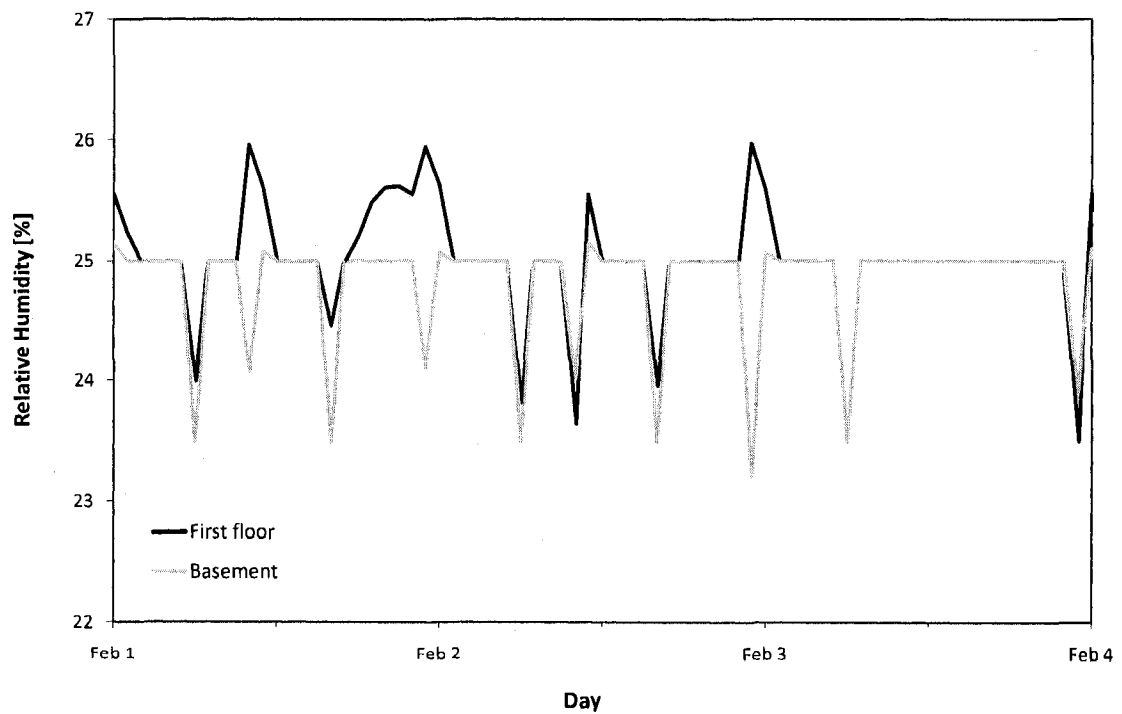
(b) Profiles of relative humidity

Figure 3.17. Representation of interior conditions in the base case house from February 1 to February 4
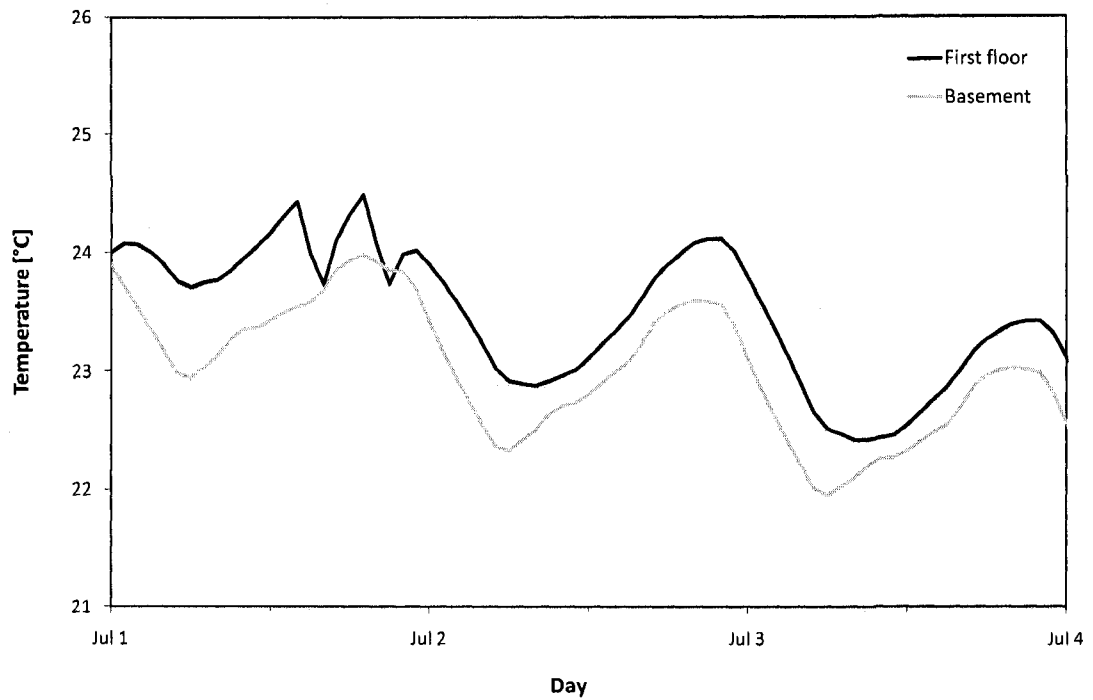
(a) Profiles of temperature
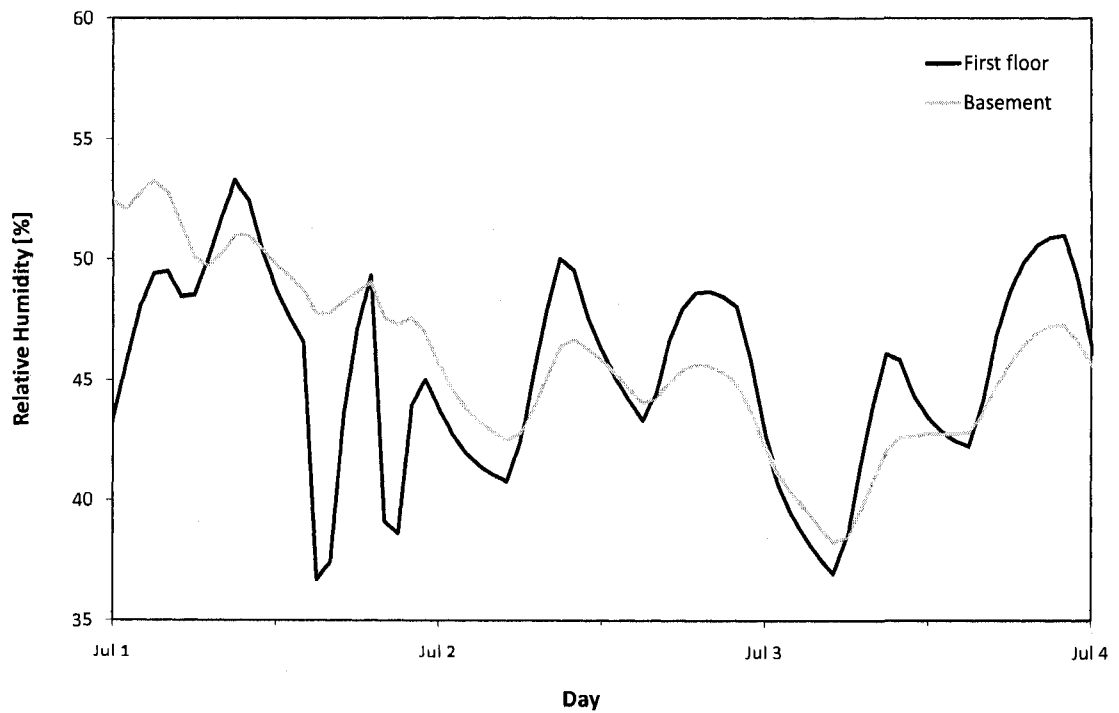
(b) Profiles of relative humidity

Figure 3.18. Representation of interior conditions in the base case house from July 1 to July 4

3.4 Life cycle analysis of the base case house

This section presents the life cycle analysis of the base case house in terms of the following indicators: life cycle energy use, life cycle emissions and life cycle cost.

3.4.1 Life cycle energy use

The life cycle energy use includes the total energy input over the entire life cycle of a building or its subsystems. Within the scope of this study, the embodied energy due to the manufacturing of the building materials in the pre-operating phase, and the total energy use in the operating phase are evaluated.

It is important to notice that: (i) the embodied energy of plumbing, heating, cooling and ventilation systems are not taken into account, and (ii) the estimation does not consider energy used for maintenance and demolition.

Embodied energy

The embodied primary energy, that represents direct and indirect energy use to extract raw materials, transport and fabrication of the final product, is estimated using the ATHENA's Environmental Impact Estimator software (ATHENA, 2003). This tool also operates the assessment of the building's GHG emissions, starting at its conception over its expected lifetime. Therefore, global warming potentials (GWPs), that constitutes a reference measure to compare the global warming effect of 1 kg of a given gas to the effect of 1 kg of CO_2 over a 100-year life span (IPCC, 2007), are computed.

The information from drawings and specifications is used to define the constituting assemblies and materials. These input data are then linked by ATHENA to the life cycle

inventory database for calculation. The building is located at Montreal (Quebec) and its life expectancy is assumed at 30 years.

The total embodied energy of the base case house is assessed at 566,907 MJ, corresponding to 2,697 MJ/m^2 of total floor area, and is equivalent to approximately five years of annual operating energy consumption. For comparison purpose, the results of previous studies are cited: Haines et al. (2007) estimated the embodied energy of a single-family dwelling, complying with the Ontario Provincial Building Code, to a value of 520,000 MJ or 2,600 MJ/m^2 of floor area, while Kassab (2002) found a value of 707,883 MJ or 2,286 MJ/m^2 of floor area for duplex-apartment house built in 2000 at Montreal, and finally, Baouendi (2003) estimated the embodied energy of a one-story detached house at 330,316 MJ or 1,278 MJ/m^2 of heated floor area. Major differences are observed with the last study but, generally speaking, a comparison is not easy since the buildings may have different dimensions, structural configuration of the exterior envelope constructions and locations.

The embodied energy per envelope component is shown in Table 3.8. The exterior and foundation walls presents the highest embodied energy (1574 MJ/m^2 of wall area), followed by floors and roofs (637 MJ/m^2), foundations (355 MJ/m^2), and doors and windows (239 MJ/m^2). The average weighted embodied energy is assessed at 836 MJ/m^2.

Table 3.8. Distribution of embodied energy per envelope component

Building component	Embodied energy		
	[MJ]	[MJ/m^2]	[%]
Foundations[1]	37,315	355	7
Walls[2]	294,741	1,574	52
Floors & Roofs	228,403	637	40
Doors & Windows	6,448	239	1
Total	566,907	836	100

[1] Represent the slab on grade.

[2] Represent below and above-ground walls.

Operating primary energy

The total operating primary energy is calculated using the electricity mix of Quebec, which considers the contribution of different energy sources, and the efficiency of the electricity generation in power plants from different energy sources (Table 3.9). Since hourly data are not available, annual average values are used. Transmission and distribution losses are assumed to be 6% (Zmeureanu and Wu, 2007). The overall power plant efficiency η_{pp} is then calculated at 73.1%.

Table 3.9. Annual average electricity mix in Quebec and power plants energy efficiencies. From Zmeureanu and Wu (2007).

Energy source	Contribution [%]	Power plant efficiency [%]
hydro-electricity	95.4	80.0
nuclear	2.0	30.0
natural gas	0.1	43.1
light fuel oil & diesel	0.1	32.8
heavy fuel oil	2.0	32.8
wood & other	0.3	43.4[1]

[1] From Statistics Canada (2005).

Assuming that the operating energy use remains constant over the 30-year life span of the system, regardless of the efficiency decrease of the mechanical systems or equipments, the total operating energy consumption is thus equal to 30 times the annual operating energy

use. Its value is estimated at 3,864 GJ, corresponding to 18,382 MJ/m^2 of floor area. The total life cycle energy use of the base case house, calculated as the sum of its embodied energy and the operating energy use over 30 years, is equal to 4,431 GJ.

3.4.2 Life cycle emissions

Embodied emissions

The embodied emissions of the base case house are evaluated at 29.75 tons CO_2 eq. by the software ATHENA. The distribution per envelope component is shown in Table 3.10. The exterior and foundation walls presents the highest embodied energy (73 kg CO_2 eq./m^2 of wall area), followed by doors and windows (38 kg CO_2 eq./m^2), foundations (35 kg CO_2 eq./m^2), and floors and roofs (32 kg CO_2 eq./m^2). The average weighted embodied energy is assessed at 44 kg CO_2 eq./m^2.

Table 3.10. Distribution of embodied emissions per envelope component

Building component	Embodied emissions		
	[kg CO_2 eq.]	[kg CO_2 eq./m^2]	[%]
Foundations[1]	3,674	35	12
Walls[2]	13,600	73	46
Floors & Roofs	11,442	32	38
Doors & Windows	1,031	38	3
Total	29,747	44	100

[1] Represent the slab on grade.

[2] Represent below and above-ground walls.

Operating emissions

The emissions of pollutants due to the house operation are investigated by considering the contribution of each energy source to the off-site production of electricity (Table 3.9) as well as the transmission and distribution losses. Therefore, the greenhouse gases emissions due

to electricity generation in power plant are estimated using the equivalent CO_2 emissions data presented by Gagnon et al. (2002). The following expression is calculated:

$$CO_{2,pp} = \frac{\alpha_1 E_{hydro} + \alpha_2 E_{gas} + \alpha_3 E_{oil} + \alpha_4 E_{coal} + \alpha_5 E_{nuclear}}{1000} \qquad (3.5)$$

where:

- $CO_{2,pp}$ is the equivalent CO_2 emissions at the generating power plant level [kg CO_2 eq.];

- E_{hydro}, E_{gas}, E_{oil}, E_{coal}, $E_{nuclear}$, correspond to the annual primary energy generated by hydro, natural gas, heavy oil, coal, and nuclear power plant respectively [kWh/yr];

- α_{1-5} are the equivalent CO_2 emissions due to the generation of electricity in power plants [kt CO_2/TWh];

- $\alpha_1 = 15$ kt CO_2/TWh, for hydro power plant with reservoir;

- $\alpha_2 = 443$ kt CO_2/TWh, for natural gas (+ 2000 km delivery) power plant;

- $\alpha_3 = 778$ kt CO_2/TWh, for heavy oil power plant;

- $\alpha_4 = 1050$ kt CO_2/TWh, for modern coal (2% S) power plant with SO_2 scrubbing;

- $\alpha_5 = 15$ kt CO_2/TWh, for nuclear power plant.

Consequently, for the base case house, the annual operating emissions are estimated at 1,875 kg CO_2 eq. annually and at 56.24 tons CO_2 eq. over the 30-years building's lifetime.

The life cycle emissions are equal to 85.98 tons CO_2 eq. The embodied emissions represent 35% of the life cycle emissions while the embodied energy represents only 13% of the total life cycle energy use. This can be explained by the fact that the energy used to manufacture

materials and transport produce more emissions per unit of energy than the energy used for the house operation, due to the low impact on the environment of hydro power plants in Quebec.

3.4.3   Life cycle cost

Construction phase

The initial cost of the base house is estimated using Residential Cost Data from RSMeans (2007), including the total cost of building materials, labor, contractor profit and overhead cost. Seven categories are identified including: site work, foundation, framing, exterior walls, windows and doors, roofing and interior partitions. Costs are taken from the assemblies and materials tables listed in the database. Then, total costs are multiplied by a city factor to account for the impact of the local market (1.21 for Montreal) and divided by a factor of 1.01 to assume the present exchange rate from US dollars to Canadian dollars. The construction cost of the base case house is finally evaluated at 204,576 $ or 973 $/m^2 of floor area.

Operating phase

Typically, operating costs include energy and maintenance costs during the life span of the building, along with demolishing costs at the end of the building life. However, for this study, only the cost of the energy use is considered. The annual energy use is supposed to remain constant during the lifetime of the building.

The heating cost is calculated with respect to the electricity rates of Hydro-Quebec (2008) as follows:

- 0.4064 $ as a fixed charge per day; plus

— 0.0540 \$ per kWh for first 30 kWh per day; plus

— 0.0733 \$ per kWh for the remaining consumption.

The Present Worth method (PW), which converts any present and future expenses to the same basis on today's dollars, is applied to evaluate the present value of money for the total operating energy cost over the life cycle of the building. The following equation (ASHRAE, 2007) is used:

$$PW_N = \frac{C\left(1 + j_E\right)^{N-1}}{\left(1 - i'\right)^{N}} \tag{3.6}$$

where:

PW_N =   present worth of operating energy cost at the end of the year N [\$];

C =   operating energy cost during the first year [\$];

j_E =   inflation rate of electricity [-];

i' =   effective interest rate [-]; and

N =   number of years [-].

The effective interest rate i' is calculated as:

$$i' = \frac{i - j}{1 + j} \tag{3.7}$$

where:

i =   discount rate (including inflation) [-]; and

j =   inflation rate [-].

Finally, the Present Worth over N years is:

$$PW = \sum_{N=1}^{N} PW_N \qquad (3.8)$$

The price of electricity is assumed to increase by 2% each year. Average values of the discount rate and the interest rate from 1998 to 2008 are used (Statistics Canada, 2008). So, $i = 5.54\%$, $j = 2.24\%$ and the resulting value of i' is 3.22%. Based on TRNSYS simulation results, the annual operating cost is equal to 1,878 \$ (9 \$/m^2) and the PW over the life cycle period of 30 years is calculated at 46,193 \$ (220 \$/m^2).

3.4.4 Summary of the results

The results obtained from previous sections are summarized in Table 3.13.

Table 3.13. Life cycle profile of the base case house

		Construction phase	Operating phase	Life cycle
Life cycle energy use	[GJ]	567	3,864	4,431
	[%]	13	87	100
Life cycle emissions	[tons CO$_2$ eq.]	29.75	56.24	85.98
	[%]	35	65	100
Life cycle cost	[\$]	204,576	46,193	250,769
	[%]	82	18	100

3.5 Life cycle analysis of design alternatives

In this section, several design alternatives are proposed in order to quantify their potential effect on a life cycle perspective. The thermal resistance of the exterior envelope of the base case house is improved to different levels of insulation. In addition, modifications on window-to-wall ratios (WWR) and infiltration rates are investigated.

66

3.5.1 Improvement of the thermal resistance of the building envelope

Choice of insulation materials

In order to facilitate the selection of design alternatives, a comparison between common insulation materials presenting the same thermal resistance of 3 $(m^2 \cdot {}^\circ C)/W$ in terms of embodied energy, embodied emissions and costs, is illustrated in Table 3.14. Results are taken from ATHENA (2003) and RSMeans (2007).

Table 3.14. Comparison between typical insulation materials

Insulation material	Embodied energy [MJ/m^2]	Embodied emissions [kg CO_2 eq./m^2]	Cost [\$/m^2]
Fiberglass batt (108 mm)	83.25	3.93	6.07
EPS (105 mm)	180.33	7.88	23.36
XPS (87 mm)	297.52	13.05	30.77
Blown cellulose (128 mm)	9.79	0.40	8.70
PIR (78 mm)	1.56	2.81	29.10

The PIR (polyisocyanurate) has the lowest embodied energy with 1.56 MJ/m^2, in opposition with the XPS (extruded polystyrene) with 297.52 MJ/m^2, while the blown cellulose has almost zero embodied emissions, compared with 3.93 kg CO_2 eq./m^2 for the fiberglass batt.

Table 3.14 emphasizes very well the fact that building designers need to be cautious with their choice of insulation materials since the overall performance, and not only the thermal resistance or cost, has to be considered in a sustainable approach.

Presentation of selected design alternatives

The first two design alternatives are elaborated to comply with the minimum insulation levels according to the Quebec Energy Code (Province of Quebec, 1992) and the Model National Energy Code of Canada for Houses (MNECCH, 1997).

Since the windows area of the base case house is quite low, a third alternative presenting similar insulation materials than the second one, but that with larger windows on the south facade, is suggested. Therefore, the window-to-wall ratio, which is the proportion of window area compared to the total wall area where the window is located (DOE, 2008), is increased from a value of 0.09 to 0.20 on the south facade to maximize solar heat gains. This alternative is named MNECCH+.

One last alternative, called "best case", is proposed in order to meet higher insulation levels with an particular emphasis aimed at "sustainable" insulation materials. Therefore, based on the analysis of Table 3.14, blown cellulose and polyisiocyanurate are preferred. All windows are upgraded using the best double-glazed window available in TRNSYS library, corresponding to a U-value of 1.26 $W/(m^2 \cdot {}^\circ C)$. The WWR is kept at a value of 0.20 for the south facade, similarly to the MNECCH+ alternative. The air infiltration rate is reduced at 1.5 ach_{50}, as recommended by the R-2000 program (NRCan, 2005). To achieve this objective, sprayed applied PIR is assumed to fill the gaps around windows and doors, at the junction of the main floor framing and the foundation, at tops of exterior and partition walls.

Table 3.15 reviews the thermal resistance and U-value of each component of the building envelope for all the studied design alternatives. The resulting overall thermal resistance (weighted average) is presented.

The thermal resistance of each component of the envelope is calculated using different insulation materials. Table 3.16 summarizes insulation materials and related thickness used for each component and design alternative. Proposed design alternatives are established with the perspective to comply with the minimum resistance required by the code. It

Table 3.15. Summary of building envelope's thermal characteristics for each design alternatives

Building component	Design alternative				
	Base case	Quebec	MNECCH	MNECCH+	"Best case"
Airtightness [ach$_{50}$]	3.5	3.5	3.5	3.5	1.5
WWR (south facade)	0.09	0.09	0.09	0.20	0.20
	Thermal resistance [(m$^2 \cdot$°C)/W]				
Ceiling/roof	6.08	6.08 (5.3)	7.61 (7.0)	7.61 (7.0)	7.61
Exterior walls	4.11	4.11 (3.4)	4.11 (4.1)	4.11 (4.1)	6.49
Foundation walls	1.09	2.87 (2.2)	3.56 (3.1)	3.56 (3.1)	4.74
Basement floor	0.99	1.36 (1.2)	1.36 (1.1)	1.36 (1.1)	2.82
Exterior doors	0.47	0.47	0.47	0.47	0.47
Garage door	1.89	1.89	1.89	1.89	1.89
	U-value [W/(m$^2 \cdot$°C)]				
Windows	1.40	1.40	1.40	1.40	1.26
Overall thermal resistance	**3.37**	**3.61**	**4.05**	**4.01**	**5.29**

Note: The number between the parentheses represents the minimum thermal resistance required by the code associated with the design alternative.

is important to notice that these propositions are not limited since many other design

alternatives can be chosen.

Table 3.16. Insulation materials used in design alternatives

Alternative	Ceiling/roof	Exterior wall	Foundation wall	Slab on grade
Base case	203 mm batt	89 mm batt +25.4 mm XPS	25.4 mm EPS	25 mm EPS
Quebec	203 mm batt	89 mm batt +25.4 mm XPS	25.4 mm EPS +63.5 mm batt	38 mm EPS
MNECCH	305 mm CEL	89 mm batt +25.4 mm XPS	25.4 mm EPS +89 mm batt	38 mm EPS
MNECCH (WWR+)	305 mm CEL	89 mm batt +25.4 mm XPS	25.4 mm EPS +89 mm batt	38 mm EPS
"Best case"	305 mm CEL	89 mm SPIR +50.8 mm PIR	25.4 mm EPS +89 mm SPIR	89 mm EPS

Notes: CEL represents the blown cellulose and SPIR the spray applied polyisiocyanurate (PIR).

Using the computer programs TRNSYS, ATHENA and the RSMeans database, the life cycle energy use, emissions and cost are estimated for each design alternative. A summary of results is shown in Table 3.17 as well as savings compared with the base case house.

Table 3.17. Summary of performance of proposed design alternatives

Design alternative	Life cycle energy use [GJ]			Life cycle emissions [tons CO$_2$ eq.]			Life cycle cost [$]		
	Embodied	Operating	Life cycle	Embodied	Operating	Life cycle	Initial	Operating	Life cycle
Base case	567	129	4,431	29.75	1.87	85.98	204,576	1,878	250,769
Quebec	571	119	4,132	29.92	1.73	81.75	208,173	1,727	250,644
	+0.7%	-8.5%	-7.2%	+0.6%	-8.5%	-5.2%	+1.7%	-8.8%	+0.0%
MNECCH	558	117	4,056	29.30	1.70	80.21	209,247	1,696	250,951
	-1.6%	-10.5%	-9.2%	-1.5%	-10.5%	-7.2%	+2.2%	-10.8%	+0.1%
MNECCH+	569	115	4,033	29.92	1.68	80.35	211,001	1,677	252,239
	+0.3%	-11.5%	-9.9%	+0.6%	-11.5%	-7.0%	+3.0%	-12.0%	+0.6%
"Best case"	546	93	3,327	28.84	1.35	69.33	212,569	1,334	245,390
	-3.9%	-38.9%	-33.2%	-3.1%	-38.9%	-24.0%	+3.8%	-40.7%	-2.2%

Note: Percentages represent the increase compared with the base case house.

Table 3.18. Reduction of embodied energy use, emissions of greenhouse gases and initial costs compared with the base case house

Design alternative	Overall thermal resistance [(m²·°C)/W]	Embodied energy increase [%]	Embodied emissions increase [%]	Initial cost increase [%]
Quebec	3.61	+0.7	+0.6	+1.7
MNECCH	4.05	-1.6	-1.5	+2.2
MNECCH+	4.01	+0.3	+0.6	+3.0
"Best case"	5.29	-3.9	-3.1	+3.8

As seen in Table 3.18, the improvement of the overall thermal resistance the base case is not directly associated with a reduction of embodied energy, emissions and initial cost, since the selection of insulation materials has a significant influence on the final results. The "best case" design alternative gives higher initial savings. Therefore, the initial use of Table 3.14 as a selection tool of materials for this design alternative seems appropriate.

Table 3.19. Reduction of annual energy use, emissions of greenhouse gases and operating costs compared with the base case house

Design alternative	Overall thermal resistance [(m²·°C)/W]	Annual energy increase [%]	Annual emissions increase [%]	Annual cost increase [%]
Quebec	3.61	-8.5	-8.5	-8.8
MNECCH	4.05	-10.5	-10.5	-10.8
MNECCH+	4.01	-11.5	-11.5	-12.0
"Best case"	5.29	-38.9	-38.9	-40.7

The annual energy use, emissions of greenhouse gases and operating costs are all reduced by the proposed design alternatives (Table 3.19). Reductions are quite similar but those for yearly operating cost appears to be slightly higher. The MNCEEH+ design alternative gives more savings that the MNECCH alternative, despite a lower overall thermal resistance, underlining the importance to consider solar heat gains. Yet, the "best case" alternative is definitively the most efficient choice since it gives the higher savings in terms of annual energy consumption, emissions and cost.

Table 3.20. Reduction of life cycle energy use, emissions, and cost for the different design alternatives compared with the base case house

Design alternative	Overall thermal resistance [(m²·°C)/W]	Life cycle energy [GJ]	Life cycle emissions [tons CO_2 eq.]	Life cycle cost [$]
Quebec	3.61	-7.2	-5.2	+0.0
MNECCH	4.05	-9.2	-7.2	+0.1
MNECCH+	4.01	-9.9	-7.0	+0.6
"Best case"	5.29	-33.2	-24.0	-2.2

The life cycle energy use and life cycle emissions are reduced for all the proposed design alternatives (Table 3.20). Life cycle costs for the "Best case" alternative are reduced by 2.2% while costs are similar in other cases. This can be seen as a direct consequence of the low rates of electricity in Quebec, compared to other Canadian provinces (BC Hydro, 2003). The most significant reductions are those for energy use, ranging from 7.2% to 33.2%. Higher insulation levels also gives emissions savings but the resulting effect is limited due to the influence of life cycle performance of some insulation materials. It is interesting to see that the MNECCH+ alternative offers roughly the same energy savings and emissions as the MNECCH alternative, despite a higher cost. The "best case" alternative is definitively the most efficient solution as it gives the higher savings in terms of energy, emissions and cost on a life cycle perspective.

Chapter 4

Modelling of a seasonal thermal storage

In this chapter, the modelling of a solar combisystem with a long-term thermal storage capacity, associated with a hydronic radiant heating floor, is presented. The TRNSYS environment is used for this purpose. The "best case" alternative (see Chapter 3) is chosen as the starting point in the development of the model. A sensitivity analysis, based on a certain set of design parameters, is achieved to evaluate the repercussions of those parameters on the overall performance of the system.

4.1 General description of the system

The long term thermal storage system is designed to supply hot water for space heating and domestic hot water for one year using only the solar energy, that is without the need of an auxiliary heating element (Figure 4.1).
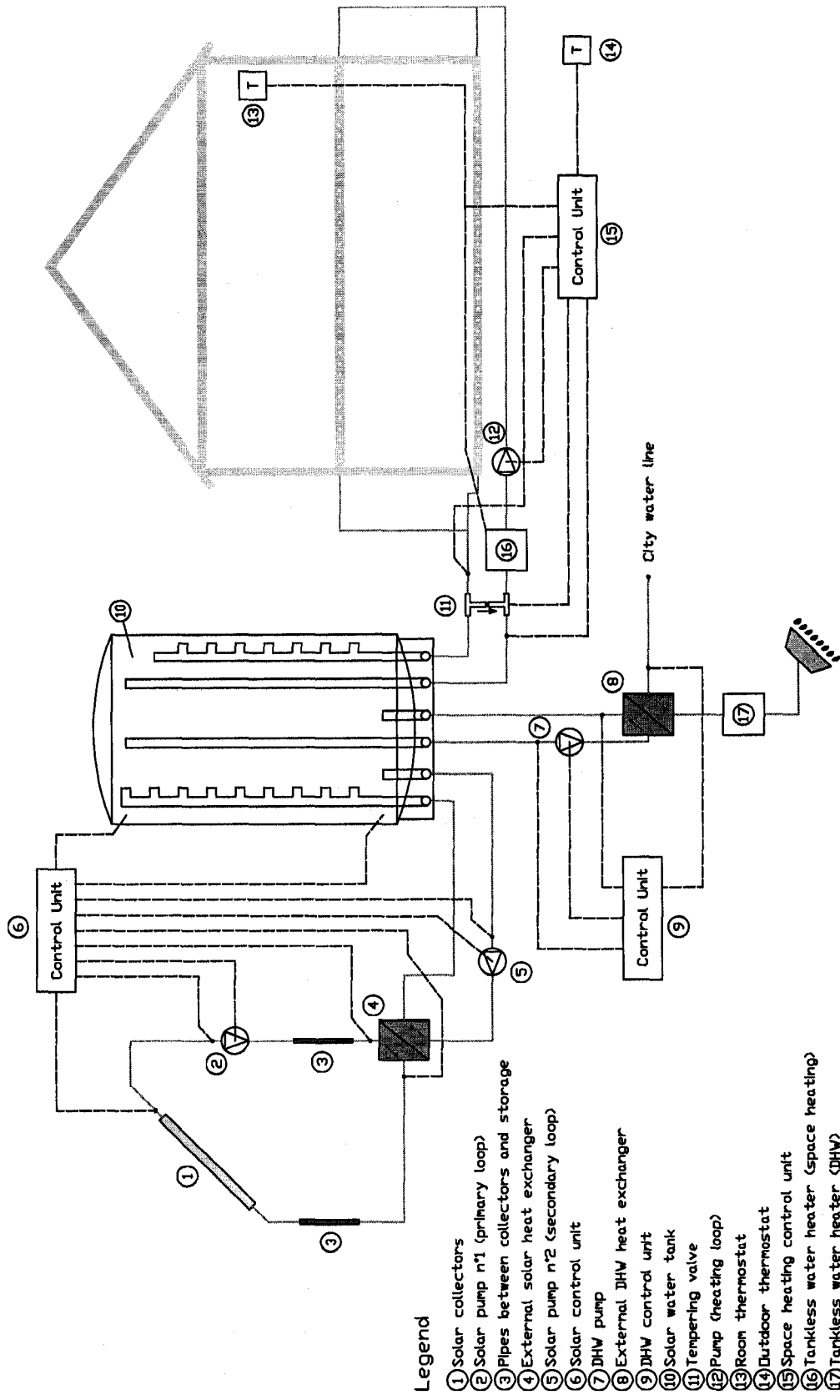
Figure 4.1. Modelling of the system

Legend

1. Solar collectors
2. Solar pump n°1 (primary loop)
3. Pipes between collectors and storage
4. External solar heat exchanger
5. Solar pump n°2 (secondary loop)
6. Solar control unit
7. DHW pump
8. External DHW heat exchanger
9. DHW control unit
10. Solar water tank
11. Tempering valve
12. Pump (heating loop)
13. Room thermostat
14. Outdoor thermostat
15. Space heating control unit
16. Tankless water heater (space heating)
17. Tankless water heater (DHW)

The combisystem consists of evacuated tube solar collectors (point 1 in Figure 4.1) placed on the roof of the house, the heat transfer loop and a pump (point 2) that includes the antifreeze fluid, and the external heat exchanger (point 4) that transfers the heat collected from the primary loop into a secondary loop where circulates the water. Hot water from the secondary loop, circulated by a pump (point 5), enters a large cylindrical water storage tank (point 10). A stratifier device improves the stratification by avoiding the mixing of layers of different temperature inside the tank. Hot water is supplied to radiant heating floors of the house by a variable speed pump (point 12) controlled by a thermostat located on the first floor (point 13). An external heat exchanger (point 8) and a variable speed pump (point 7) enable the control of domestic hot water at around 45°C at the user-end.

4.2 Heat management approach

4.2.1 Solar loop

Solar energy is captured by evacuated tube collectors since their use is recommended in cold climates (RETScreen, 2007). The variable flow rate pump (point 5) circulates the hot water on the secondary loop from the external solar heat exchanger (point 4) to the tank, at a maximum temperature of 95°C. Both pumps (points 2 and 5) start only when the inlet temperature of the heat exchanger, on the primary loop, is higher than the water temperature at the bottom of the tank.

4.2.2 Space heating

The space heating is provided by a hydronic radiant floor heating system as it represents typically a better choice for low energy buildings (Keller, 1998), it brings higher exergy

efficiency (Zmeureanu and Wu, 2007) and increases thermal comfort (ASHRAE, 2004). Cross-linked polyethylene (PEX) (Liu et al., 2000) flexible piping is integrated in the radiant floor to circulate the hot water. The garage floor is not heated.

A constant setpoint temperature control is applied on the operative temperature which is a better indicator of the thermal comfort for radiant systems than the air temperature, while improving the energy performance (Van der Veken et al., 2005). Therefore, a proportional-integral-derivative (PID) controller modifies the flow rate of the hot water circulating pump (point 12) to maintain the operative temperature on the first floor at the fixed setpoint of 20°C. In addition, a thermostat (point 14), located outside of the house, adjusts the water temperature as a function of outdoor temperature.

4.2.3 Domestic hot water

The cold water from the water city line enters the external DHW heat exchanger (point 8), and leaves at about 45°C (Aguilar et al., 2005) at the user-end by controlling the pump (point 7) water flow rate.

4.2.4 Auxiliary heating

Two electric tankless water heaters (points 16 and 17) are used to ensure a correct water temperature for space heating and domestic hot water. Such external devices are preferred to electric heating elements submerged in the storage tank as they heat water only when it is needed, which avoids standby heat loss through the tank and water pipes (NRCan, 2008).

4.3 Description of TRNSYS components used for modelling

The system is modelled by using the TRNSYS environment. Table 4.1 presents the additional components required for the simulation comparatively to the previous chapter (Table 3.1).

Table 4.1. List of TRNSYS types used for modelling the seasonal storage system

Type	Description	Name
2	ON/OFF Differential Controller	In-OutQ, TmaxTank, TmaxPump, AuxHeaton
5	Cross Flow Heat Exchanger	Solar HX, DHW HX
9	Data Reader For Generic Data Files	DHW data, Loads data
11b	Tempering valve	Type11b
11h	Tee piece	Type11h
23	PID controller	Type 23
24	Quantity Integrator	Simulation integration
534	Cylindrical Storage Tank	Type 534
538	Evacuated tube solar collector	Type 538, 538-2, 538-3
647	Fluid Diverting Valve	Type 647, Type 647-2
649	Mixing valve for fluids	Type 649, Type 649-2
656	Variable Speed Pump	Solar pump 1, Solar pump 2, DHW pump, Heating pump
659	Auxiliary Heater with Proportional Control	Type659, Type 659-2
709	Circular, Fluid-Filled Pipe	Type 709, Type 709-2

The following sections present a detailed description of the components used in TRNSYS to model the solar loop, the space heating system and the domestic hot water.

4.3.1 Solar loop

Type 538: Solar collectors

The Type 538 developed by TESS (2007) is used to simulate the evacuated tube solar collectors. An array of identical elements is mounted on the south side of the roof (azimuth = 0°, tilt angle = 45°). Figure 4.2 shows three rows of collectors, connected in parallel. Type 647-2 divides the total flow rate among the different solar collectors, and Type 649-2 collects the outlet flow rates. Solar radiation is given by Type 16g, while Type 33e gives the outside temperature required to calculate collectors efficiency as explained in the following sections.
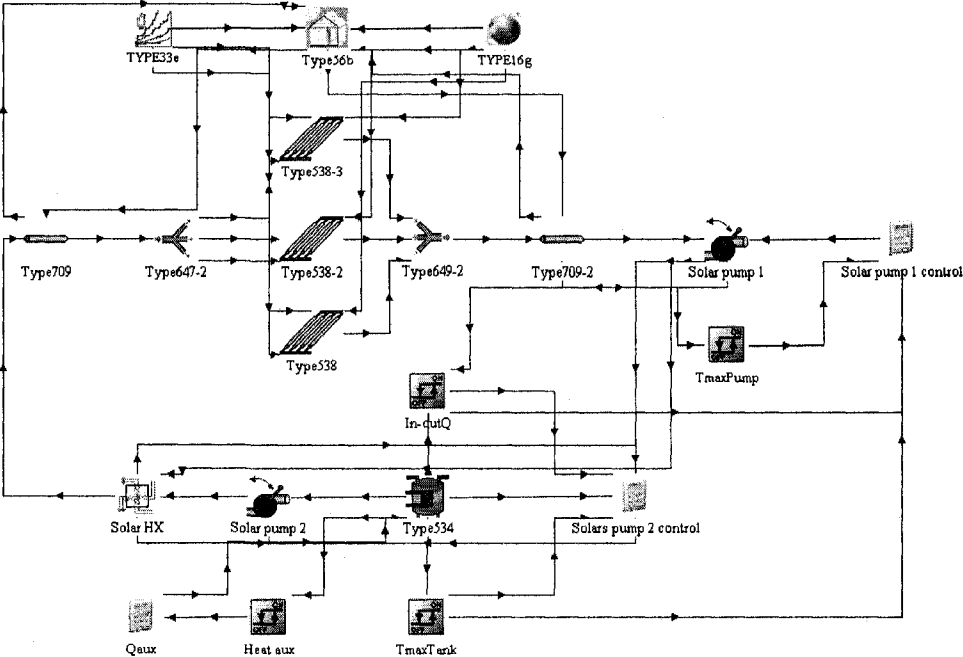
Figure 4.2. TRNSYS components used to model the solar loop

The solar collector model Vitosol 300 SP3 with 30 evacuated tubes from Viessmann (2008) is chosen in this study (see technical specifications, Appendix C). Each tube contains a sealed copper pipe (heat pipe) that is attached to a black copper fin absorber plate (Figure 4.3).

79

As the sun shines on the black surface of the fin, alcohol within the heat tube is heated and hot vapour rises to the top of the pipe. A mix of antifreeze and distilled water flows through a manifold recovering the heat, while the alcohol condenses and flows back down into the tube by gravity.

Ⓐ Connecting chamber
Ⓑ Thermal insulation made from melamine epoxy foam
Ⓒ Flow pipe
Ⓓ Coaxial manifold and distributor pipe
Ⓔ Coaxial heat exchanger pipe
Ⓕ Absorber
Ⓖ Evacuated glass tube
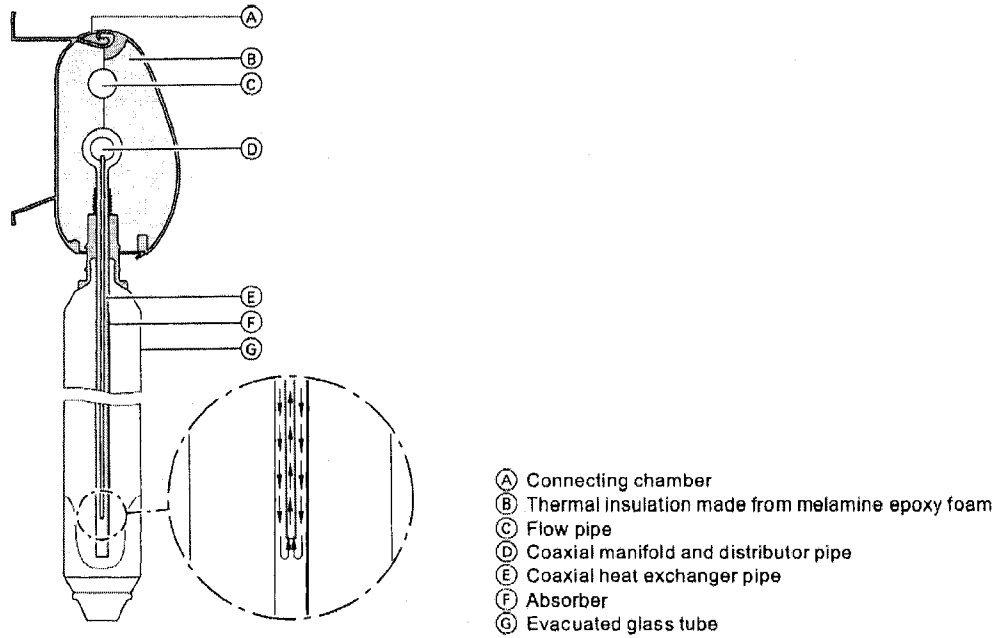
Figure 4.3. Evacuated tube collector based on the heat pipe principle. From Viessmann (2008).

The model computes the solar thermal efficiency of collectors by using the following correlation-based model (Duffie and Beckman, 2006):

$$\eta = a_0 K_\theta - a_1 \frac{(T_i - T_o)}{G_T} - a_2 \frac{(T_i - T_o)^2}{G_T} \qquad (4.1)$$

where:

η = collector efficiency [-];

a_0 = optical efficiency [-];

80

K_θ =   incidence angle modifier [-];

a_1 =   first-order coefficient in collector efficiency equation [W/(m$^2\cdot$K)];

a_2 =   second-order coefficient in collector efficiency equation [W/(m$^2\cdot$K^2)];

T_i =   inlet fluid temperature [°C];

T_o =   outdoor (air) temperature [°C]; and

G_T =   global solar radiation on the collector [W/m^2].

Parameters a_0, a_1 and a_2 are obtained by experimental testing of collectors in accredited laboratories (SRCC, 2008). Values are presented in Table 4.3.

Table 4.3. Solar collector technical data (SRCC, 2008)

Gross area		[m^2]	4.287
Net aperture area		[m^2]	3.760
Flow rate at test conditions		[kg/s]	0.059
Optical efficiency	a_0	[-]	0.5079
Heat loss coefficient	a_1	[W/(m$^2\cdot$K)]	0.9156
	a_2	[W/(m$^2\cdot$K^2)]	0.0030

Note: test fluid = propylene glycol & water

The incidence angle modifier K_θ in Equation 4.1 is a correction factor that accounts for changes in output performance of the solar collector as a function of the sun's incidence angle θ. As pointed out by Morrison et al. (2005), this may have a significant influence on the energy collected, particularly when rays of the sun hit the collector's surface with a high angle of incidence θ. Since evacuated tube collectors are not optically-symmetric, incidence angle modifiers are typically estimated for transversal and longitudinal directions.

The longitudinal incidence angle θ_l is measured in the longitudinal plane that is perpendicular to the absorber plane. The corresponding incidence angle modifier K_{θ_l} is referred as longitudinal. The transversal incidence angle θ_t is measured in the transversal plane that

is perpendicular to the collector absorber and the longitudinal plane. The corresponding incidence angle modifier K_{θ_t} is referred as transversal. As shown in Figure 4.4, the collector test report (SRCC, 2008) provides values of K_{θ_t} for different θ_t (at $\theta_l = 0$) and K_{θ_l} for different θ_l (at $\theta_t = 0$). These data are set in an input file. Then, the model approximates the incidence angle modifier K_θ for any θ_l and θ_l by multiplying $K_{\theta_l,0}$ and K_{0,θ_t}.
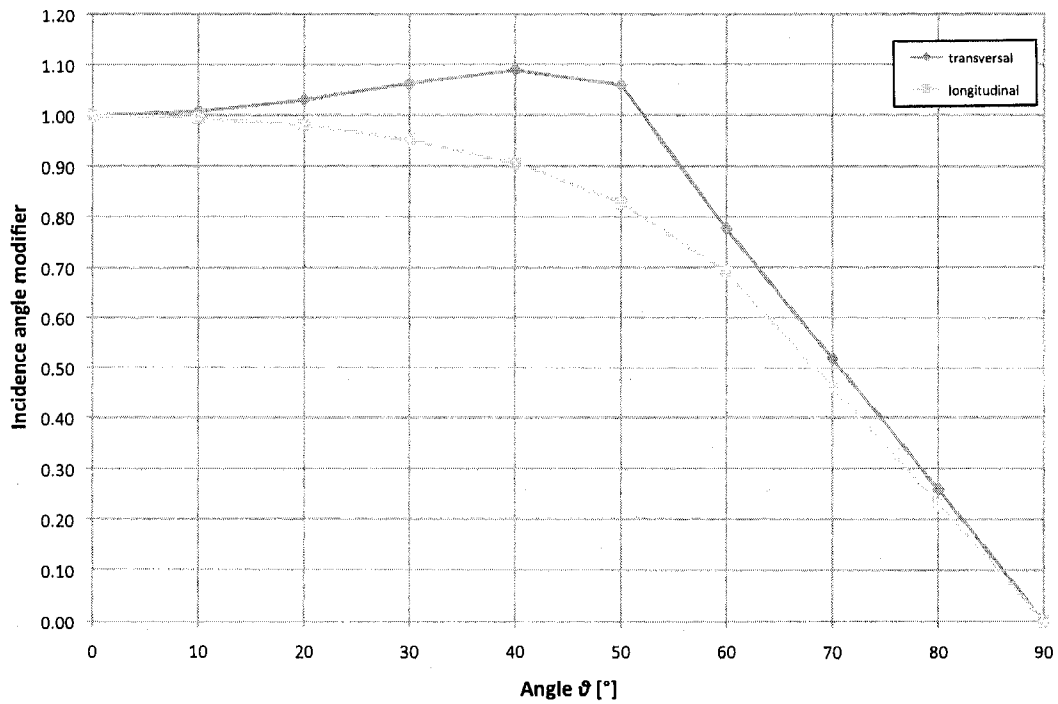
Figure 4.4. Incidence angle modifiers based on SRCC (2008) test results

As an example and in order to illustrate the performance of the collector, the solar collector thermal efficiency for three different weather conditions are calculated based on Equation 4.1, assuming K_θ equal to 1 (Figure 4.5). If the temperature difference $T_i - T_o = 50°C$, the collector efficiency is about 31% on a clear day and 9% on a cloudy day.
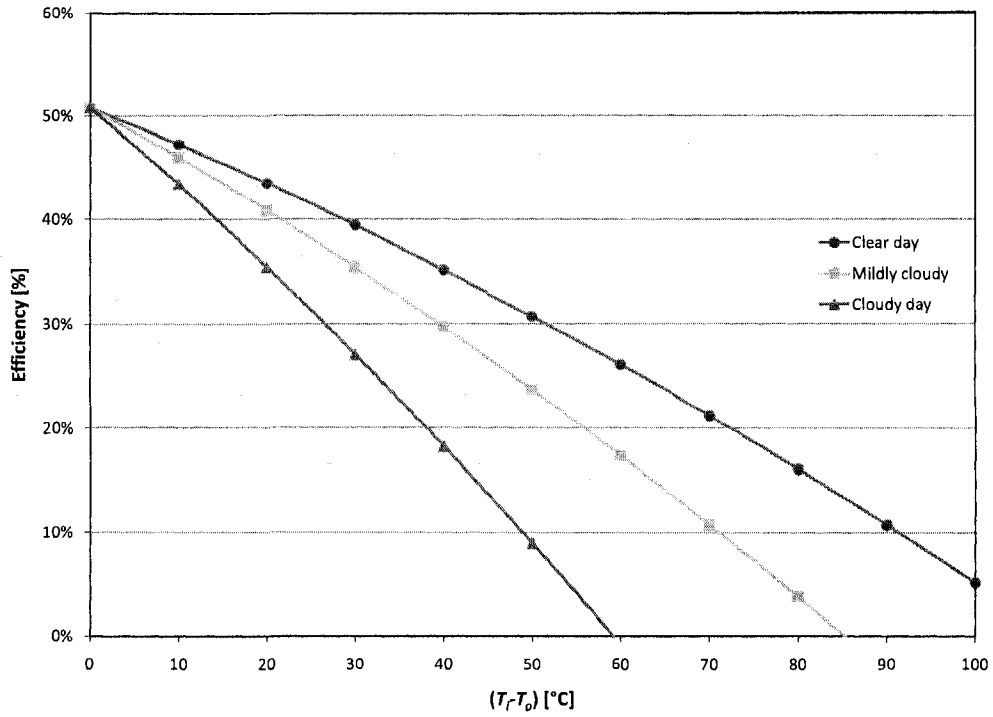
Figure 4.5. Solar collector efficiency

Type 538 requires additional informations to apply analytical corrections to the ideal efficiency curve to account for operating at flow rates other than values at test conditions and for the number of identical collectors mounted in series. Yet, these corrections required linear efficiency curves and Equation 4.1 is converted as:

$$\eta = \frac{Q_u}{A_c G_T} = F_R \left(\tau\alpha\right)_n K_\theta - F_R U_L' \frac{(T_i - T_o)}{G_T} \tag{4.2}$$

where:

Q_u = useful energy gain [W];

A_c = total collector array (gross) area [m^2];

G_T = global solar radiation on the collector [W/m^2];

F_R = overall collector heat removal efficiency factor [-];

$(\tau\alpha)_n$ = product of the cover transmittance and the absorber absorptance at normal incidence [-];

K_θ = incidence angle modifier [-];

U_L' = modified first-order collector efficiency [W/(m²·°C)];

T_i = inlet temperature of fluid to collector [°C]; and

T_o = outdoor (air) temperature [°C].

$F_R(\tau\alpha)_n$ and $F_R U_L'$ are equal to 0.5093 and 1.0948 W/(m²·°C), respectively (SRCC, 2008). To consider the effect of the operating flow rate to the efficiency, both values are multiplied by the correction factor r_1:

$$r_1 = \frac{\dfrac{\dot{m}_{use} C_p}{F' U_L} \left(1 - e^{\frac{-F' U_L}{\dot{m}_{use} C_p}}\right)}{\dfrac{\dot{m}_{test} C_p}{F' U_L} \left(1 - e^{\frac{-F' U_L}{\dot{m}_{test} C_p}}\right)} \tag{4.3}$$

where:

r_1 = correction factor [-];

$\dot{m}_{use}$ = mass flow rate at use conditions [kg/s];

C_p = specific heat of collector fluid [J/(kg·°C)];

F' = collector efficiency factor [-];

U_L = overall thermal loss coefficient per unit area [W/(m²·°C)]; and

$\dot{m}_{test}$ = mass flow rate at test conditions [kg/s];

The value of $F'U_L$ is calculated at test conditions:

$$F'U_L = -\frac{\dot{m}_{test}C_p}{A_c} \ln\left(1 - \frac{F_R U'_L A_c}{\dot{m}_{test}C_p}\right)$$ (4.4)

For instance, if the operating flow rate is 0.03 kg/s and the flow rate at test conditions is 0.059 kg/s (Table 4.3), the correction factor r_1 equals 0.994.

To consider the number of identical collectors mounted in series N_S, a second correction factor r_2 multiplies $F_R (\tau\alpha)_n$ and $F_R U'_L$:

$$r_2 = \frac{1 - \left(1 - \frac{A_c F_R U'_L}{\dot{m}_{use}C_p}\right)^{N_S}}{N_S \frac{A_c F_R U'_L}{\dot{m}_{use}C_p}}$$ (4.5)

For instance, if the operating flow rate is 0.03 kg/s and four collectors are mounted in series $(N_S = 4)$, then $r_2 = 0.965$.

Thermophysical properties of the fluid

The solar collector's manufacturer recommends the use of propylene glycol as antifreeze solution, with concentrations from 0 to 70% (Viessmann, 2008). Since the freezing temperature is a direct function of the concentration, it has to be selected carefully in order to avoid damages to the collectors during cold months.

The freezing temperature T_F, expressed in [K], is as a function of polypropylene glycol concentration ξ (M. CONDE Engineering, 2002):

$$\frac{T_F}{273.15} = 1 - 0.03736\xi - 0.40050\xi^2$$ (4.6)

The concentration of antifreeze is set at 50% (Cruickshank and Harrison, 2006). Based on Equation 4.6, this corresponds to a freezing temperature T_F of 240.7 K (-32.5°C) which is way below the outdoor design dry-bulb temperature for heating recommended by ASHRAE (2005) of 250.15 K (-23°C).

The thermophysical properties of the fluid are required in several TRNSYS components such as pumps, pipes, heat exchangers and solar collectors. However, these values can only be set as fixed parameters and not as input variables, which implies that an average operating temperature needs to be assumed.

The density, specific heat and thermal conductivity are calculated in terms of glycol's concentration ξ and the average operating temperature T. Each property is represented by P_x (M. CONDE Engineering, 2002), as follows:

$$P_x = A_1 + A_2\xi + A_3\frac{273.15}{T} + A_4\xi\frac{273.15}{T} + A_5\left(\frac{273.15}{T}\right)^2 \tag{4.7}$$

The computation of the dynamic viscosity μ is performed using a sightly different expression (M. CONDE Engineering, 2002), as follows:

$$\ln(\mu) = A_1 + A_2\xi + A_3\frac{273.15}{T} + A_4\xi\frac{273.15}{T} + A_5\left(\frac{273.15}{T}\right)^2 \tag{4.8}$$

The value of parameters A_1, A_2, A_3, A_4 and A_5 are presented in Appendix D. The resulting density, specific heat, thermal conductivity and dynamic viscosity are illustrated from Figures 4.6 to 4.9.
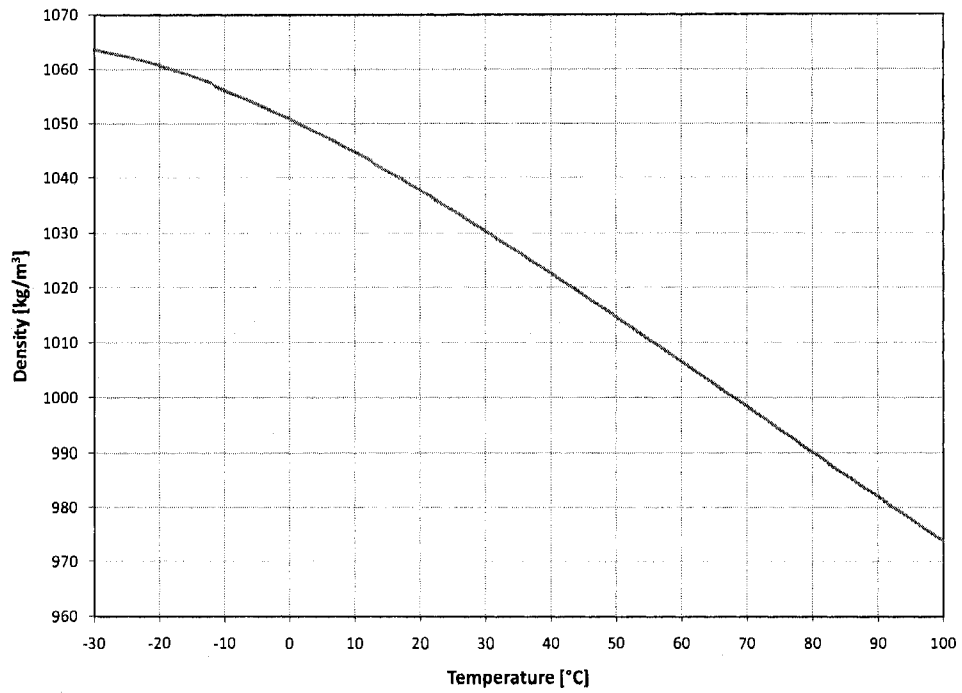
Figure 4.6. Variation of density of propylene glycol with temperature
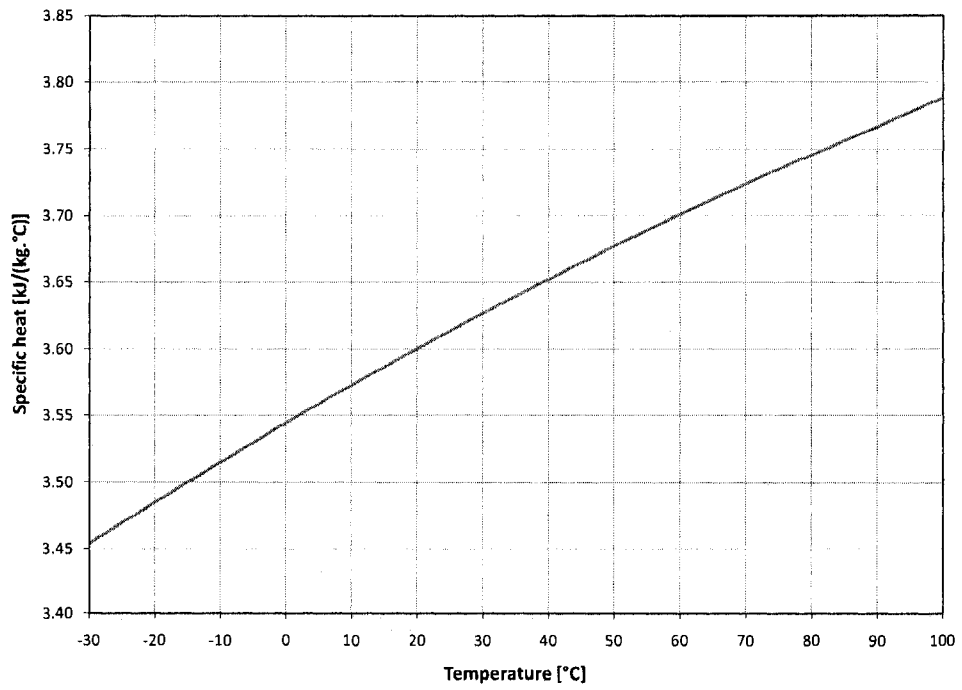
Figure 4.7. Variation of specific heat of propylene glycol with temperature

87
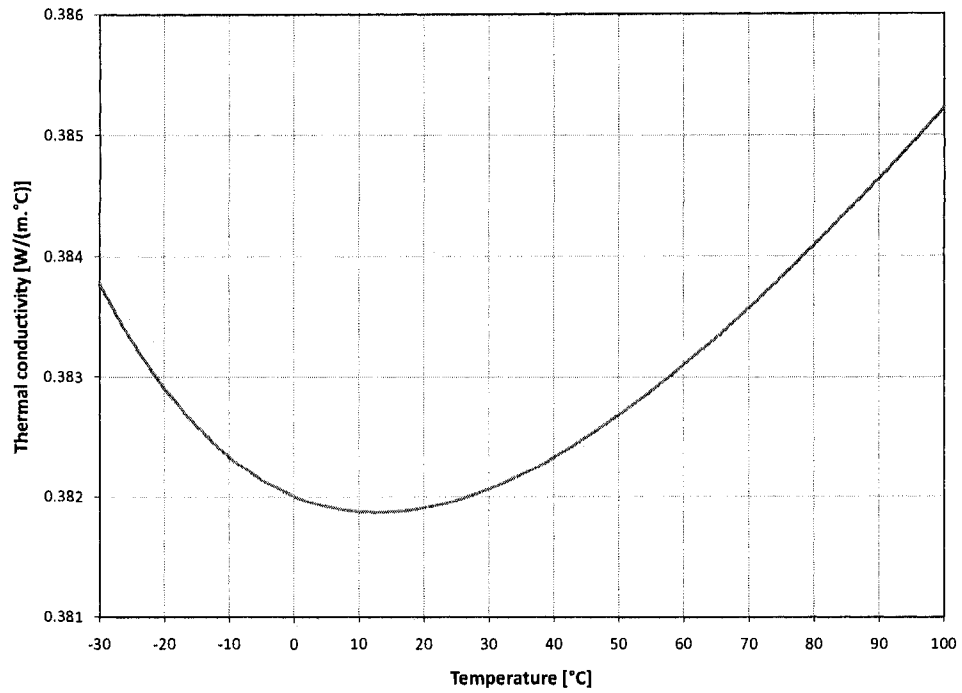
Figure 4.8. Variation of thermal conductivity of propylene glycol with temperature
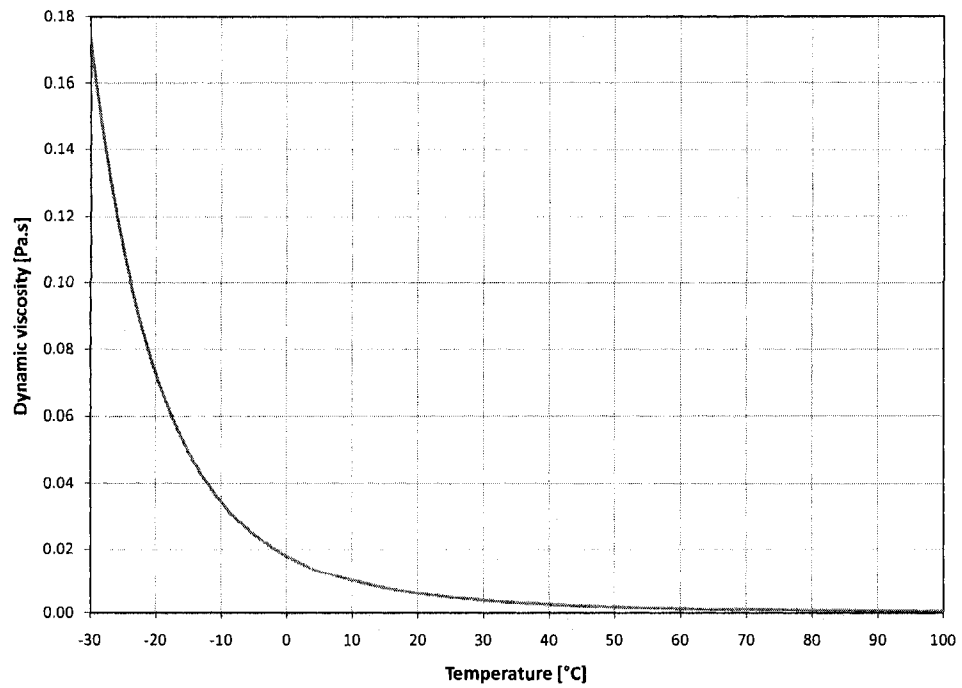
Figure 4.9. Variation of dynamic viscosity of propylene glycol with temperature

The density and specific heat curves vary almost linearly with the operating temperature (Figures 4.6 and 4.7). The dynamic viscosity and thermal conductivity, however, present a different trend (Figure 4.8 and Figure 4.9). The average operating temperature of the antifreeze is assumed at 80°C, which corresponds to the average temperature of the antifreeze in the collector as calculated by the computer model. The corresponding thermophysical properties used further in this study are shown in Table 4.6.

Table 4.6. Thermophysical properties of glycol used in the study

ρ [kg/m^3]	C_p [kJ/(kg·°C)]	λ [W/(m·°C)]	μ [Pa·s]	T_F [°C]
990	3.746	0.384	0.00087	-32.5

Piping between collectors and storage

Two Types 709, one for cold side and one for hot side, are used to model copper pipes between solar collectors and the water tank. Each pipe is divided in three segments to represent the transit of the fluid through the attic, first floor and basement. So, the indoor air temperature is set as input and the computed environment losses are established as another source of heat gains in these three zones (Figure 4.2). Pipes length is approximated at 10 m for the cold side and 10 m as well for the hot side. They are covered by a 40 mm thick insulation material able to resist to high temperature, with a thermal conductivity of 0.04 W/(m·°C).

In order to limit the hydraulic head, the flow velocity inside the copper pipes is between 0.4 m/s and 0.7 m/s (Viessmann, 2008). Therefore, the standard size is selected as a function of the design flow rate and according to data provided in Table 4.7.

Table 4.7. Recommended dimensions of pipes. From Viessmann (2008).

Standard size [mm]	12.7	15.9	19.1	25.4	31.8	38.1
Outside diameter [mm]	15.9	19.1	22.2	28.6	34.9	41.3
Inside diameter [mm]	13.4	16.6	18.9	25.3	31.6	37.6
Flow rate (total collector area) [l/h]	Velocity of flow rate [m/s]					
200	0.42	0.28	0.18	0.11	0.07	0.05
250	0.52	0.35	0.22	0.14	0.09	0.06
300	0.63	0.41	0.27	0.17	0.10	0.07
350	0.73	0.48	0.31	0.20	0.12	0.08
400	0.84	0.55	0.35	0.23	0.14	0.09
450	0.94	0.62	0.40	0.25	0.16	0.10
500	1.04	0.69	0.44	0.28	0.17	0.12
600	1.25	0.83	0.53	0.34	0.21	0.14
700	1.46	0.97	0.62	0.40	0.24	0.16
800	1.67	1.11	0.71	0.45	0.28	0.19
900	1.88	1.24	0.80	0.51	0.31	0.21
1000	2.09	1.38	0.88	0.57	0.35	0.23
1500	3.14	2.07	1.33	0.85	0.52	0.35
2000	4.19	4.14	1.77	1.13	0.69	0.47
2500	5.23	4.84	2.21	1.41	0.86	0.58
3000	6.28	3.09	2.65	1.70	1.04	0.70

Type 534: Storage tank

The vertical cylindrical storage tank, installed on the basement floor, is developed using Type 534 since it has the ability to model stratifiers (TESS, 2007). The tank diameter is calculated based on its volume and its total height, which is assumed at 5.2 m, corresponding to the cumulative height of the basement and the first floor.

The tank is divided into ten horizontal isothermal layers of equal volume (Figure 4.10) to consider the stratification effect. A previous study (Braun et al., 1981) showed that ten layers are sufficient to model accurately the stratification of a seasonal storage tank.

90
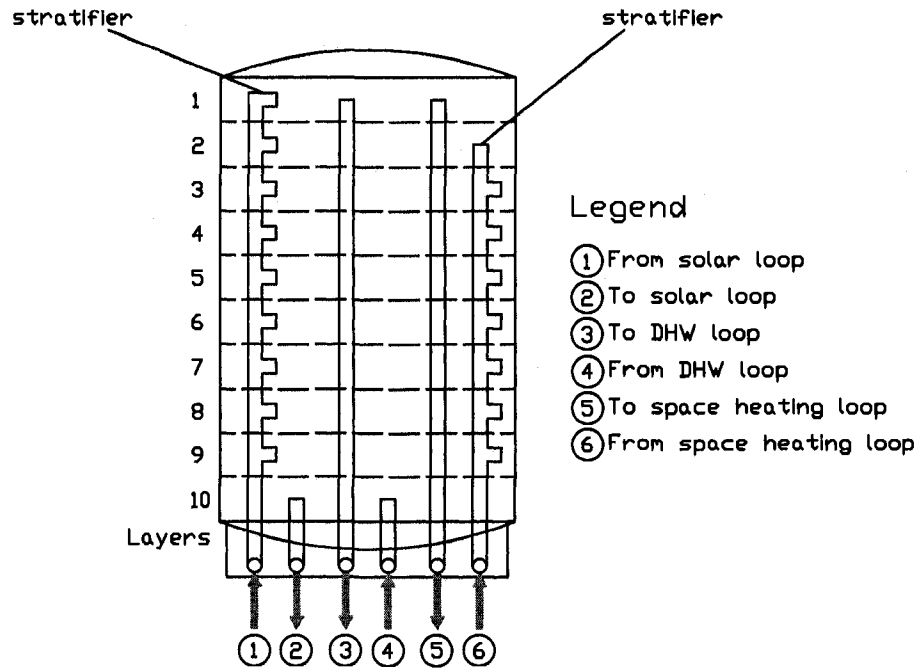
Figure 4.10. Inlets and outlets locations in the seasonal storage tank

To reduce the time of simulation, heat losses (or gains) between the storage tank and the environment are neglected since the level of insulation is assumed to be extremely high. The heat balance of each layer is performed, including the effect of inlet/outlet flows, and the conduction heat transfer between adjacent layers inside the tank. Type 534 uses two different "modes" to distinguish the way the water enters into the tank.

The first mode, called *fixed inlet and outlet*, is applied to set fixed inlet and outlet locations of streams coming from and going to the DHW loop. The inlet temperature and mass flow rate are provided as input data to the model. The position of outlet stream is supposed to be in layer n°2 and the inlet stream at the bottom of the tank. At every time step, the model considers a complete mixing between the entering fluid and the layer. Then, the fluid advances to the next layer. The direction of the fluid flow is assumed from the inlet to the

91

outlet layer. At any time, the temperature at the outlet equals the average temperature of the layer containing it.

The second mode, called *temperature seeking inlets with fixed outlets*, is used to simulate the effect of stratifier devices for the solar and heating loops. For each inlet, the temperature and mass flow rate are provided as input data. Then, the model directs the water into the layer closest in temperature to the incoming water temperature. The position for the radiant heating floor is in layer n°1, and the outlet position for the solar loop is at the bottom of the tank. With the inlet location knowns, the outlet temperature is then calculated as in the first mode.

Type 656: Pumps

In the solar loop, two Type 656 components are used to model the variable speed pumps that supply any mass flow rate up to the rated value (TESS, 2007). The pump starting transient characteristics are not modeled.

The role of Solar pump n°1 (point 2 in Figure 4.1) located on the primary loop is to circulate the antifreeze solution from the solar collectors to the external solar heat exchanger. The operating mass flow rate $\dot{m}_{solar}$ is directly proportional to the total solar collector area and is chosen equal to 40 kg/(h·m^2). The pump Wilo-Stratos ECO-ST from Wilo (2008) is chosen. The rated power $\dot{P}_{rated}$ is 40 W, the rated flow rate $\dot{m}_{rated}$ is 2,500 kg/h and the maximum inlet fluid temperature is 110°C.

Based on the curve presented in the technical documentation, the electrical power input $\dot{P}$

is modeled using a polynomial:

$$\dot{P} = \dot{P}_{rated}\left(0.30 + 6.38\gamma - 19.87\gamma^2 + 31.12\gamma^3 - 18.88\gamma^4 + 1.95\gamma^5\right) \qquad (4.9)$$

where:

$\dot{P}$ =   electrical power [W];

$\dot{P}_{rated}$ =   rated power of the pump [W]; and

γ =   pump control signal [-].

The control signal of the pump γ is:

$$\gamma = \frac{\dot{m}_{solar}}{\dot{m}_{rated}} \qquad (4.10)$$

The electric power of the pump is illustrated in Figure 4.11.
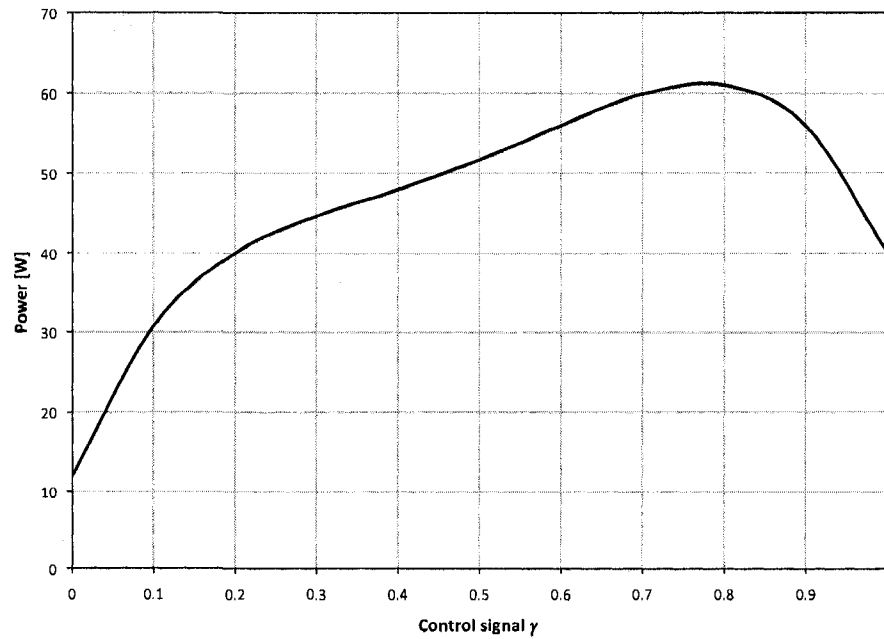
Figure 4.11. Electric power of Solar pump n°1 as a function of the control signal

93

The Solar pump n°2 (point 5 in Figure 4.1) circulates the hot water in the secondary loop from the external solar heat exchanger to the storage tank. The operating mass flow rate $\dot{m}_{pump}$ that is required to increase the temperature of water supplied to the tank to a maximum of 95°C (Viessmann, 2008) needs to be estimated:

$$\dot{m}_{pump} = \dot{m}_{solar} \cdot \frac{T_{oc} - T_{hi}}{95 - T_t} \cdot \frac{C_{p,fluid}}{C_{p,water}} \qquad (4.11)$$

where:

$\dot{m}_{pump}$ =   operating mass flow rate of the pump [kg/h];

$\dot{m}_{solar}$ =   mass flow rate of antifreeze coming from collectors [kg/h];

T_{oc} =   outlet temperature of collectors that is equal to the inlet temperature of the pump [°C];

T_{ho} =   high temperature of fluid leaving the heat exchanger [°C];

$T_{tank,bottom}$ =   temperature at the bottom of the tank [°C];

$C_{p,fluid}$ =   specific heat of antifreeze [kJ/(kg·°C)]; and

$C_{p,water}$ =   specific heat of water [kJ/(kg·°C)].

The variable speed pump Wilo-Stratos ECO (Wilo, 2008) is selected and presents identical technical proporties as Solar pump n°1. The control signal γ is:

$$\gamma = \frac{\dot{m}_{pump}}{\dot{m}_{rated}} \qquad (4.12)$$

External solar heat exchanger

Type 5 models the external cross flow heat exchanger (point 4 in Figure 4.1) required to transfer the heat from the primary loop (hot side) where circulates the propylene glycol to

the secondary loop (cold side) where circulates water. Fluids are unmixed. The heat transfer capacity rate of the heat exchanger is based on the correlation developed by Heimrath (2003) in Task 26 (IEA SHC, 2007):

$$(UA)_{HX} = (88.561 A_c + 328.19) \qquad (4.13)$$

where:

$(UA)_{HX}$ = heat transfer capacity rate [W/°C]; and

A_c = total collector array (gross) area [m^2].

Control strategy

The control strategy of the solar loop is achieved with three Type 2 controllers. The first controller (In-OutQ) checks if the collectors outlet temperature is higher than the temperature at the bottom of the tank, with an upper and lower dead band equals to 10°C and 3°C, respectively (Heimrath, 2003). The second controller (TmaxPump) checks if the collectors outlet temperature is lower than 110°C to avoid damaging the Solar pump n°1 (Wilo, 2008). Finally, the third controller (TmaxTank) checks if the temperature inside the tank is lower than 95°C (Viessmann, 2008).

A solar control unit, modeled with a calculator, starts the Solar pump n°1 when all the controllers output are equal to 1, at the same time. Solar pump n°2 is turned on when In-OutQ and TmaxTank output are equal to 1.

4.3.2   Space heating

The components used to model the radiant floor heating system are presented in Figure 4.12.
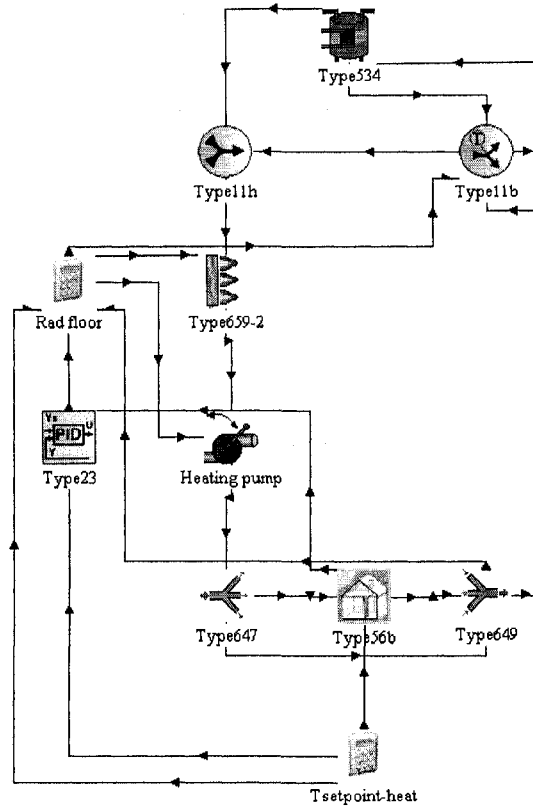
Figure 4.12. TRNSYS components used to model the heating loop

Radiant floor

For modelling the radiant heating floor, an "active layer" is added to floor definition in Type 56 (multizone building). The layer is called "active" because it contains fluid filled pipes that either add or remove heat from the surface. Parameters used to define active layers are the pipe spacing (10 cm), pipe outside diameter (2 cm), pipe wall thickness (0.2 cm) and PEX pipe wall conductivity (0.35 W/m·°C) (Liu et al., 2000). Also, the number of fluid loops is set at 10 for each floor. This is used for calculating the pipe length, as:

$$\text{pipe length} = \frac{\text{floor surface area}}{\text{pipe spacing} \cdot \text{number of loops}} \qquad (4.14)$$

Type 56 also requires that the inlet mass flow rate exceeds a minimum value. Using a process called "autosegmentation", the model splits automatically the floor surface area into a number of smaller segments to comply with the minimum flow rate on each segment. In order to limit the number of segments and to limit the calculation time, a value of 1 kg/(h.m^2), corresponding to a total of 186 kg/h for each heated floor, is assumed.

The supply water temperature to the floor heating system is an input to the building model and is controlled in terms of the outdoor temperature (Figure 4.13).

The chart shows supply temperature on the vertical axis (20 to 50 °C) versus outdoor temperature on the horizontal axis (-30 to 30 °C). The curve is constant at 45 °C up to -23°C, then decreases linearly following $T_{supply} = -0.4878 \, T_{out} + 33.78$ until 18°C, then remains constant at 25 °C.
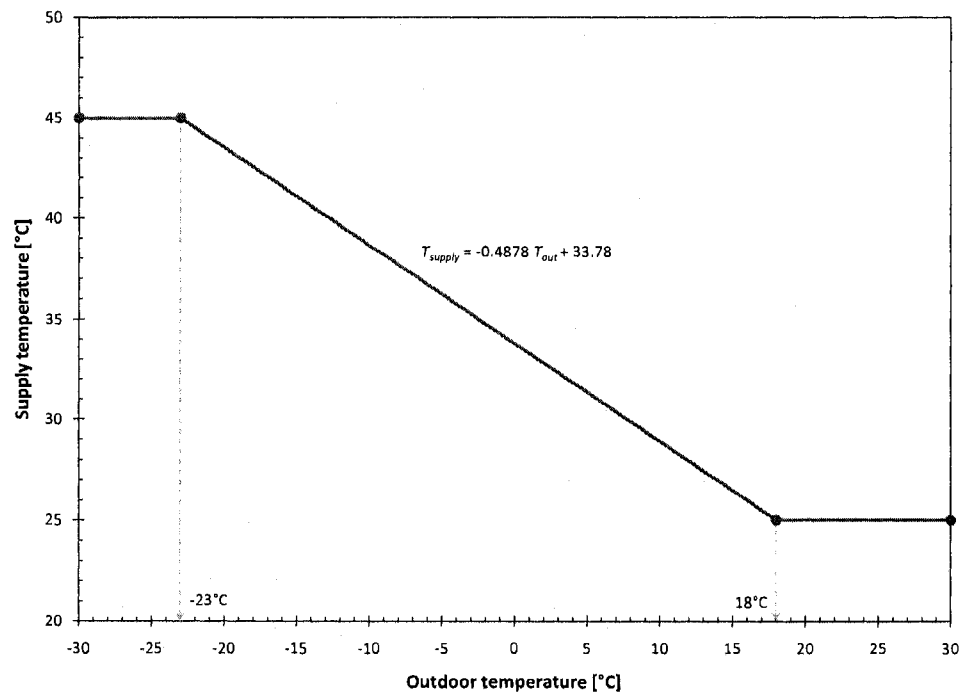
Figure 4.13. Supply temperature as a function of outdoor temperature

As shown in Figure 4.13, the maximum supply temperature is 45°C when the outdoor temperature is equal or lower that the design outdoor air temperature for heating of -23°C. The hot water is supplied at a minimum temperature of 25°C when the outdoor temperature is 18°C or higher. The values vary linearly between these boundary conditions. This can

be expressed as:

$$T_{supply} = -0.4878 \cdot T_o + 33.78 \qquad (4.15)$$

Using an Equation-Type (calculator), the final supply temperature is defined as the maximum temperature between the temperature calculated in Equation 4.15 and the return temperature given by Type 56. This value is then sent back to Type 56 as input data.

Control strategy

Type 23 is used to model a Proportional, Integral and Derivative (PID) controller that adjusts the pump flow rate, in order to maintain the operative temperature on the first floor at the setpoint of 20°C. That temperature, calculated by Type 56, is defined as input data in Type 23. The value of the calculated flow rate $\dot{m}_{calc}$ is between the rated flow rate of the pump and the minimum inlet flow rate (186 kg/h). The remaining parameters of the model such as the gain constant, integral and derivative time are selected equal to 744, 8 h and 0.5 h, respectively.

To ensure that the supply water temperature T_{supply} complies with Equation 4.15, a tempering valve is modeled (Type 11b) to adjusts the amount of return fluid that "bypasses" the storage tank (point 11 in Figure 4.1). The bypassed return water is mixed with water coming from the hot source by a tee piece (Type 11h).

Tankless water heater

Type 659-2 models the tankless water heater used to boost the temperature of hot water for space heating if necessary. The 15 kW Eemax Series Two (Eemax, 2008) electric water

heater is chosen. The thermal losses are not considered and its efficiency is assumed at 100%. The device is turned on if the temperature of water coming from Type 11h is lower than the calculated value in Equation 4.15, and if the operative temperature (controlled by the Type 2 AuxHeaton) on the first floor goes below 20°C. The auxiliary energy transmitted to the fluid by the heating element is:

$$\dot{Q}_{aux} = \dot{m}_{calc} C_{p,water} \left(T_{supply} - T_i \right) \tag{4.16}$$

where:

$\dot{Q}_{aux}$ =   auxiliary energy added to the fluid by the heater [kJ/h];

$\dot{m}_{calc}$ =   flow rate calculated by Type 23 [kg/h];

$C_{p,water}$ =   specific heat of water [kJ/(kg·°C)];

T_{supply} =   temperature of hot water calculated in Equation 4.15 [°C]; and

T_i =   temperature of water coming from Type 11h [°C].

Heat distribution

Like the Solar pump n°2, the Wilo-Stratos ECO is selected as the variable speed pump for the radiant floors (point 12 in Figure 4.1). The rated power $\dot{P}_{rated}$ is 40 W and the rated flow rate $\dot{m}_{rated}$ is 2,500 kg/h. During the heating season, from October 1 to May 15, the control signal of the pump γ is:

$$\gamma = \frac{\dot{m}_{calc}}{\dot{m}_{rated}} \tag{4.17}$$

where:

$$\gamma \qquad = \quad \text{pump control signal [-];}$$

$$\dot{m}_{calc} \quad = \quad \text{flow rate calculated by Type 23 [kg/h]; and}$$

$$\dot{m}_{rated} \quad = \quad \text{rated flow rate [kg/h].}$$

During the rest of the year, the pump is turned off and γ equals 0. The electrical power input is modeled using Equation 4.9.

Using Type 647, the water flow rate is then split to delivers hot water to the basement and first floors, while Type 649 collects the return water and send it back to the storage tank (Figure 4.12).

4.3.3 Domestic hot water

The components used to model the preparation of domestic hot water are presented in Figure 4.14.
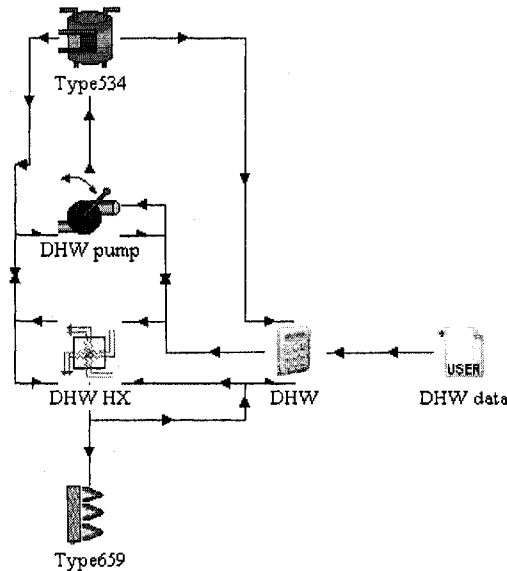
Figure 4.14. TRNSYS components used to model the DHW loop

DHW pump

The variable speed DHW pump (Wilo-Stratos ECO) (point 7 in Figure 4.1) circulates the hot water on the primary loop of the DHW external heat exchanger (point 8 in Figure 4.1). The operating water flow rate $\dot{m}_{pump}$ that is required to increase the water temperature from the city line to 45°C at the user-end is computed as:

$$\dot{m}_{pump} = \dot{m}_{DHW} \cdot \frac{45 - T_{city}}{T_{hi} - T_{ho}} \tag{4.18}$$

where:

$\dot{m}_{pump}$ = operating water mass flow rate of the pump [kg/h];

$\dot{m}_{DHW}$ = domestic hot water consumption from the given profile [kg/h];

T_{city} = city line water temperature [°C];

T_{hi} = temperature of hot water coming from the tank [°C]; and

T_{ho} = temperature of water going back to the tank [°C].

The control signal of the pump equals the ratio of the calculated operating flow rate to the rated flow rate (Equation 4.12).

External DHW heat exchanger

Type 5 models the external cross flow heat exchanger (point 8 in Figure 4.1) used to transfer the heat from the hot water coming out of the solar tank (hot side) to the water from the city line (cold side). Fluids are unmixed. Based on the results of a parameters identification process (Bales and Persson, 2003) and considering the hot water load profile, the heat transfer coefficient of the heat exchanger $(UA)_{HX}$ is set to 6190 W/°C.

Tankless water heater

Type 659 models the 15 kW Eemax "Series Two" (Eemax, 2008) tankless water heater used to boost the temperature of domestic hot water if necessary. The device is turned on if the temperature of water coming from the external heat exchanger is lower than 45°C. The auxiliary energy transmitted to the fluid by the heating element is:

$$\dot{Q}_{aux} = \dot{m}_{DHW} C_{p,water} \left(45 - T_i\right) \tag{4.19}$$

where:

$\dot{Q}_{aux}$ = auxiliary energy added to the fluid by the heater [kJ/h];

$\dot{m}_{DHW}$ = domestic hot water consumption from the given profile [kg/h];

$C_{p,water}$ = specific heat of water [kJ/(kg·°C)]; and

T_i = temperature of water coming from the external heat exchanger [°C].

4.4 Preliminary design method

In the following section, a preliminary design method developed by Braun et al. (1981) is used to predict the storage tank volume required to achieve heating and DHW needs without any auxiliary heating source. This methodology is compared with the TRNSYS results for storage volume to collector area ratios greater than 200 l/m².

Since the storage tank is very large, the inside water temperature is not expected to vary throughout each month, so an average collector inlet temperature is assumed. Consequently, the utilizability ($\overline{\phi}$) method developed by Duffie and Beckman (2006) is used.

4.4.1 System description and simulation model

The schematic of the closed-loop space heating system with sensible storage is shown in Figure 4.15. Solar energy Q_u is collected and transmitted to a water storage tank through an external heat exchanger. The primary source for heating and domestic hot water is the energy supplied $Q_{supplied}$ from storage. The tank is assumed very well insulated and the heat losses are not considered. The water in the tank is supposed to be fully-mixed and, therefore, the stratification is not considered. The return temperature from the heating and domestic hot water loads is always at or above T_{min}. A bypass valve makes sure that the temperature coming from the heat exchanger is always at or below T_B. An auxiliary heating element covers the additional energy demand Q_{aux}, if necessary. An energy balance

Figure 4.15. Schematic of a closed-loop space heating system (Braun et al., 1981)

on the tank for a one-month period is performed, as:

$$\Delta U = Q_u - Q_{supplied} \qquad (4.20)$$

where:

ΔU = monthly change in internal energy of storage [GJ];

Q_u = useful energy gain [GJ]; and

$Q_{supplied}$ = energy supplied by the storage tank [GJ].

The radiation level must exceed a critical value before useful output is produced. This critical level is expressed as follows:

$$I_{Tc} = \frac{F_R U'_L \left(\overline{T}_t - \overline{T}_{do}\right)}{F_R \left(\tau\alpha\right)_n} \qquad (4.21)$$

where:

I_{Tc} = monthly critical level radiation [W/m^2];

F_R = overall collector heat removal efficiency factor [-];

U'_L = modified first-order collector efficiency [W/(m$^2\cdot$°C)];

$\left(\tau\alpha\right)_n$ = product of the cover transmittance and the absorber absorptance at normal incidence [-];

$\overline{T}_t$ = monthly average tank temperature [°C]; and

$\overline{T}_{do}$ = monthly average daytime outdoor temperature [°C].

The daily utilizability $\overline{\phi}$ is calculated using the correlation method developed by Duffie and Beckman (2006). The useful energy gain of collectors $N \sum \overline{Q}_u$, characterized as the difference between the absorbed radiation and the radiation losses to the surroundings over a time period is calculated over each month:

$$N \sum \overline{Q}_u = \overline{\phi} A_c \overline{G}_T F_R \overline{(\tau\alpha)} \qquad (4.22)$$

where:

N =   number of days in the month [-];

$\overline{Q_u}$ =   monthly average of daily useful energy gain [GJ];

$\overline{\phi}$ =   daily utilizability [-];

A_c =   total collector array (gross) area [m^2];

G_T =   global solar radiation on the collector [W/m^2];

F_R =   overall collector heat removal efficiency factor [-]; and

$\overline{(\tau\alpha)}$ =   monthly average product of the cover transmittance and the absorber

                        absorptance [-]; assumed equal to 0.96 (Duffie and Beckman, 2006).

The energy supplied to the load from storage $Q_{supplied}$ is assumed to be the minimum of the loads Q_{loads} and the quantity of energy that could be supplied if the heat exchanger operates continuously throughout the month:

$$Q_{supplied} = \min\left(\epsilon C_{min}\left(\overline{T}_T - T_R\right)\Delta t, Q_{loads}\right) \tag{4.23}$$

where:

$Q_{supplied}$ =   energy supplied by the storage tank [GJ];

ϵC_{min} =   product of the effectiveness of the heat exchanger and the minimum

                     capacitance rate of the heat exchanger [W/°C];

$\overline{T}_t$ =   monthly average tank temperature [°C];

T_R =   room temperature [°C];

Δt =   length of time in the month [s]; and

Q_{loads} =   sum of space heating and domestic hot water loads [GJ].

The ϵC_{min} product is selected to respect the following condition (Braun et al., 1981):

$$0.4 < \frac{\epsilon C_{min}}{(UA)_{house}} < 2 \tag{4.24}$$

where $(UA)_{house}$ is the overall loss conductance of the "best case" house.

The annual solar fraction of the solar combisystem is finally computed as:

$$\mathscr{F} = 1 - \frac{\int^{year} Q_{aux} \, dt}{\int^{year} Q_{loads} \, dt} \tag{4.25}$$

where:

$\mathscr{F}$ = annual solar fraction [-];

Q_{aux} = auxiliary energy [GJ]; and

Q_{loads} = sum of space heating and domestic hot water loads [GJ].

Since Q_{loads} is equal to the sum of the energy supplied by the storage tank $Q_{supplied}$ and Q_{aux}, Equation 4.25 is rewritten as:

$$\mathscr{F} = \frac{\int^{year} Q_S \, dt}{\int^{year} Q_{loads} \, dt} \tag{4.26}$$

4.4.2 Methodology

Given an initial storage tank temperature $\overline{T}_i$ at the start of the month of March, for example, the average temperature of the same month $\overline{T}_t$ is guessed. The final tank temperature at

the end of the month is given by:

$$\overline{T}_f = 2 \cdot \overline{T}_t - \overline{T}_i \qquad (4.27)$$

$\overline{T}_t$ is used to calculate the critical radiation level I_{Tc} (Equation 4.21) and the resulting utilizability $\overline{\phi}$. The tank energy balance is then applied to estimate the tank temperature at the end of the month:

$$\overline{T}_f = \frac{\Delta U}{cap_S} + \overline{T}_i = \frac{Q_u - Q_{supplied}}{cap_S} + \overline{T}_i \qquad (4.28)$$

The thermal capacitance of the storage medium cap_S, expressed in GJ/°C, is:

$$cap_S = V_t \cdot \rho \cdot C_p \qquad (4.29)$$

where:

V_t =   volume of the tank [m³];

ρ =   density [kg/m³]; and

C_p =   specific heat [GJ/(kg·°C)].

This calculated temperature is compared with the assumed value (Equation 4.27), and if they agree, the computation continues with the next month. If the temperature difference exceeds 0.1°C, another monthly average temperature is estimated and a new final tank temperature is calculated until the agreement is reached between the guessed value of $\overline{T}_t$ and the calculated value. The process is repeated for all twelve months, and the final tank temperature $\overline{T}_f$ is compared with the initial guess made for March. If they agree, the

calculations are stopped; if they disagree, the calculations are repeated.

4.4.3 Input data

An array of twelve identical Vitosol 300 SP3 solar collectors is assumed to cover as much as possible the area on the south part of the roof. The resulting absorber surface area is equal to 51.4 m^2. Meteorological, outdoor temperature and solar radiation data are extracted from the weather file used by TRNSYS. The parameters used for the preliminary design method are presented in Table 4.21.

Table 4.21. Parameters used in the preliminary design method

Solar collector		
A_c	[m^2]	51.44
$F_R(\tau\alpha)_n$	[-]	0.5093
$F_R U'_L$	[W/(m$^2\cdot$°C)]	1.0948
Tilt angle	[°]	45
Orientation	[-]	South
T_B	[°C]	95
Load		
$(UA)_L$	[W/°C]	120
T_R	[°C]	20
Load heat exchanger		
ϵC_{min}	[W/°C]	168
T_{min}	[°C]	25
Thermal storage		
Medium	[-]	Water
C_p	[kJ/(kg·°C)]	4.19
ρ	[kg/m^3]	1000

4.4.4 Results

For a total collector area of 51.4 m^2, the annual solar fraction of 100%, synonym of a seasonal storage system, is achieved when the tank volume comes close to 38,600 l (Figure 4.16). The ratio of the tank volume to the collector area is equal to 750 l/m^2.
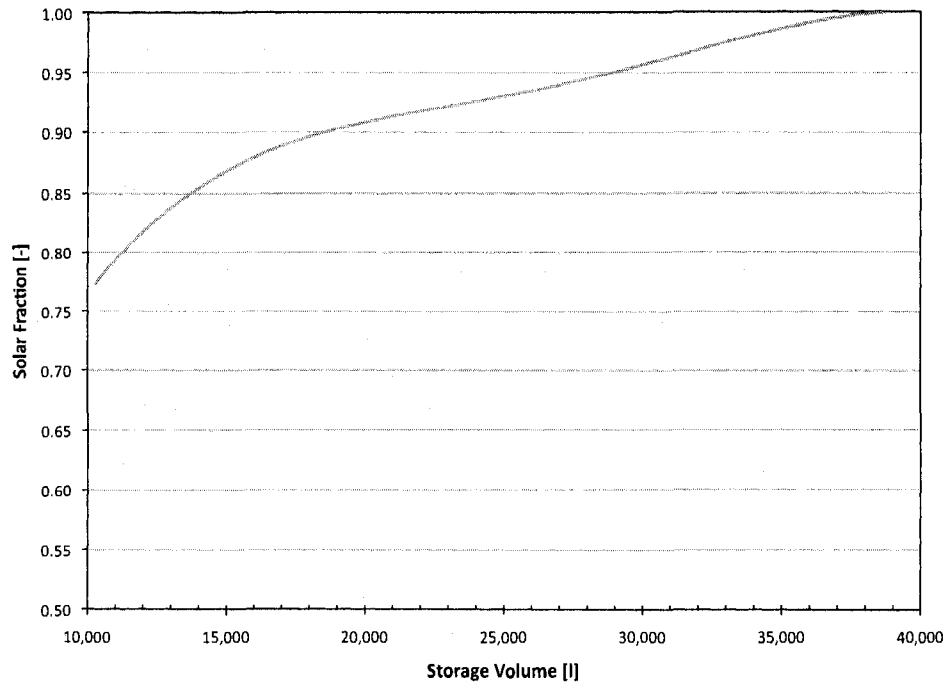
Figure 4.16. Solar fraction as a function of the storage volume

4.5   TRNSYS simulation results and discussion

This section presents the TRNSYS simulation results for the seasonal storage system associated with a hydronic radiant heating floor and domestic hot water, as described previously. The model runs over two years since initial temperature of the storage tank is unknown. Therefore, each layer is assumed at a temperature of 60°C at the beginning of the first year. Results at the end of the first year are input as initial conditions for the simulation of the second year. Since the first year of operation is not representative, only the results of the second year are presented.

Using information available for the domestic hot water consumption profile (Jordan and Vajen, 2001), the simulation time step is reduced to six minutes in order to provide a more

109

realistic representation of temperature variation inside the tank. The flow rate of the Solar pump n°1 is fixed at 40 kg/(h·m²).

4.5.1 Overall performance

According to the TRNSYS simulation results, the total house electricity use is equal to 8,300 kWh (29,880 MJ), corresponding to 45 kWh/m² (161 MJ/m²) of heated floor area. Compared to the total eletricity use of 18,830 kWh of the "best case" (without solar energy), this represents a drastic decrease as the total energy use is divided by a factor bigger than 2.

The monthly repartition of electricity use during the year as well as its distribution among end-uses are shown in Table 4.22. The Heating & DHW part represents the eletricity use due to the circulating pumps. The winter months have the highest contribution to the consumption due mainly to the ventilation system since the outdoor air needs to be heated up to the temperature of 20°C. During summer, the months of July and August present higher demand as a result of the cooling system.

Table 4.22. Monthly repartition and distribution of electricity use

Electricity use [kWh]	Month												
	Jan	Feb	Mar	Apr	May	Jun	Jul	Aug	Sep	Oct	Nov	Dec	Tot
Heating & DHW	24	24	29	20	4	2	1	2	1	4	18	21	150
Humidification	205	173	125	37	1	-	-	-	-	4	51	167	764
Cooling	-	-	-	-	7	146	310	231	47	-	-	-	740
Lighting	133	108	102	88	72	65	68	81	96	121	141	146	1,220
Ventilation	670	593	590	469	347	285	294	294	285	429	523	642	5,421
Total	1,035	900	846	613	432	498	673	608	429	558	732	976	8,300

Figure 4.17 presents a comparison between the monthly electricity use in the base case and the solar combisystem. It shows a drastic decrease from April to October. However, the difference is less sensible during the period where the heating system is turned off.

110
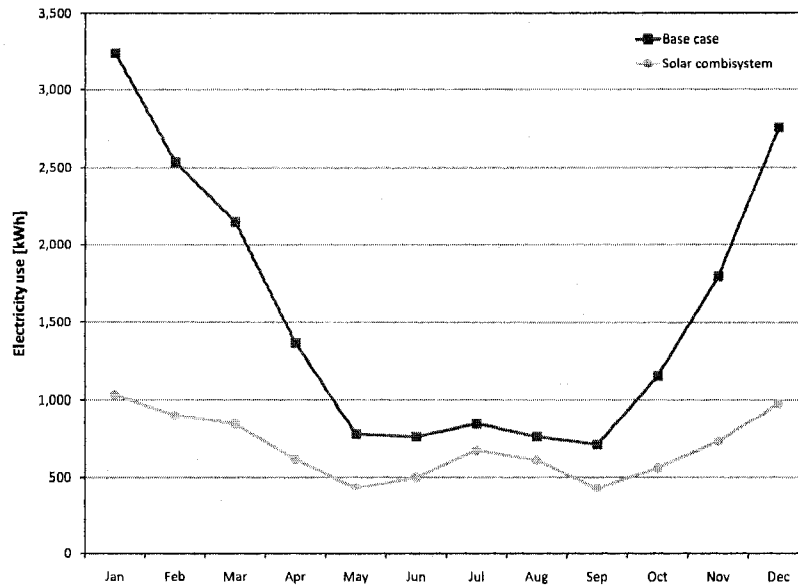
Figure 4.17. Comparison between the base case and the solar combisystem

The annual distribution of energy use is detailed in Figure 4.18. The ventilation has the highest contribution to the energy use as it accounts for 65.3% of the total value, followed by lighting with 14.7%, humidification with 9.2% and cooling with 8.9%. The combination of space heating and domestic hot water production accounts for only 1.8%.
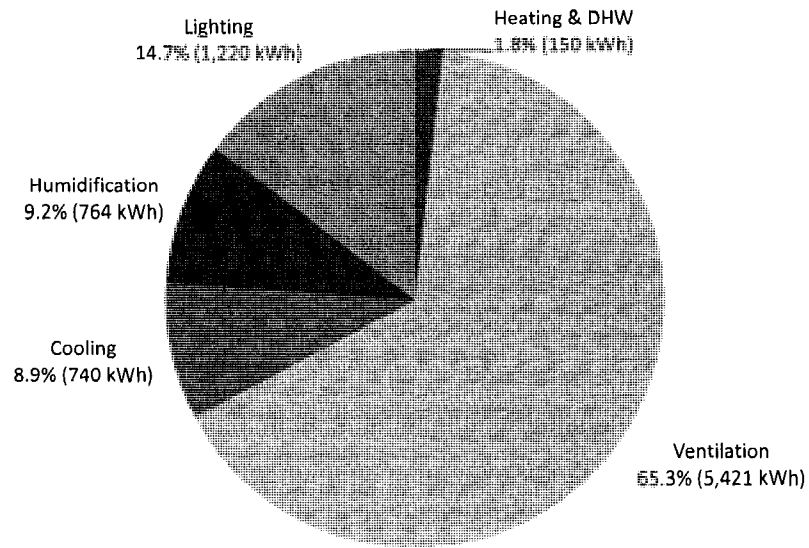
Figure 4.18. Annual distribution of electricity use

The monthly average operative temperature of the first floor is shown in Figure 4.19. During the cooling season, the cooling system is able to maintain the temperature around 24°C. During the heating season, the temperature is systematically above the design setpoint of 20°C by approximately 0.5°C.
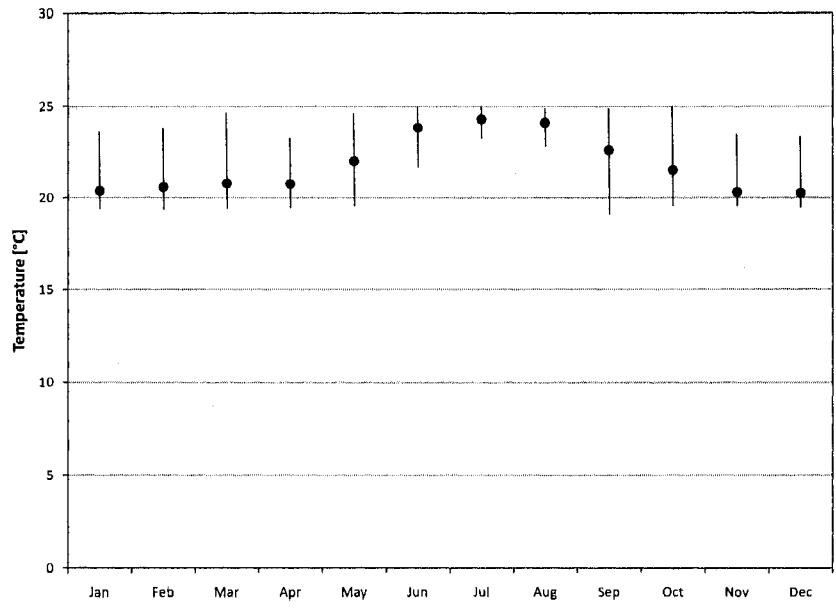
Figure 4.19. Monthly average of operative temperature

This overheating phenomenon is very well illustrated in Figure 4.20 for the first three days of February since the operative temperature goes up to a maximum of 23.5°C in the afternoon of February 2.

Higher temperatures observed on February 2 can be seen as the direct result of exterior conditions since the outdoor temperature and horizontal solar radiation present superior values that particular day (Figure 4.21).
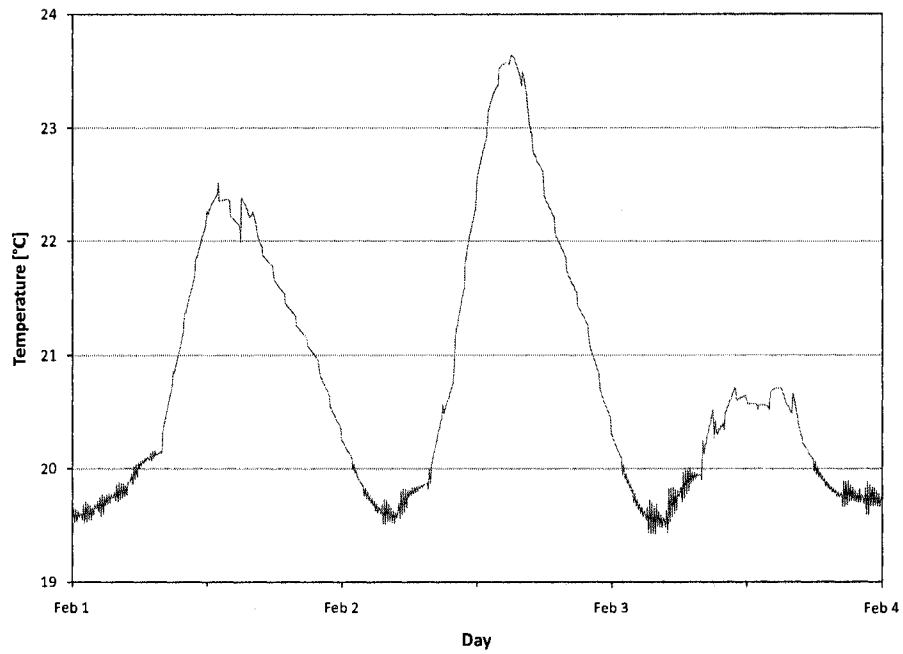
Figure 4.20. Operative temperature in February
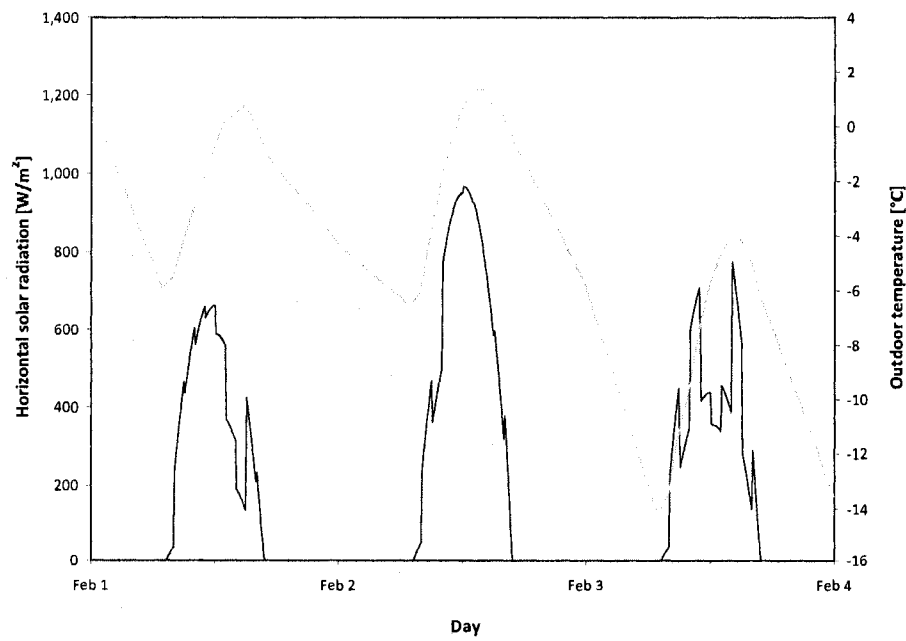
Figure 4.21. Horizontal solar radiation and outdoor temperature

114

The surface temperature of the first floor is investigated in order to see if values comply with allowable range of 19 and 29°C proposed by ASHRAE (2004). The minimum temperature observed is 20°C and the maximum 28°C. Hence, the condition is well respected.
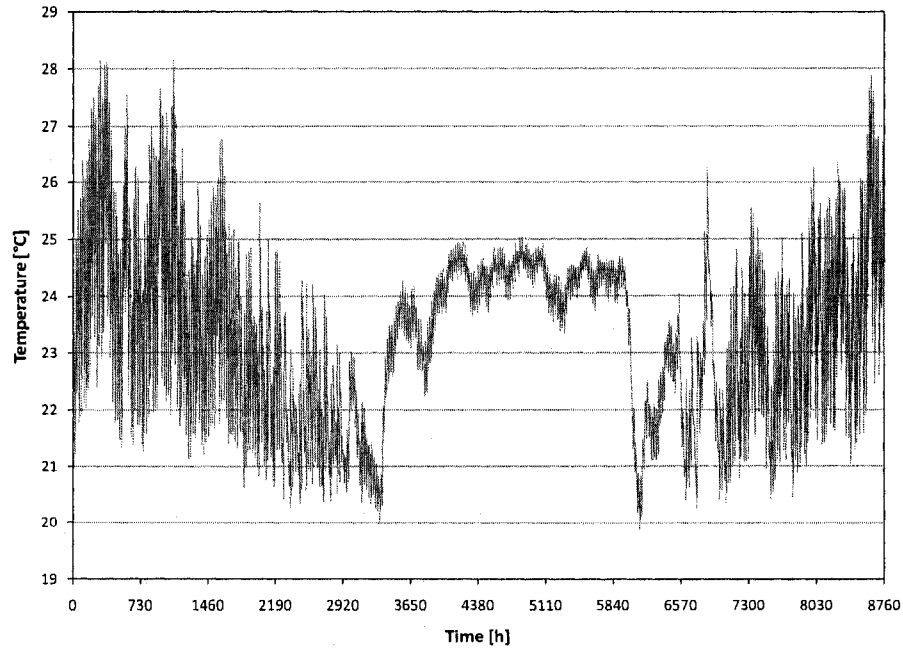
Figure 4.22. Inside surface temperature on the first floor

4.5.2 Performance of the solar combisystem

The following sections present the performance analysis of the seasonal storage system as well as its various components, based on the TRNSYS simulation.

Storage tank

For indication only, the top layer, bottom layer and average tank temperatures are presented during the first year of operation (Figure 4.23). The bottom and average temperatures drop drastically during the first part of January. In the middle of February, the top temperature starts to go up until the top layer reaches its maximum of 95°C. That temperature is

115

maintained until the end of November. However, the average and bottom tank temperatures starts to drop in the middle of October due to a higher heating demand. It is observed that the top layer temperature falls consequently one month and a half later, in December.

The temperature profile for the second year of operation (Figure 4.24) presents similarities with the previous chart. The minimum temperature of the top layer occurs at the end of January and is approximately 46-47°C. Since the hot water supplied to the radiant floor is extracted from the top layer (Figure 4.10), this suggests that the combisystem may be properly sized as the temperature is higher, but not significantly, than the maximum supply temperature for space heating of 45°C (Figure 4.13).
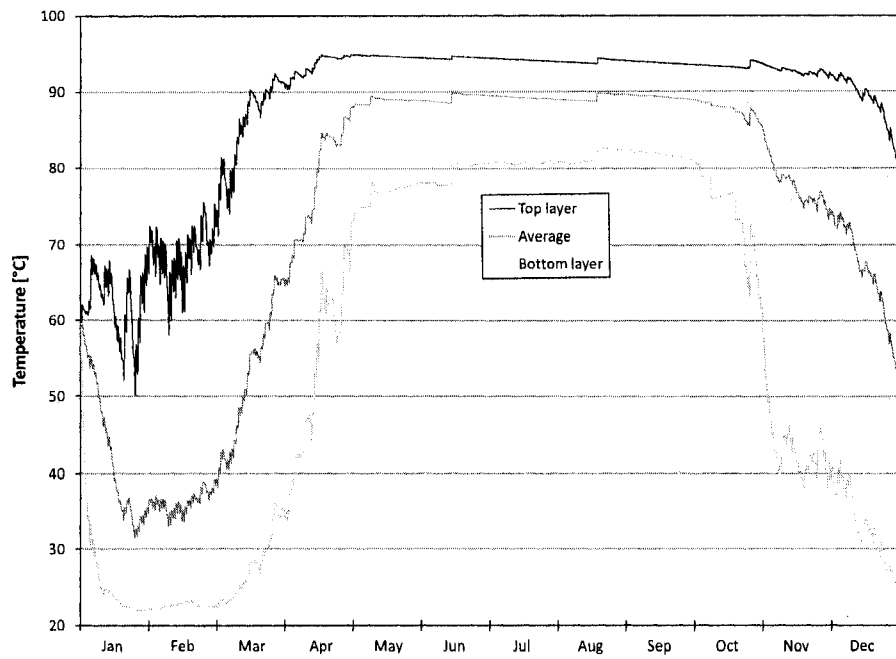
Figure 4.23. Temperatures in the storage tank during the first year of operation
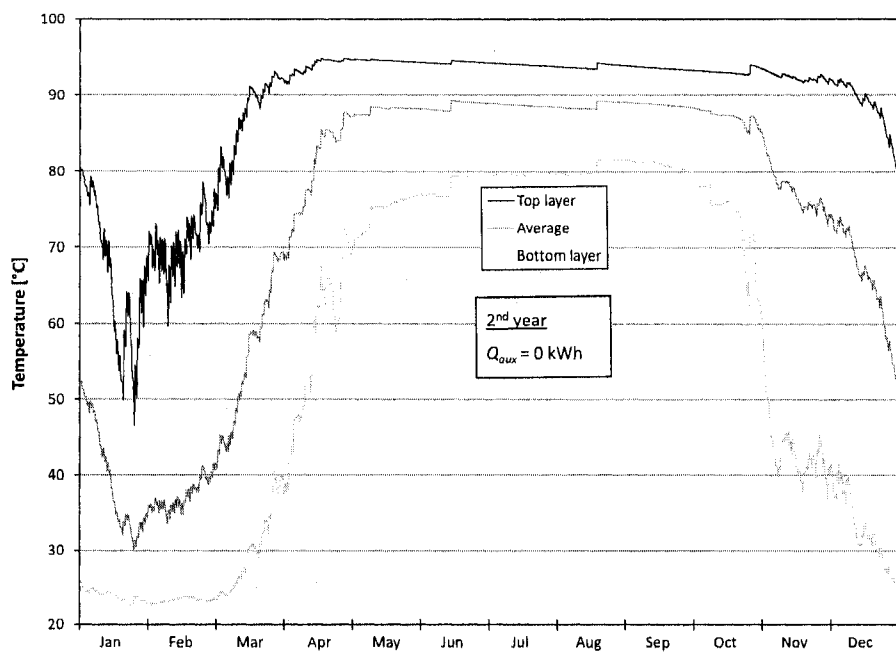
Figure 4.24. Temperatures in the storage tank during the second year of operation

The profile of average tank temperature is illustrated in Figure 4.25 on a monthly basis. Minimum values are noticed in January and February. During summer months, the temperature comes close to 95°C, which is a sign that the input of solar energy coming from the collectors maybe too elevated.
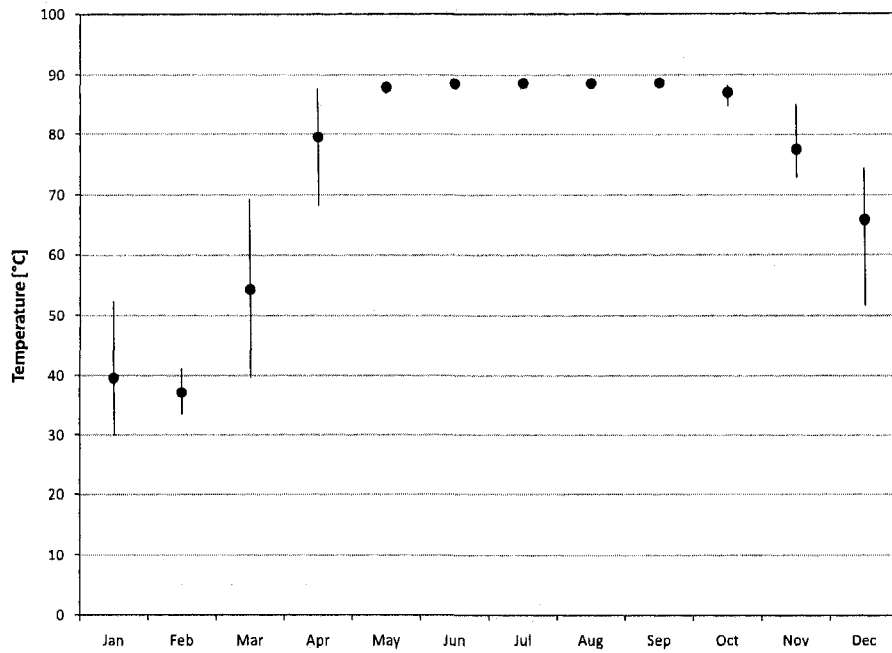
Figure 4.25. Monthly average water temperature in the storage tank

Pumps

The time of operation and average mass flow rate of pumps are shown in Table 4.23. The pumps are turned on mainly during the heating season to supply higher heating and DHW demands.

Table 4.23. Time of operation and average mass flow rate of pumps

Time of operation [h]	Month											
	Jan	Feb	Mar	Apr	May	Jun	Jul	Aug	Sep	Oct	Nov	Dec
Solar pump n°1	219	248	315	212	61	26	16	26	12	28	155	170
Solar pump n°2	167	201	245	164	35	14	6	11	5	17	111	121
Pump for heating	199	144	124	69	4	-	-	-	-	52	170	213
Pump for DHW	15	13	15	12	10	11	9	9	13	15	12	16
Mass flow rate [kg/h]	Month											
	Jan	Feb	Mar	Apr	May	Jun	Jul	Aug	Sep	Oct	Nov	Dec
Solar pump n°2	82	96	121	181	382	1,023	2,077	1,401	2,208	670	78	81
Pump for heating	436	457	405	345	307	-	-	-	-	311	344	397
Pump for DHW	76	43	36	31	27	26	22	20	23	26	30	36

The mass flow rate of Solar pump n°1 is not presented as it remains constant at 40 kg/m^2 of collector area. From November to April, the monthly average mass flow rate of Solar pump n°2 fluctuates between 78 and 181 kg/h (Figure 4.26). During the period when the average tank temperature comes closer to 95°C (Figure 4.25), the values are increased substantially up to a maximum of 2,208 kg/h in September. These high values could have negative impact on the stratifiers performance since the flow rates are higher than 8 kg/min or 480 kg/h (see Chapter 2).

The flow rate profile of the pump for space heating presents less variations, as values range between 307 and 457 kg/h (Figure 4.27). The mass flow rate is directly related to the heating demand, as higher values are observed during colder months, and to the supply water temperature, which has higher values during the cold days.

Mass flow rates of variable speed pump for domestic hot water is associated to the storage tank temperature (Figure 4.25). Indeed, as the temperature is low, the mass flow rate is increased to ensure a 45°C hot water at the user end at all times (Figure 4.28).
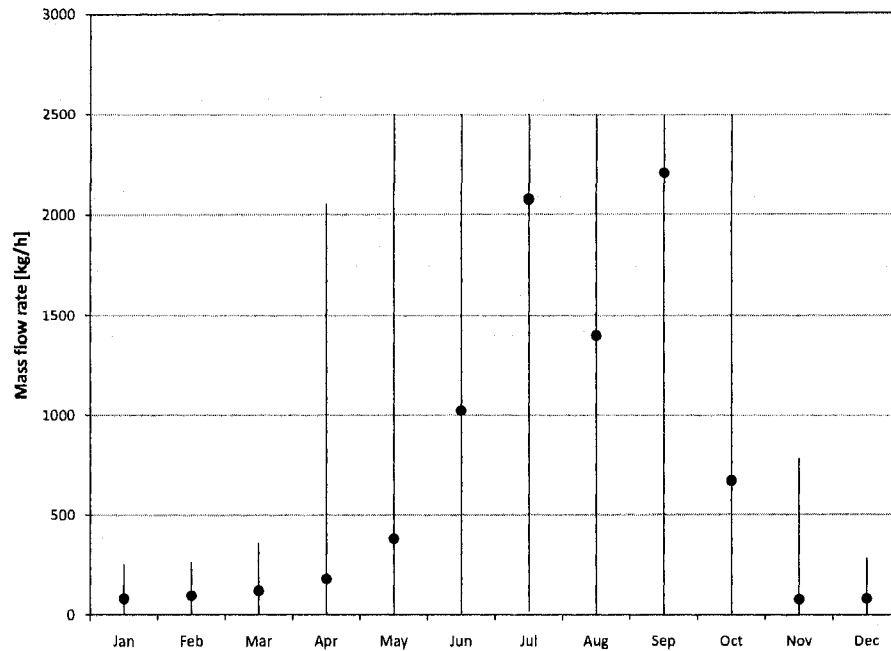
Figure 4.26. Solar pump n°2 mass flow rates
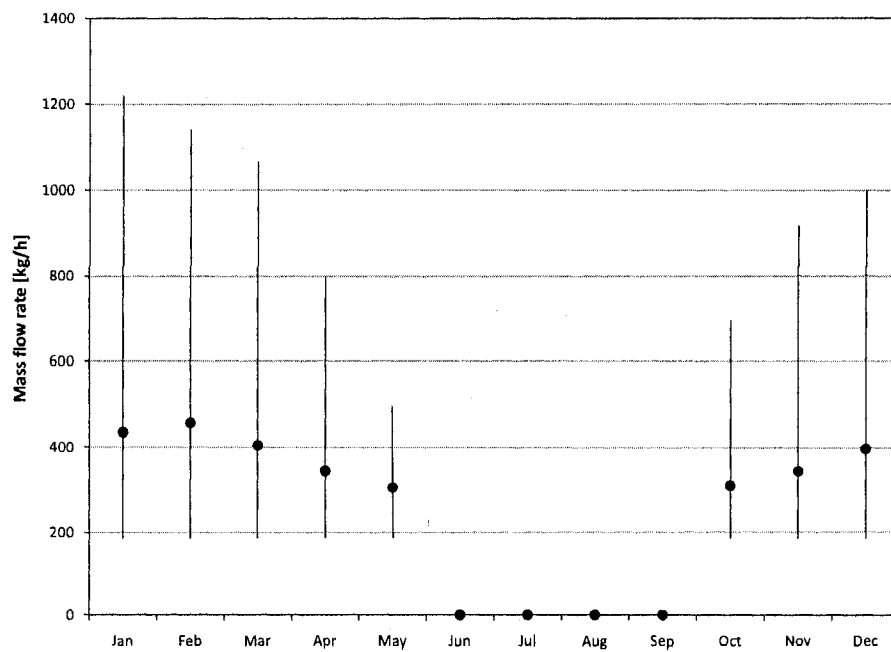
Figure 4.27. Mass flow rates of the pump used for space heating

120
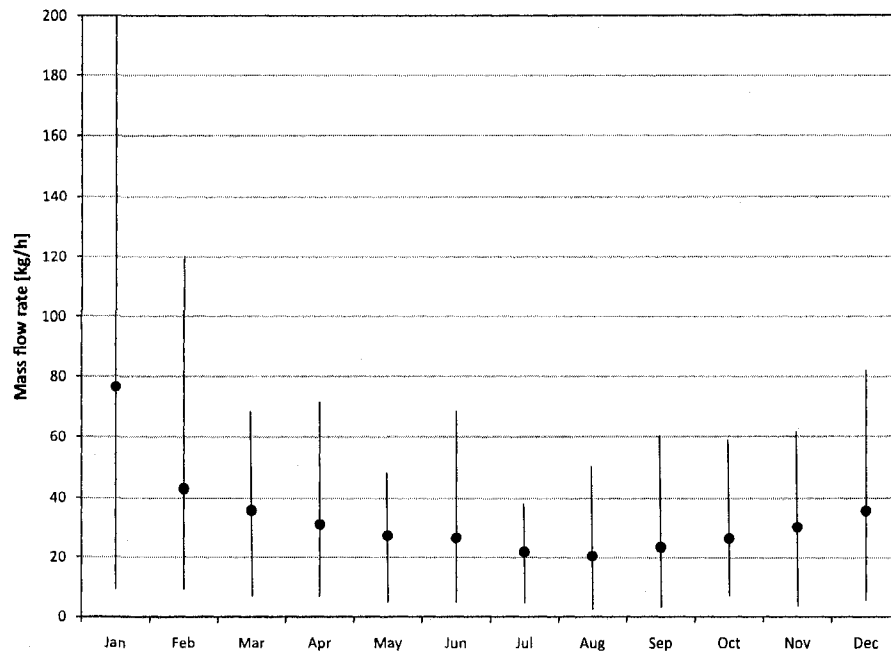
Figure 4.28. Mass flow rates of the pump used for space DHW

Solar collectors

The outlet collectors temperature is presented on a monthly basis in Figure 4.29. The average temperature oscillates between 65 and 85°C during the year. The maximum temperature is limited to 110°C to avoid damaging the pump.
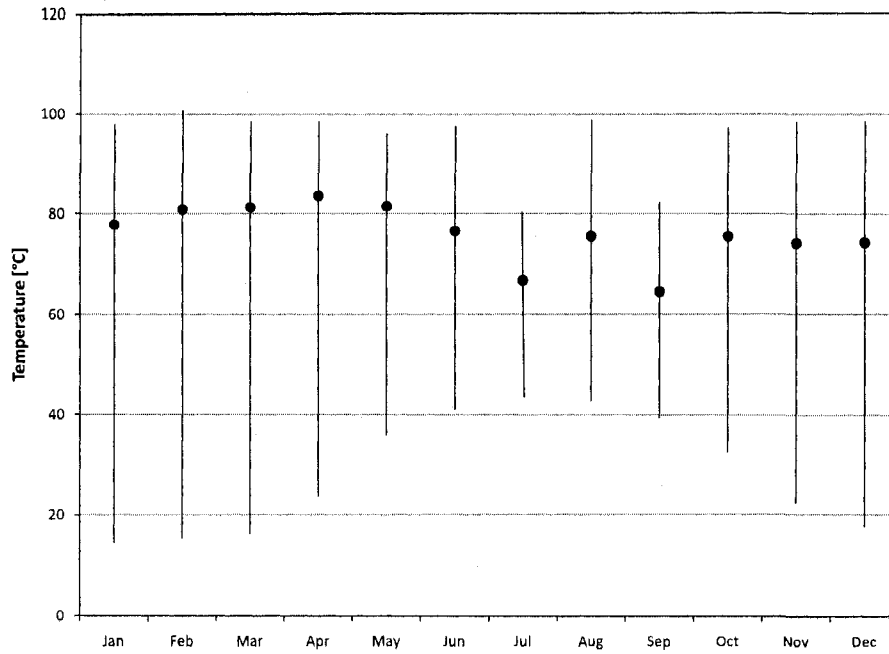
Figure 4.29. Monthly outlet collectors temperature

The TRNSYS results show that the yearly average of the outlet temperature of collectors is 80°C and the corresponding inlet temperature is 76°C. Therefore, the average temperature in the collectors is equal to 78°C, which corresponds to the initial guess of 80°C used to estimate the thermophysical properties of the antifreeze.

The rate of useful energy gain of collectors is calculated by TRNSYS as:

$$Q_u = \dot{m}C_p\left(T_o - T_i\right) \tag{4.30}$$

where:

Q_u = rate of useful energy gain [W];

$\dot{m}$ = the pump fluid flow rate through the collector [kg/s];

C_p = specific heat of collector fluid [J/(kg·°C)];

T_i = inlet temperature of fluid to collector [°C]; and

T_o = outlet temperature of fluid from collector [°C].

The rate of useful energy gain Q_u is integrated over the second year is equal to 9,335 kWh.

4.5.3 Collection efficiency

A measure of collector performance is the collection efficiency η_{TH}, defined as the ratio of the useful energy gain over a year to the incident solar energy on the collectors over the same period (Duffie and Beckman, 2006):

$$\eta_{TH} = \frac{\int^{year} Q_u \, dt}{A_c \int^{year} G_T \, dt} = 0.257 \qquad (4.31)$$

where:

η_{TH} = efficiency of collectors [-];

Q_u = rate of useful energy gain [W];

A_c = total collector array (gross) area [m^2]; and

G_T = global solar radiation on the collector [W/m^2].

If the electric energy use of pumps Q_{pumps} is considered, the collection efficiency is:

$$\eta_{TH+ELEC} = \frac{\int^{year} Q_u \, dt}{A_c \int^{year} G_T \, dt + \int^{year} Q_{pumps} \, dt} = 0.256 \qquad (4.32)$$

4.5.4 Solar fraction

No auxiliary heating is required to provide additional heat in the storage tank during the second year of operation. Therefore, the solar fraction of the system is:

$$\mathscr{F}_{TH} = 1 - \frac{\int^{year} Q_{aux} \; \mathrm{d}t}{\int^{year} Q_{loads} \; \mathrm{d}t} = 1 \tag{4.33}$$

where:

$\mathscr{F}_{TH}$ =   annual solar fraction [-];

Q_{aux} =   energy supplied to the storage tank by the tankless water heaters [kWh]; and

Q_{loads} =   sum of space heating and hot water loads [kWh].

The solar fraction that considers the energy use of the circulating pumps is:

$$\mathscr{F}_{TH+ELEC} = 1 - \frac{\int^{year} (Q_{aux} + Q_{pumps}) \; \mathrm{d}t}{\int^{year} Q_{loads} \; \mathrm{d}t} = 0.975 \tag{4.34}$$

4.5.5 Coefficient of performance

The coefficient of performance (COP) of the solar combisystem is calculated using the following equation:

$$\text{COP} = \frac{\int^{year} (Q_{heat} + Q_{DHW}) \; \mathrm{d}t}{\int^{year} Q_{pumps} \; \mathrm{d}t} = 49.3 \tag{4.35}$$

The energy supplied for space heating Q_{heat} is calculated as:

$$Q_{heat} = m_{heat} C_p \left(T_{supply} - T_{ret} \right) \tag{4.36}$$

124

where:

Q_{heat} =   energy supplied for space heating [W];

m_{heat} =   mass flow rate of hot water supplied by the circulating pump [kg/s];

C_p =   specific heat of water [J/(kg·°C)];

T_{supply} =   supplied temperature [°C]; and

T_{ret} =   return temperature [°C].

The energy supplied for domestic hot water preparation Q_{DHW} is calculated as:

$$Q_{DHW} = m_{DHW} C_p \left(45 - T_{city} \right) \qquad (4.37)$$

where:

Q_{DHW} =   energy supplied for domestic hot water preparation [W];

m_{DHW} =   domestic hot water consumption profile [kg/s];

C_p =   specific heat of water [J/(kg·°C)]; and

T_{city} =   city line temperature [°C]; and

4.6 Sensitivity analysis

In this section, a sensitivity analysis based on a certain set of design parameters is performed in order to evaluate the repercussions of those parameters on the seasonal storage system and to improve its performance. A comparison between evacuated tube and flat-plate collectors is presented. For each type of collectors, several alternatives are proposed based on the parameters that are expected to have a significant impact. Modifications are investigated on:

- storage tank volume;

- solar collector area;

- insulation of the storage tank;

- operating mass flow rate of Solar pump n°1;

- tilt angle.

4.6.1 Evacuated tube collectors

The solar combisystem described in previous sections is considered as the base case for the sensitivity analysis.

Influence of the storage tank volume

The volume of the storage tank is reduced by 10, 20 and 30% to see the resulting performance of the system. Compared to the base case, the alternative 1 has almost no impact as the solar fraction remains close to 100% (Table 4.29). However, for alternatives 2 and 3, a drastic decrease of performance occurs as the COP is divided by a factor 2 each time that

the tank volume is reduced by 10%. The collection efficiency remains constant around

25.4-25.8%.

Table **4.29.** Performance of the solar combisytem for different storage tank volumes

Alternative	Volume [m^3]	η_{TH} [%]	$\eta_{TH+ELEC}$ [%]	Q_{aux} [kWh]	Q_{pumps} [kWh]	$\mathscr{F}_{TH}$ [%]	$\mathscr{F}_{TH+ELEC}$ [%]	COP [-]
Base case	38.6	25.7	25.6	-	151	100.0	97.5	49.3
1	34.7	25.7	25.6	9	151	99.8	97.3	46.5
2	30.9	25.8	25.7	151	154	97.5	94.9	24.3
3	27.0	25.4	25.3	388	157	93.5	90.8	13.5

Influence of the solar collector area

The total area of collectors is reduced by substracting 1, 2 and 3 collectors. As shown in

Table 4.30, the fact to remove one element has almost no impact on the performance of the

system. However, for alternatives 2 and 3, the COP is divided approximately by a factor 2

each time that one collector is removed.

Table **4.30.** Performance of the solar combisytem for different collector areas

Alternative	Area [m^2]	η_{TH} [%]	$\eta_{TH+ELEC}$ [%]	Q_{aux} [kWh]	Q_{pumps} [kWh]	$\mathscr{F}_{TH}$ [%]	$\mathscr{F}_{TH+ELEC}$ [%]	COP [-]
Base case	51.4	25.7	25.6	-	151	100.0	97.5	49.3
1	47.1	25.6	25.4	5	159	99.9	97.2	45.3
2	42.8	25.6	25.5	82	168	98.6	95.8	29.6
3	38.5	25.4	25.2	307	180	94.8	91.8	15.1

Influence of the tank insulation

To give a more realistic perspective of the system, it is required to estimate the impact of

the storage tank heat losses to the environment. Therefore, a blanket of mineral wool with

a thickness 20 cm is assumed to cover the tank entirely. The resulting edge loss coefficient is

equal to 0.20 W/(m$^2\cdot$°C). That value, as well the air temperature of the surrounding space

(given by Type 56), are set as input in Type 534 for each of the tank layers. Reciprocally, the tank losses are set as new heat gains in Type 56.

As presented in Table 4.31, the solar fraction of the system $\mathscr{F}_{TH+ELEC}$ is lowered by 5.7%. The COP presents the most radical decrease as it drops from 49.3 to 12.8.

Table 4.31. Influence of the tank insulation on the performance of the solar combisystem

Alternative	η_{TH} [%]	$\eta_{TH+ELEC}$ [%]	Q_{aux} [kWh]	Q_{pumps} [kWh]	$\mathscr{F}_{TH}$ [%]	$\mathscr{F}_{TH+ELEC}$ [%]	COP [-]
Base case	25.7	25.6	-	151	100.0	97.5	49.3
1	25.5	25.4	288	196	95.1	91.8	12.8

Since these results are more representative of a real system, it is decided to pursue the sensitivity analysis using the alternative 1 (insulated tank) as the "new base case".

Influence of the operating mass flow rate of Solar pump n° 1

The mass flow rate of the thermal fluid circulating in the collectors $\dot{m}_{solar}$ is varied between 25 and 51 kg/(h·m^2). The minimum value corresponds to the minimum flow rate recommended by the manufacturer to assure an appropriate circulation and a turbulent flow in the collectors (Viessmann, 2008); and the maximum corresponds to the maximum flow rate of Solar pump n°1 (2,500 kg/h).

Table 4.32 shows that the alternative 1 lowers the energy use of the pumps since it is directly proportional to the flow rate (Equation 4.9). Therefore, the solar fraction ($\mathscr{F}_{TH+ELEC}$) of the base case is increased by 4% and the COP is almost doubled. Such system is preferred as it also reduces the piping size (Table 4.7).

Table 4.32. Performance of the solar combisytem for different values of $\dot{m}_{solar}$

Alternative	Flow rate [kg/(h·m²)]	η_{TH} [%]	$\eta_{TH+ELEC}$ [%]	Q_{aux} [kWh]	Q_{pumps} [kWh]	$\mathscr{F}_{TH}$ [%]	$\mathscr{F}_{TH+ELEC}$ [%]	COP [-]
Base case	40	25.5	25.4	288	196	95.1	91.8	12.8
1	25	26.5	26.4	90	161	98.5	95.8	24.3
2	33	26.0	25.9	193	178	96.8	93.7	16.5
3	51	18.8	18.7	662	201	88.9	85.5	7.3

Influence of the tilt angle

Four alternatives are proposed for the tilt angle. At 37.5°, the solar fraction $\mathscr{F}_{TH+ELEC}$ is reduced by about 3.6% and the COP by 3.9 (Table 4.33). Then, by incrementing the tilt angle by 7.5° up to 60°, the performance is clearly enhanced as the solar fraction comes close to 95% and the COP to 20.

Table 4.33. Performance of the solar combisytem for different tilt angles

Alternative	Tilt angle [°]	η_{TH} [%]	$\eta_{TH+ELEC}$ [%]	Q_{aux} [kWh]	Q_{pumps} [kWh]	$\mathscr{F}_{TH}$ [%]	$\mathscr{F}_{TH+ELEC}$ [%]	COP [-]
Base case	45.0	25.5	25.4	288	196	95.1	91.8	12.8
1	37.5	24.9	24.8	497	204	91.6	88.2	8.9
2	52.5	25.7	25.6	151	192	97.5	94.2	18.0
3	60.0	25.6	25.5	123	191	97.9	94.7	19.6
4	67.5	25.0	24.9	197	202	96.7	93.3	15.5

129

Table 4.34 shows the monthly average temperature of the storage tank for the top layer and the entire tank. On all cases, the lower temperatures occurs during the month of January where the heating load is the most important (Table 3.6). During that month, the maximum tank temperatures are observed for a tilt angle of 60°, which corresponds precisely to the highest performances of the solar combisystem (Figures 4.30 and 4.31). For its actual configuration, this implies that the system has to be designed to deliver high temperatures in the storage tank during the "peak period" of heating loads, in order to achieve greater solar fraction and COP values.

Table 4.34. Temperature in the storage tank for different tilt angles

Tilt angle	Top layer temperature												
[°]	Jan	Feb	Mar	Apr	May	Jun	Jul	Aug	Sep	Oct	Nov	Dec	Year
37.5	33.2	38.8	71.8	88.4	86.6	80.5	83.5	84.7	83.7	77.9	75.0	68.3	72.9
45.0	38.4	44.7	78.3	89.0	85.9	82.3	85.6	82.2	84.0	82.0	77.2	71.6	75.3
52.5	42.4	47.4	79.4	88.7	87.4	84.0	84.6	82.5	84.9	82.9	79.1	74.2	76.6
60.0	43.3	54.8	82.0	89.1	86.2	84.1	82.8	83.0	84.1	81.8	77.8	73.6	77.0
67.5	40.8	55.2	81.7	88.3	84.8	82.3	82.2	82.4	86.0	82.1	77.1	74.1	76.5
Tilt angle	Average temperature												
[°]	Jan	Feb	Mar	Apr	May	Jun	Jul	Aug	Sep	Oct	Nov	Dec	Year
37.5	25.9	27.8	41.5	67.9	81.1	76.7	78.2	78.7	77.9	72.6	62.2	48.1	61.7
45.0	27.7	29.5	45.6	71.4	81.0	77.5	80.1	77.4	76.3	73.9	64.0	51.2	63.2
52.5	29.5	30.3	46.7	71.6	81.9	79.1	79.6	76.8	77.7	75.0	65.9	53.9	64.2
60.0	29.8	32.2	49.6	73.3	81.6	79.1	77.8	76.4	76.2	73.7	64.2	52.9	64.0
67.5	28.6	32.2	49.2	71.3	78.2	76.3	75.4	74.3	77.3	75.3	64.5	53.4	63.1
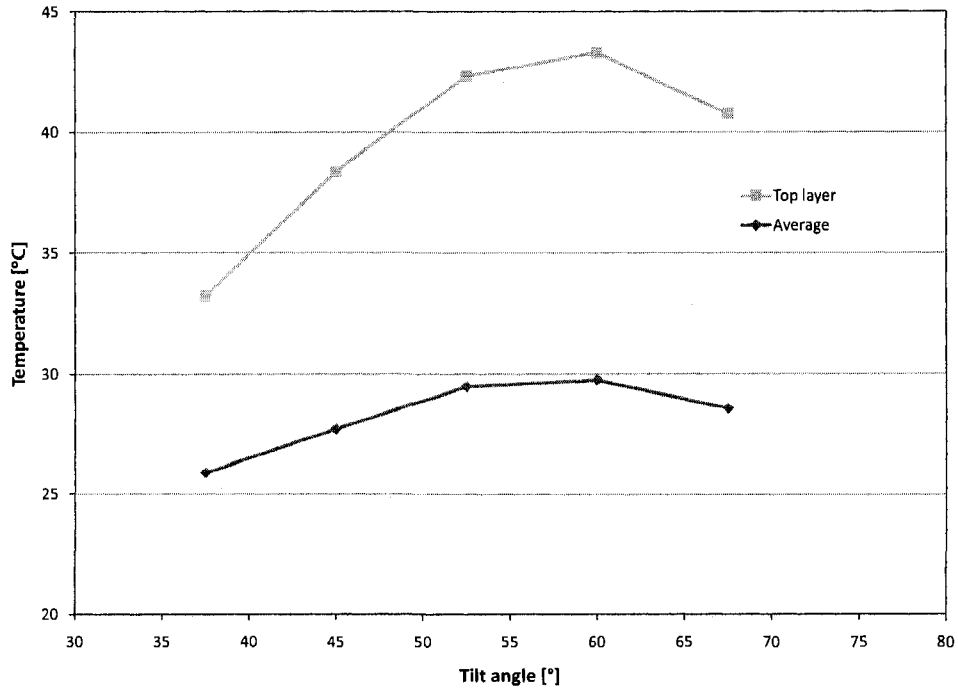
Figure 4.30. Variation of the storage tank temperature with the tilt angle during the month of January
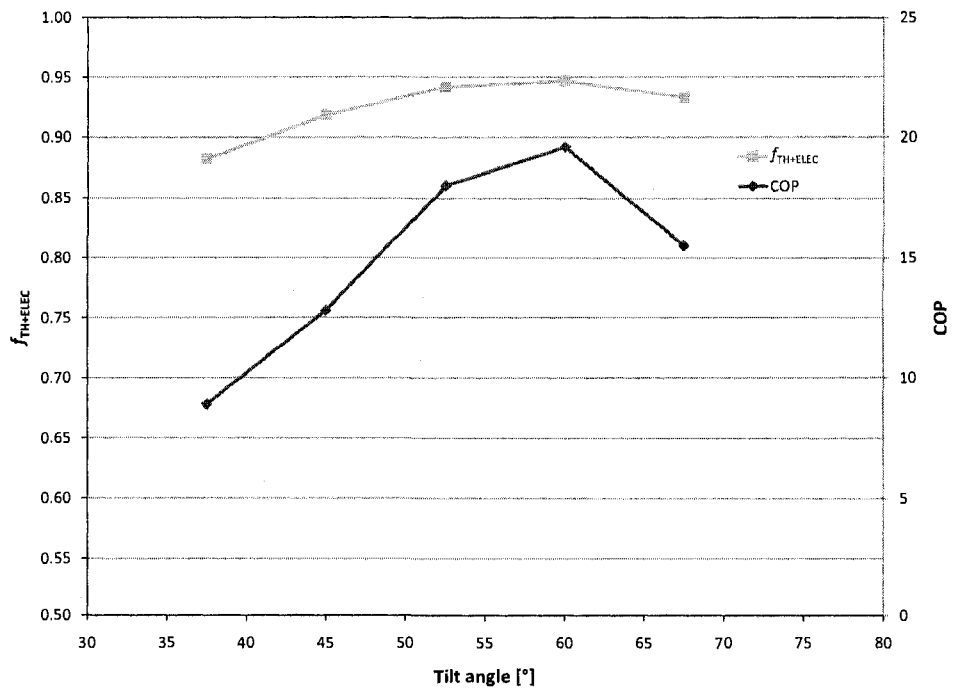
Figure 4.31. Variation of $\eta_{TH+ELEC}$ and the COP with the tilt angle

131

4.6.2 Flat-plate collectors

To consider the impact of flat-plate collectors on the solar combisystem, Type 538, previously used to model the Vitosol 300 SP3 evacuated tubes solar collector, is replaced by Type 537. The model Vitosol 100 SV1 from Viessmann (2008) is selected. Some technical data are shown in Table 4.35 (see full specifications, Appendix E). Since its gross area is relatively smaller than the Vitosol 300 (Table 4.3), three rows of seven collectors are required so that the total area is 53.0 m^2, which is similar to 51.4 m^2 for the evacuated tube collectors. The storage tank volume remains at 38.6 m^3, the flow rate of the Solar pump n°1 at 40 kg/(h·m^2) of collectors, and the tilt angle at 45°.

Table 4.35. Solar collector technical data (SRCC, 2008)

Gross area		[m^2]	2.523
Net aperture area		[m^2]	2.334
Flow rate at test conditions		[kg/s]	0.050
Optical efficiency	a_0	[-]	0.7162
Heat loss coefficient	a_1	[W/(m^2·K)]	3.0562
	a_2	[W/(m^2·K^2)]	0.1232

Note: test fluid = propylene glycol & water

As an example and in order to illustrate the performance of the collector, the solar collector thermal efficiency for three different weather conditions are calculated based on Equation 4.1, assuming K_θ equal to 1 (Figure 4.32). If the temperature difference $T_i - T_o = 50°C$, the collector efficiency is about 8% on a clear day and is null on a cloudy day. Therefore, compared to evacuated tube collectors, the performance is much more affected by cold outside temperatures (Figure 4.5).
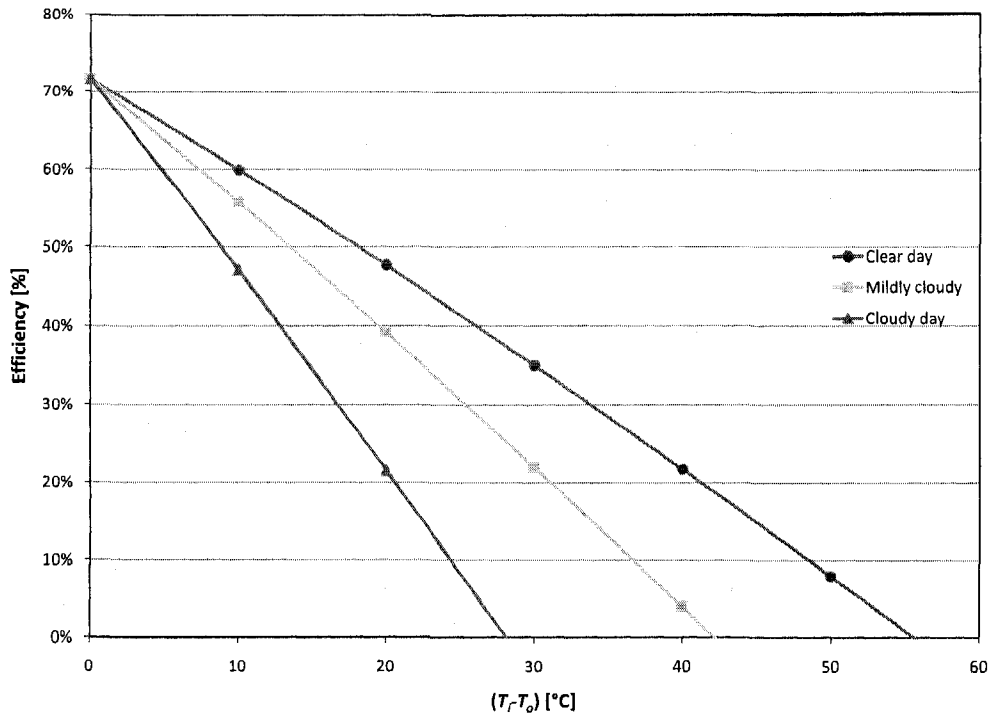
Figure 4.32. Solar collector efficiency

Influence of the tank insulation

The performance of the solar combisystem is presented in Table 4.36 with (base case) and without (alternative 1) the consideration of the tank insulation. Results shows that the collection efficiency is reduced from values around 25.6% for evacuated tube collectors (Table 4.29) to approximately 20%. This implies a significant drop for the solar fraction as it goes down to less than 90%. Consequently, it is decided not to proceed to further investigations on consequences of a reduction of the storage tank volume and the number of collectors, as it would not represent exactly the concept of a seasonal storage system. Finally, the alternative 1 (insulated tank) is considered as the "new base case".

Table 4.36. Influence of the tank insulation on the performance of the solar combisystem

Alternative	η_{TH} [%]	$\eta_{TH+ELEC}$ [%]	Q_{aux} [kWh]	Q_{pumps} [kWh]	$\mathscr{F}_{TH}$ [%]	$\mathscr{F}_{TH+ELEC}$ [%]	COP [-]
Base case	19.0	18.9	700	167	88.2	85.4	8.5
1	20.8	20.7	1,079	191	81.8	78.6	5.0

Influence of the operating mass flow rate of Solar pump n° 1

The mass flow rate of antifreeze circulating in the collectors $\dot{m}_{solar}$ is varied between 15 and 51 kg/(h·m^2). The minimum value corresponds to the minimum flow rate recommended by the manufacturer for flat-plate collectors (Viessmann, 2008). The best performance is achieved by the alternative 2 as it is the only to increase the solar fraction and the COP. Such system is preferred as it also reduces the piping size. It is noteworthy to observe that, despite higher operating flow rates, the alternative 3 has a lower energy use for pumps. It can be explained by the fact that the Solar pump n°1 is turned on and off constantly during the summer. Indeed, since the efficiency of the collector is higher at this period, the outlet temperature becomes too hot too quickly and the pump has to be stopped.

Table 4.37. Performance of the solar combisytem for different values of $\dot{m}_{solar}$

Alternative	Flow rate [kg/(h·m^2)]	η_{TH} [%]	$\eta_{TH+ELEC}$ [%]	Q_{aux} [kWh]	Q_{pumps} [kWh]	$\mathscr{F}_{TH}$ [%]	$\mathscr{F}_{TH+ELEC}$ [%]	COP [-]
Base case	40	20.8	20.7	1,079	191	81.8	78.6	5.0
1	15	19.8	19.8	1,150	167	80.6	77.8	4.8
2	27	20.8	20.7	954	172	83.9	81.0	5.6
3	51	21.0	21.0	1,144	158	80.7	78.1	4.9

Influence of the tilt angle

Five alternatives are proposed for the tilt angle. At 37.5°, the solar fraction $\mathscr{F}_{TH+ELEC}$ is reduced by about 5.6% and the COP by 1.1 (Table 4.38). Then, by incrementing the tilt angle by 7.5° up to 67.5°, the performance is improved as the solar fraction goes up to

88.9% and the COP to 9.6.

Table 4.38. Performance of the solar combisytem for different tilt angles

Alternative	Tilt angle [°]	η_{TH} [%]	$\eta_{TH+ELEC}$ [%]	Q_{aux} [kWh]	Q_{pumps} [kWh]	$\mathscr{F}_{TH}$ [%]	$\mathscr{F}_{TH+ELEC}$ [%]	COP [-]
Base case	45.0	20.8	20.7	1,079	191	81.8	78.6	5.0
1	37.5	20.2	20.2	1,406	195	76.3	73.0	3.9
2	52.5	20.6	20.6	787	193	86.8	83.5	6.5
3	60.0	20.4	20.3	605	196	89.8	86.5	7.9
4	67.5	19.2	19.2	451	207	92.4	88.9	9.6
5	75.0	17.9	17.9	488	223	92.3	88.5	9.4

Table 4.39 shows the monthly average temperature of the storage tank for the top layer and the entire tank. The average temperature of the storage tank during summer is superior by approximately 9-10°C compared to the case where evacuated tube collectors are used (Table 4.34). Indeed, more solar energy is transmitted to the solar tank thanks to the higher efficiency of flat-plate collectors during warmer months (Figure 4.32). However, as soon as the outdoor temperature decreases significantly (typically in November), the top layer and average temperature drops at a faster pace since less energy is collected. This results in lower temperatures (compared to the case with evacuated tube collectors) in the storage tank during two first months of the year.

Table 4.39. Temperature in the storage tank for different tilt angles

Tilt angle	Top layer temperature												
[°]	Jan	Feb	Mar	Apr	May	Jun	Jul	Aug	Sep	Oct	Nov	Dec	Year
37.5	29.5	28.0	52.5	79.5	89.9	91.9	91.2	88.8	88.8	88.4	79.7	68.8	73.3
45.0	31.4	29.7	57.3	80.7	89.6	91.8	91.0	87.8	88.3	88.4	79.2	70.7	74.1
52.5	34.8	31.4	59.3	80.5	88.3	92.5	90.0	89.5	88.2	86.3	77.6	71.2	74.4
60.0	37.2	32.4	59.2	78.7	85.5	91.5	91.7	88.9	88.9	87.6	79.4	74.2	74.8
67.5	40.3	32.8	57.1	74.8	80.4	85.1	88.9	90.4	91.4	88.0	81.3	76.0	74.1
75.0	41.2	32.1	50.8	66.4	71.4	74.4	76.9	81.5	89.5	90.3	81.0	75.7	69.5

Tilt angle	Average temperature												
[°]	Jan	Feb	Mar	Apr	May	Jun	Jul	Aug	Sep	Oct	Nov	Dec	Year
37.5	24.8	23.6	30.0	47.0	73.8	91.2	90.9	88.5	88.4	87.9	73.7	52.2	64.6
45.0	25.5	24.2	31.7	49.0	73.5	90.9	90.8	87.6	88.0	87.9	73.2	53.8	64.9
52.5	26.7	24.9	32.8	49.4	70.5	89.5	89.1	88.9	88.0	86.0	71.3	53.6	64.4
60.0	27.7	25.3	32.9	47.4	64.3	82.6	90.4	88.4	88.4	87.1	73.4	56.8	63.9
67.5	29.2	25.4	31.8	43.1	55.3	68.0	77.1	85.8	90.6	87.3	75.2	59.1	60.9
75.0	29.8	25.2	29.7	36.8	43.9	51.4	57.1	64.2	77.1	87.9	74.7	58.6	53.2

In February, the maximum tank temperatures are observed for a tilt angle of 67.5°, which corresponds to the highest performances of the solar combisystem (Figures 4.33 and 4.34).
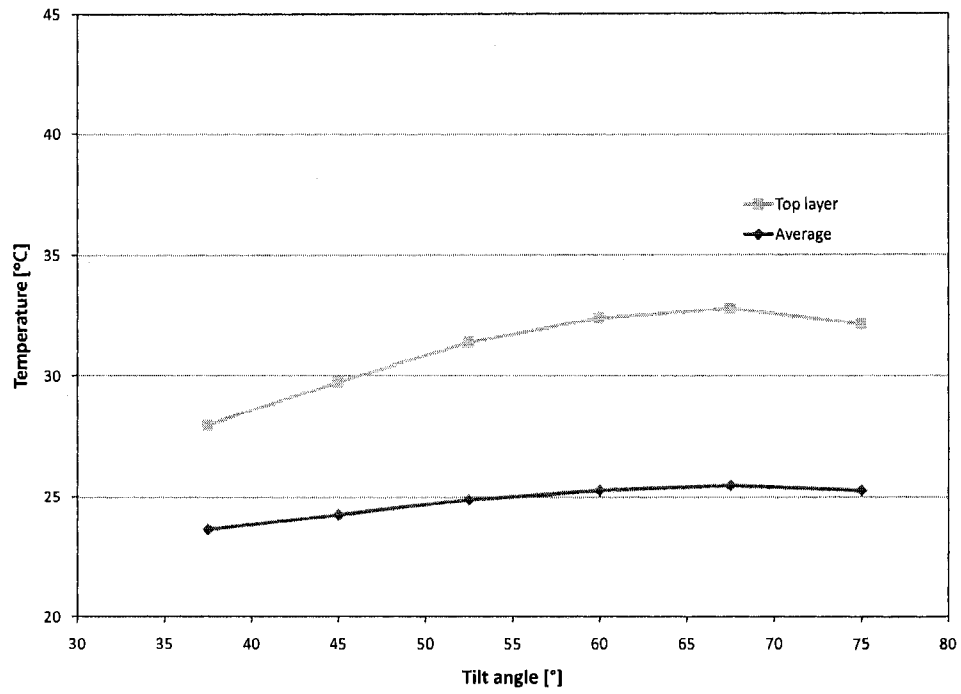
Figure 4.33. Variation of the storage tank temperature with the tilt angle during the month of February
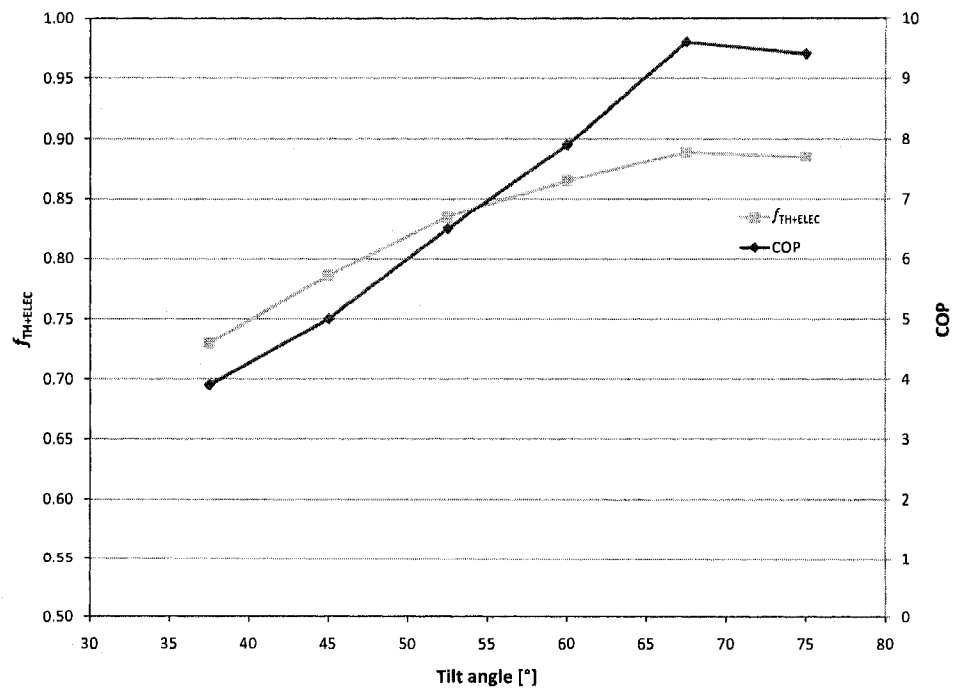
Figure 4.34. Variation of $\eta_{TH+ELEC}$ and the COP with the tilt angle

137

4.6.3 Solutions proposed

Based on the sensitivity analysis, two final design alternatives are proposed to pursue this study (Table 4.40).

Table 4.40. Proposed design alternatives

Alternative	Type of collector	Area [m^2]	Tank volume [m^3]	$\dot{m}_{solar}$ [kg/(h·m^2)]	Tilt angle [°]
1	Evacuated tube	47.1	34.7	25	60.0
2	Flat-plate	53.0	38.6	27	67.5

These two alternatives can not be seen exactly as total seasonal storage systems since a small quantity of auxiliary energy is required (Table 4.41). Yet, this remains limited since values of solar fraction are superior to 90%. The total electricity use of the solar combisystem Q_{combi} required to provide space heating and hot water is equal to the sum of the energy use required by the pumps and the auxiliary energy, which gives 365 kWh (1.3 GJ) for the alternative 1 and 567 kWh (2.0 GJ) for alternative 2. This represents a considerable reduction compared to the electricity use of 10,704 kWh (38.5 GJ) in the "best case" house using the baseboard heaters and the conventional electric water heater.

Table 4.41. Performance of the design alternatives

Alternative	η_{TH} [%]	$\eta_{TH+ELEC}$ [%]	Q_{aux} [kWh]	Q_{pumps} [kWh]	$\mathscr{F}_{TH}$ [%]	$\mathscr{F}_{TH+ELEC}$ [%]	COP [-]	Q_{combi} [kWh]
1	26.7	26.6	200	165	96.6	93.9	17.0	365
2	19.1	19.0	382	185	93.6	90.5	11.1	567

Chapter 5

Life cycle performance of the seasonal storage system

This chapter presents the analysis of the life cycle cost and life cycle energy use of the two seasonal storage alternatives previously studied in Chapter 4.

5.1 Life cycle cost

The life cycle cost of the seasonal storage system, defined as the sum of its initial cost and the Present Worth (PW) of the operating cost over a 30 years period, is investigated in this section. The simple and improved payback are calculated to assess the return on investment.

5.1.1 Initial cost

A rough approximation is proposed to estimate the initial cost of the system as several important assumptions are used:

- The costs do not include the installation and maintenance;

- The storage tank is manufactured in Switzerland and only available in Europe (Jenni, 2008);

139

— The costs of the two external heat exchangers are not considered since no information has been found;

— The costs of the control units are assumed based on the solar tank manufacturer's documentation.

Since the combisytem provides space heating and domestic hot water, the electric baseboard heaters and the conventional electric water heater are not necessary. Therefore, both alternatives are credited with the initial costs of these systems. However, the additional cost of cross-linked polyethylene pipes (PEX) integrated in the radiant heating floor needs to be considered. Also, the flat-plate collectors are supposed integrated to the roof, which implies the substitution of an equivalent surface of asphalt shingles.

The initial cost is estimated at 58,162 $ for alternative 1 and 39,949 $ for alternative 2 (Table 5.1). The main cost difference comes from the collectors where evacuated tube (35,603 $) represent more than twice the price of flat-plate collectors (17,238 $).

Table 5.1. Initial cost of the solar combisystem

System component	Alternative 1 [$]	Alternative 2 [$]	Source of data
Storage tank	12,031	13,023	Jenni (2008)
Tank insulation	4,777	5,138	Jenni (2008)
Conventional storage tank	-1,053	-1,053	RSMeans (2007)
Electric baseboard heaters	-3,097	-3,097	RSMeans (2007)
Radiant floor (PEX pipes)	2,502	2,502	RSMeans (2007)
Solar collectors	35,603	17,238	Viessmann (2008)
Shingles (credit for integrated mounting)	-	-1,201	RSMeans (2007)
Control unit	2,280	2,280	Jenni (2008)
Pumps Stratos ECO	1,328	1,328	Wilo (2008)
Pump Stratos ECO-ST (Solar pump n°1)	474	474	Wilo (2008)
Tankless water heaters	1,331	1,331	Eemax (2008)
Copper pipes	1,784	1,784	RSMeans (2007)
Piping insulation	202	202	RSMeans (2007)
Total	58,162	39,949	

5.1.2 Operating cost

Based on the total electricity use of the solar combisystem Q_{combi} (Table 4.41) and using the electricity rates of Hydro-Quebec (2008), the annual operating costs are estimated at 26 $ for the alternative 1 and 40 $ for the alternative 2.

The inflation rate of electricity is assumed at 2% and the effective interest rate at 3.22% , which corresponds to default economic conditions used in Chapter 3. The degradation of performance is not considered. Based on Equations 3.6 and 3.8, the PW and the life cycle cost are then equal to 637 $ and 58,799 $ for the design alternative 1; 990$ and 40,939 $ for the alternative 2.

5.1.3 Simple payback

The simple payback of the solar combisystem is calculated as:

$$\text{Payback} = \frac{C_i}{\text{Solar Savings}} \tag{5.1}$$

where:

Payback = simple payback [years];

C_i = initial cost [$]; and

Solar Savings = savings for space and water heating, due to the proposed design alternative during the first year of operation [$].

As shown in Table 5.3, the simple payback is 79.4 years for alternative 1 and 55.6 years for alternative 2.

Table 5.3. Simple payback of the design alternatives

Alternative	Electricity use [kWh]	Operating cost[1] [$]	Solar Savings [$]	Simple payback [years]
"Best case"	10,704	759	-	-
1	365	26	733	79.4
2	567	40	719	55.6

[1] Based on Hydro-Quebec electricity rates (see Chapter 3).

5.1.4 Improved payback

Compared to the simple payback, the improved payback is a much more realistic approach as it considers the time value of money. Defined as the period required for the cumulative savings to equal the initial cost of the system, it is found by solving the following equation for N (ASHRAE, 2007):

$$C_i = \frac{\text{Solar Savings} \, (1 + j_E)^{N-1}}{(1 - i')^N} \tag{5.2}$$

where:

C_i =   initial cost of the design alternative [$];

Solar Savings   =   savings due to the proposed design alternative during the first

         year of operation [$];

j_E =   inflation rate of electricity [-];

i' =   effective interest rate [-]; and

N =   number of years [-].

The inflation rate of electricity is assumed at 2% and the effective interest rate at 3.22%. Based on these assumptions, the cumulative savings are calculated from Equation 5.2.

As shown in Figure 5.1, the solar combisystem is not able to payback its installation costs. Yet, 50% of the installation costs are recovered after 55 years for the alternative 1, and 34 years for the alternative 2.
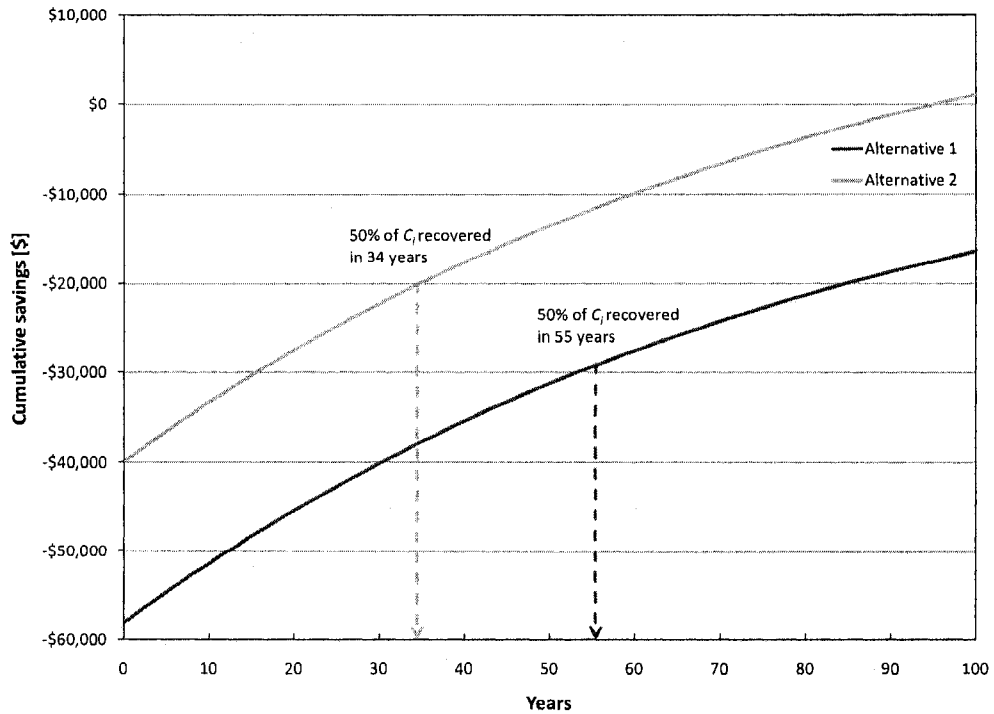
Figure 5.1. Cumulative savings of the design alternatives

If the inflation rate of electricity goes up to 4%, the curve of cumulative savings presents a different shape as the payback period for the alternative 1 is achieved after 64 years and after 48 years for the alternative 2 (Figure 5.2).

143
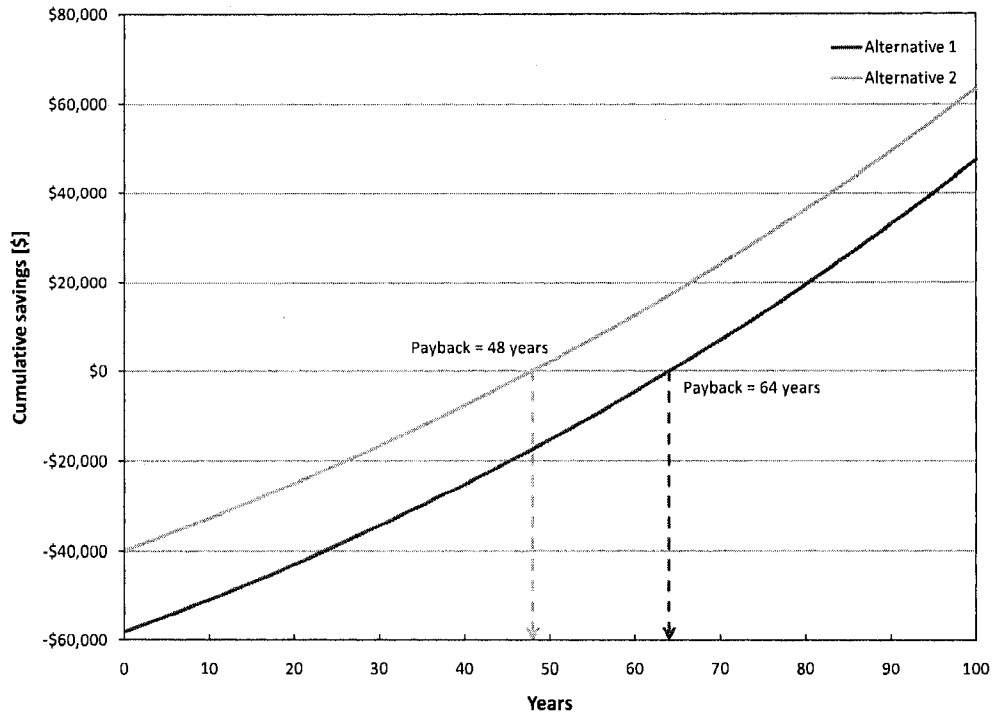
Figure 5.2. Impact of the inflation rate of electricity on cumulative savings

Through its ecoEnergy Retrofit program, Natural Resources Canada provides financial support to homeowners to help them implement energy saving projects that reduce energy-related greenhouse gases and air pollution (NRCan, 2008). It offers a 500 $ grant for the installation of a solar domestic hot water system.

Recently, the inflation rate j has surged and is now measured at 3.5% in Canada (Statistics Canada, 2008). So, by considering the ecoEnergy rebate, the current discount rate i of 4.75% (August 2008) and assuming the inflation of electricity j_E equals to the inflation, the system is now able to recover its installation costs over a 45 years period for the alternative 1, and over 36 years for alternative 2 (Figure 5.3).

As illustrated previously, a grant of 500 $ is not sufficient to reduce significantly the payback period of the seasonal storage system. Much more "generous" programs than ecoEnergy

144
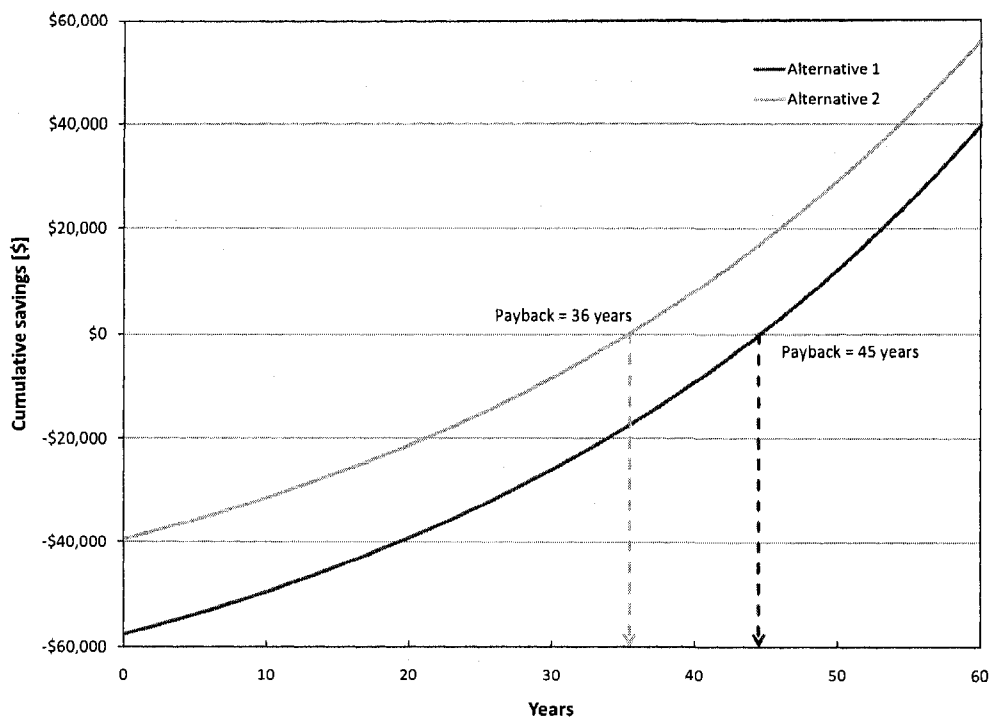
Figure 5.3. Impact of recent economical data and ecoEnergy program on cumulative savings

exist in other part of the world. For instance, in Belgium, the federal government covers up to 40% of the investment costs (with a maximum of 5,200 $) as tax rebates for the installation of a solar thermal system (SPF Economy, 2008). The Walloon Region adds a grant of 2,280 $ for systems with a net aperture area of collectors ranging between 2 and 4 m², and 150 $ per additional m² (Walloon Region Ministry, 2008). Also, residents of the Wallonia's capital (Namur) benefit from an additional 380 $ from the city authorities (City of Namur, 2008). So, if such a program would exist in Canada, the total of grants would be 12,748 $ for alternative 1 and 14,679 $ for alternative 2. Using the same rates as the previous scenario, this would imply a payback time period of 38 years for alternatives 1 and 26 years for alternative 2.
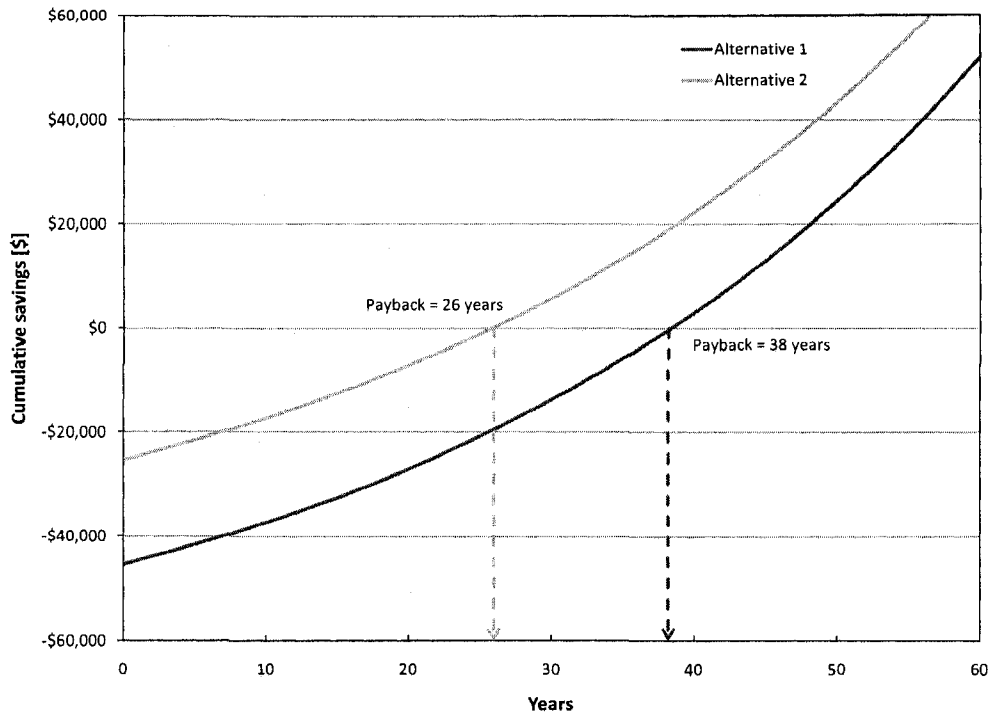
Figure 5.4. Impact of incentives on cumulative savings

5.1.5 Discussion

The (improved) payback period of the seasonal storage system is quite long as, depending on the economic scenario, it ranges from 55 to 38 years for the alternative 1, and from 34 to 26 years for the alternative 2 (Table 5.5). The only way to obtain a payback period lower than the 30-years life span of the system, is to benefit from substantial incentives. These results are seen as the direct consequence of the high initial costs of the systems in addition to the low rates of electricity in Quebec, compared to other Canadian provinces (BC Hydro, 2003).

Table 5.5. Improved payback for different economic situations

i [%]	j [%]	i' [%]	j_E [%]	Grant [$]	Payback$_{50\%}$ [years]	Payback [years]	Grant [$]	Payback$_{50\%}$ [years]	Payback [years]
					Alternative 1			Alternative 2	
5.54	2.24	3.22	2.00	-	55	-	-	34	-
5.54	2.24	3.22	4.00	-	36	64	-	26	48
4.75	3.50	1.21	3.50	500	28	45	500	21	36
4.75	3.50	1.21	3.50	12,748	18	38	14,679	7	26

5.2 Life cycle energy use

The life cycle energy use relates to the total energy input over the entire life span of the solar combisystem. Within the scope of this study, the embodied energy of the system's components and the total operating energy use are evaluated. The estimation does not take into account the energy required for the unit packing, transportation, installation and maintenance.

5.2.1 Embodied energy

The estimation of the embodied energy of the two design alternatives is based on some important assumptions:

- The embodied energy of the storage tank, pumps, piping and external heat exchangers is limited to an approximation of the embodied energy of materials;

- The tankless water heaters providing auxiliary energy for space heating and hot water are not considered.

The embodied energy of the evacuated tube collectors is based on one study due to the lack of detailed information available in the literature. Therefore, the embodied energy is assumed at 1,521 MJ/m^2, and 71,717 MJ for the total collector area of 47.1 m^2(Gürzenich and Mathur, 1998). The assessment of the total embodied (primary) energy required to produce

a complete flat-plate collector is based on several studies (Table 5.6). The results show some dissimilarities since (i) the materials used in the solar collectors are not all identical, and (ii) the authors are coming from distinct countries implying different calculation of the primary energy. Considering these limits, the average value of 1,732 MJ/m^2 is then considered. For the total collector area (53 m^2), the embodied energy is calculated at 91,766 MJ.

Table 5.6. Embodied energy of flat-plate solar collectors

A_c [m^2]	Embodied energy [MJ]	[MJ/m^2]	Country	Authors
2.13	3,513	1,649	Italy	Ardente et al. (2005)
1.35	2,663	1,973	Cyprus	Kalogirou (2008)
5.00	6,408	1,282	Germany	Streicher et al. (2004)
5.00	8,633	1,727	Germany	Streicher et al. (2004)
6.15	11,450	1,862	Germany	Gürzenich and Mathur (1998)
5.76	9,790	1,700	Germany	Gürzenich and Mathur (1998)
2.00	3,604	1,802	India	Gürzenich and Mathur (1998)
	Average	1,732		

The calculation of the total embodied energy is shown in Table 5.7. The storage tank is supposed entirely made of stainless steel (16.3 MJ/kg) and recovered by 20 cm of mineral wool (15.6 MJ/kg). Copper pipes (48.7 MJ/kg) between the collectors and the storage tank have a diameter of 31.8 mm and are insulated with fiberglass (30.3 MJ/kg) over a total length of 20 m. The heat exchangers are made of stainless steel (16.3 MJ/kg) (GEA, 2008); the pumps of stainless steel and grey cast iron (32.8 MJ/kg) (Wilo, 2008).

The electric baseboard heaters previously used to heat the "best case" house are assumed exclusively made of aluminium (58.5 MJ/kg). They are deducted from the total as well as the conventional electric water heater (6,155 MJ) (Streicher et al., 2004) and the roof shingles (76.6 MJ/m^2). The additional embodied energy due the PEX pipes (103.0 MJ/kg) integrated in the radiant floor is considered.

Table 5.7. Total embodied energy of the design alternatives

Element	Flat-plate			Evacuated tube		
	$[m^2]$	$[MJ/m^2]$	$[MJ]$	$[m^2]$	$[MJ/m^2]$	$[MJ]$
Collectors	53.0	1,732	91,766	47.1	1,521	71,717
Shingles (credit for roof integration)	53.0	76.6	-4,058	-	-	-
	$[kg]$	$[MJ/kg]^1$	$[MJ]$	$[kg]$	$[MJ/kg]^1$	$[MJ]$
Storage tank (stainless steel)[2]	3,744.2	16.3	62,918	3,369.8	16.3	54,927
Insulation (20 cm, mineral wool)	260.2	15.6	4,064	260.2	15.6	4,064
Piping (copper)	30.9	48.7	1,504	30.9	48.7	1,504
Piping insulation (fiberglass)	2.8	30.3	85	2.8	30.3	85
Antifreeze	55.0	42	2,311	35.1	42	1,476
Solar heat exchanger	14.0	16.3	228	14.0	16.3	228
DHW heat exchanger	7.2	16.3	117	7.2	16.3	117
Pumps	12.0	24.6	295	12.0	24.6	295
Electric baseboard heaters	69.5	58.5	-4,058	69.5	58.5	-4,058
Conventional storage tank	-	-	-5,659	-	-	-5,659
		Total	157,870		Total	134,689

[1] From Yang (2005).

[2] The total weight of the storage tank is given by Jenni (2008).

The total embodied energy of the solar combisystem is approximated at 157,870 MJ for the alternative 1 and 134,689 MJ for the alternative 2.

5.2.2 Operating energy use

To assess the operating energy (primary), the annual electricity use of both combisystems Q_{combi} (Table 4.41) is divided by the overall power plant efficiency η_{pp} of 73.1% (see Chapter 3). Assuming that the annual energy use remains constant over the 30-years life span of the system, regardless of the efficiency decrease of the mechanical systems or equipments, the total operating energy use is thus equal to 30 times the annual operating energy use, and its value is calculated at 53.9 GJ for the alternative 1 and 83.8 GJ for the alternative 2.

The life cycle energy use of the seasonal storage system is the sum of its embodied energy

(Table 5.7) and the operating energy use over 30 years, which gives 188.6 GJ and 241.6 GJ.

5.2.3   Energy payback time

The energy payback time (EPT) is defined as the time (in years) in which the amount of primary energy required to manufacture the solar combisystem is compensated by the energy produced (Richards and Watt, 2007):

$$\text{EPT} = \frac{E_{input}}{W_{net,primary}} \tag{5.3}$$

where:

EPT $\quad\quad=\quad$ energy payback time [years];

$E_{input} \quad\quad=\quad$ embodied energy of the system [GJ]; and

$W_{net,primary} \quad=\quad$ annual net energy output in primary energy equivalent [GJ/yr].

The value of $W_{net,primary}$ is calculated as:

$$W_{net,primary} = \frac{Q_{loads} - Q_{combi}}{\eta_{pp}} \tag{5.4}$$

With energy payback time values of 4.9 years for the alternative 1 and 6.0 years for the alternative 2 (Table 5.9), the results are higher than the typical energy payback times of solar combisystems (without long-term storage capacity) ranging from 2.0 to 4.3 years (Streicher et al., 2004). Yet, such difference is easily explained by the higher overall efficiency of power plants in Quebec (73.1%) compared to Germany (35.0%).

150

Table 5.9. Energy payback time of the design alternatives

		Alternative 1	Alternative 2
Q_{loads}	[GJ/yr]	21.4	21.4
Q_{combi}	[GJ/yr]	1.3	2.0
E_{input}	[GJ]	134.7	157.9
$W_{net,primary}$	[GJ/yr]	27.4	26.4
EPT	[years]	4.9	6.0

5.2.4 Energy yield ratio

The energy yield ratio (EYR) is defined as "how many times the energy invested is returned by the system in its entire life" (Watt et al., 1998). Higher ratio values show better performance. Contrary to the energy payback time, this indicator considers the life span of the solar combisystem and hence provides more meaningful results. It is given by:

$$\text{EYR} = \frac{L_{combi}W_{net,primary}}{E_{input}} \tag{5.5}$$

where L_{combi} is the life span of the combisystem (30 years). So, the EYR for the alternative 1 is calculated at 6.1 and 5.0 for the alternative 2. It is quite lower than values ranging from 7.5 to 12.6 calculated for typical combisystems (without long-term storage) in Germany (Gürzenich and Mathur, 1998). As for the EPT, this difference must be credited to the higher overall efficiency of power plants in Quebec.

According to Gagnon (2008), hydropower is the most efficient solution to generate energy with EYR between 205 and 280, followed by wind power with EYR between 18 to 34. The seasonal storage system is yet an appropriate solution to mitigate climate change comparatively to other options like, for example, photovoltaics with EYR between 3 and 6, or ethanol from corn (oil and gas as energy input) with EYR of 1.3.

5.2.5 Discussion

The life cycle cost analysis shows that the proposed design alternatives do not provide rational payback periods by considering default economic conditions. However, with higher rates of inflation and with some incentives, the initial costs can be recovered after a more reasonable period of time.

The great potential of energy savings of the solar combisystem is very well demonstrated on a life cycle basis. Indeed, the energy payback time and energy yield ratio for both systems present acceptable values for such a large system. Comparatively to the second alternative using flat-plate collectors, the first performs better in terms of energy payback time and energy yield ratio. Due to the higher efficiency of evacuated tube in cold climates, it requires less collector area and less storage tank volume. Therefore, less material - meaning a lower embodied energy - is required to achieve approximately the same level of performance $(W_{net,primary})$.

Chapter 6

Conclusions, contributions and future work

6.1 Conclusions

This research has presented the development of the integrated building model of a typical single family house in Montreal by using the TRNSYS 16 simulation program. Several design alternatives have been proposed to improve the life cycle performance of the building, including the life cycle energy, environmental impacts and life cycle cost.

The modelling of a solar thermal application for space and water heating with a long-term storage capacity is carried out. The overall performance of the system is investigated and enhanced by performing a sensitivity analysis on a certain set of design parameters. The life cycle analysis is performed to assess the potential of cost and energy savings of the system during its entire life span.

The results of the present study lead to the following conclusions:

- The life cycle performance of a single family house can be significantly enhanced by combining a passive solar design, high level of thermal insulation, high performance windows and airtightness of the building envelope;

- The life cycle energy and emission of the house are reduced by choosing materials

with low embodied energy;

– The solar combisystem with seasonal storage capacity is a concept that is achievable in a cold climate like Canada;

– The system performs better with evacuated tube collectors, compared to flat-plate collectors;

– The sensitivity analysis shows the essential role of the storage tank insulation on the sizing and the overall performance of the system;

– Key design features such as the tilt angle and the mass flow rate circulating in the solar loop have to be considered carefully;

– The life cycle energy analysis shows that the systems provide substantial energy savings.

More globally, the study reveals that the life cycle cost analysis of both the house and the solar combisystem are directly "affected" by the low electricity rates in Quebec. Indeed, the results would be totally different in other Canadian provinces and the proposed solutions would lower the payback periods drastically. In addition, since 95% of electricity in Quebec is generated by cleaner alternatives like hydropower (see Chapter 3), the life cycle energy use of the house and system is reduced. Though this can be perceived as an excellent news, this has the negative effect to lower the energy payback and market penetration of such "green alternatives".

6.2 Research contributions

This study has brought the following contributions:

– Review of existing and future projects of low energy and net-zero houses in different parts of the world;

– Identification of key design features for low energy buildings and solar combisystems;

– Modelling of an advanced solar combisystem with a long-term thermal storage capacity in a cold climate;

– One-dimension sensitivity analysis of the solar combisystem based on a certain set of design parameters;

– Investigation of the life cycle energy use and life cycle cost of the solar combisystem.

6.3   Recommendations for future work

Several research directions using this thesis as a starting point can be identified.

Solar combisystem

Although many design parameters of the solar combisystem are evaluated in this research, other aspects are expected to have a considerable impact:

– PV (photovoltaic) cells can be used to power the Solar pump n°1 and provide a continual adjustment of fluid flow, and possibly improving the system performance (Al-Ibrahim, 1997). Indeed, this system can act as a fast-response sensor to solar energy and therefore pumping will only occur at the times when the thermal collector is also receiving solar radiation. Also, the use of a PV power source eliminates the demand for an auxiliary power source to operate the pump;

155

- The degree of precision to model the storage tank can be enhanced by increasing the number of layers;

- The flow rate of the Solar pump n°2 can be fixed to limit the flow in the stratifying device to the recommended range of 5-8 kg/min (see Chapter 2);

- To avoid exploiting the hottest water in the tank (located in the top layer), different outlet locations can be investigated since the maximum water temperature for space heating is only 45°C;

- Since the storage tank is expected to store water at high temperatures during summer months, a sensitivity analysis on the thickness of insulation can be achieved to see the effect on the cooling loads of the house;

- To reduce the electricity use of the ventilation system, the hot water contained in the tank can be used to preheat the cold outdoor air in winter thanks to a heat exchanger.

Finally, this research can be extent to other locations in Canada to quantify the effect of different climatic conditions on the system's design. The life cycle performance, including the life cycle cost and energy savings, would be significantly affected as well due to higher utility rates and other source of electricity generation.

References

Aguilar, C., White, D., and Ryan, D. (2005). *Domestic Water Heating and Water Heater Energy Consumption in Canada.* CBEEDAC, Canadian Building Energy End-Use Data and Analysis Centre. University of Alberta, Edmonton, AB.

Aitken, D. (2003). Transitioning to a renewable energy future. In *ISES International solar energy society white paper, Freiburg.*

Al-Ibrahim, A. (1997). *Optimum Selection of Direct-Coupled Photovoltaic Pumping System in Solar Domestic Hot Water Systems.* PhD thesis, University of Wisconsin-Madison.

Andersen, E., Furbo, S., Hampel, M., Heidemann, W., and Muller-Steinhagen, H. (2008). Investigation on stratification devices for hot water heat stores. *International Journal of Energy Research*, 32:255–263.

Ardente, F., Beccali, G., Cellura, M., and Lo Brano, V. (2005). Life cycle assessment of a solar thermal collector. *Renewable Energy*, 30:1031–1054.

ASHRAE (2001). *ASHRAE Standard 62-2001. Ventilation for acceptable indoor air quality.* American Society of Heating, Refrigerating and Air-Conditioning Engineers, Inc., Atlanta.

ASHRAE (2004). *ASHRAE Standard 55-2004. Thermal environmental conditions for human occupancy.* American Society of Heating, Refrigerating and Air-Conditioning Engineers, Inc., Atlanta.

ASHRAE (2005). *ASHRAE Handbook-Fundamentals.* American Society of Heating, Refrigerating and Air-Conditioning Engineers, Inc., Atlanta.

ASHRAE (2007). *ASHRAE Handbook-HVAC Applications.* American Society of Heating, Refrigerating and Air-Conditioning Engineers, Inc., Atlanta.

ASHRAE Montreal Chapter (2007). Website. http://www.ashrae-mtl.org/ (Last accessed March 6, 2007).

ATHENA (2003). Environmental impact estimator v 3.0. Athena Sustainable Materials Institute. Ottawa, Canada.

Athienitis, A. K. and Santamouris, M. (2002). *Thermal Analysis and Design of Passive Solar Buildngs.* James & James.

Bales, C. and Persson, T. (2003). E xternal DHW units for solar combisystems. *Solar Energy*, 74:193–204.

Baouendi, R. (2003). Development of a prototype tool for the evaluation of sustainability of canadian houses. Master's thesis, Concordia University, Montreal, Canada.

BC Hydro (2003). Electric Rates Comparison. Technical report, BC Hydro. http://www.bchydro.com/rx_files/info/info9238.pdf (Last accessed December 13, 2007).

Beasley, D. and Clark, J. (1984). Transient response of a packed for thermal energy storage bed. *International Journal of Heat and Mass Transfer*, 27:1659–1669.

BedZED & Eco-Village Development (2007). Website. http://www.bioregional.com (Last accessed March 5, 2007).

Braun, J., Klein, S., and Mitchell, J. (1981). Seasonal storage of energy in solar heating. *Solar Energy*, 26:403–411.

CEPHEUS (2001). *Final Technical Report.* http://www.passivehouse.com (Last accessed March 7, 2007).

Charron, R. (2005). A review of low and net-zero energy solar homes initiatives. Technical report, CANMET Energy Technology Centre-Varennes, NRCan. http://cetc-varennes.nrcan.gc.ca (Last accessed March 5, 2007).

City of Namur (2008). Website. http://www.energie-namur.be/ (Last accessed September 26, 2008).

Cruickshank, C. A. and Harrison, S. J. (2006). Simulation and testing of stratified multi-tank, thermal storages for solar heating systems. In *EuroSun 2006*, Glasgow, UK.

Dayan, M. (1997). High performance in low-flow solar domestic hot water systems. Master's thesis, University of Wisconsin-Madison.

Dincer, I., Dost, S., and Li, X. (1997). Performance analyses of sensible heat storage systems for thermal applications. *International Journal of Energy Research*, 21:1157–1171.

DOE (2008). Website. U.S. Department of Energy.http://www.eere.energy.gov/ (Last accessed October 5, 2008).

Duffie, J. and Beckman, W. (2006). *Solar Engineering of Thermal Processes.* John Wiley & Sons Inc. 3rd Ed.

Eemax (2008). Website. http://www.tanklesswaterheaters.ca/ (Last accessed September 14, 2008).

Ellehauge, K. (2003). Final report: Solar Combisystems. Technical report, Altener. http://www.elle-kilde.dk/altener-comb (Last accessed October 5, 2008).

EnergyPlus (2007). *EnergyPlus Engineering Reference.* US Department Of Energy.

Environment Canada (2007). Canadian Climate Normals 1971-2000. http://www.climate.weatheroffice.ec.gc.ca (Last accessed July 9, 2007).

EQuilibrium Housing (2007). Website. http://www.cmhc-schl.gc.ca (Last accessed March 5, 2007).

Frei, U., Vogelsanger, P., and Homberger, D. (2000). Domestic hot water systems: testing, development, trends. In *3rd ISES-Europe Solar Congress, EuroSun 2000, Copenhagen.*

Fujitsu (2007). Website. http://www.fujitsugeneral.com/ (Last accessed December 5, 2007).

Gagnon, L. (2008). Civilisation and energy payback. *Energy Policy*, 39:3317–3322.

Gagnon, L., Bélanger, C., and Uchiyama, Y. (2002). Life-cycle assessment of electricity generation options: The status of research in year 2001. *Energy Policy*, 30:1267–1278.

Garg, H. P., Mullick, S. C., and Bhargava, A. K. (1985). *Solar Thermal Energy Storage.* Springer.

GEA (2008). Website. http://www.flatplate.com/ (Last accessed October 2, 2008).

Gerbasi, D. (2000). The Energy Performance of the NOVTEC Advanced House. Master's thesis, Concordia University.

Gürzenich, D. and Mathur, J. (1998). Material and energy demand for selected renewable energy technologies. Technical report, DLR - International Bureau of the BMBF.

Hadorn, J.-C. (2005). *Thermal energy storage for solar and low energy buildings.* IEA SHC.

Haines, G., Org, M., Barkan, A., and Pressnail, K. (2007). An economic and environmental comparison of standard versus energy efficient homes in toronto, canada. In *Sustainable Urban Areas*, Rotterdam, Netherlands.

Hamada, Y., Nakamura, M., Ochifuji, K., Yokoyama, S., and Nagano, K. (2003). Development of a database of low energy homes around the world and analyses of their trends. *Renewable Energy*, 28(2):321–328.

Hasnain, S. (1998). Review on sustainable thermal energy storage technologies, part 1: Heat storage materials and techniques. *Energy Conversion and Management*, 39:1127–1138.

Heimrath, R. (2003). Generic System #19: Centralized Heat Production, Distributed Heat Load. Technical report, IEA SHC - Task 26. http://www.iea-shc.org/outputs/task26/ (Last accessed March 28, 2008).

Hestnes, A. G., Hastings, R., and Saxhof, B. (2003). *Solar energy houses: strategies, technologies, examples*. James & James, 2nd edition.

Hunn, B. and Calafell, D. (1977). Determination of average ground reflectivity for solar collectors. *Solar Energy*, 19:87–89.

Hydro-Quebec (2008). Website. http://www.hydroquebec.com/ (Last accessed September 22, 2008).

IEA SHC (2007). International Energy Agency. Solar Heating and Cooling. Website. http://www.iea-shc.org (Last accessed March 8, 2007).

IPCC (2007). Intergovernmental panel on climate change. website. http://www.ipcc.ch/ (Last accessed November 2, 2007).

Jenni (2008). Website. http://www.jenni.ch/ (Last accessed September 21, 2008).

Jordan, U. and Vajen, K. (2001). Realistic domestic hot-water profiles in different time scales. Technical Report V. 2.0, FB. Physik, FG. Solar. Universität Marburg.

Kalogirou, S. (2008). Thermal performance, economic and environmental life cycle analysis of thermosiphon solar water heaters. *Solar Energy*. doi:10.1016/j.solener.2008.06.005.

Kassab, M. (2002). Improving the energy performance of houses in montreal using the life-cycle analysis. Master's thesis, Concordia University, Montreal, Canada.

Kasuda, T. and Archenbach, P. (1965). Earth temperature and thermal diffusivity at selected stations in the United States. *ASHRAE Transactions*, 71:61–74.

Keller, B. (1998). Low temperature heating and cooling systems for low-energy houses. Proved in practice. In *Proceedings of the IEA workshop "Future building forum - Low temperature heating systems in buildings"*, Royal Institue of Technology, Stockholm, Sweden.

Kenjo, L., Caccavelli, D., and Inard, C. (2003). A model of low flow solar domestic hot water system. In *8th International IBPSA Conference, Eindhoven, Netherlands*.

Kjärstad, J. and Johnsson, F. (2007). The european power plant infrastructure - Presentation of the Chalmers energy infrastructure database with applications. *Energy Policy*, 35:3643–3664.

Krause, T. and Jaehnig, D. (2002). Solar heating with a storage-integrated condensing gas burner. In *Indudstry Workshop, IEA-SHC Task 26*.

Liu, W., Davidson, J., and Mantell, S. (2000). Thermal analysis of polymer heat exchangers for solar water heating: A case study. *Journal of Solar Energy Engineering*, 122(2):84–91.

Lstiburek, J. (2002). Relative humidity. In *Proceedings of the Healthy Indoor Environments Conference, April 23, 2002, Austin, Texas.*

M. CONDE Engineering (2002). Thermophysical Properties of Brines. Technical report. http://www.mrc-eng.com/Downloads/Brine%20Properties.pdf (Last accessed February 1, 2008).

MNECCH (1997). Model National Energy Code of Canada for Houses. NRC, National Research Council of Canada. Canadian Commission on Buildings and Fire Codes. Ottawa, Canada.

Morrison, G., Budihardjo, I., and Behnia, M. (2005). Measurement and simulation of flow rate in a water-in-glass evacuated tube solar water heater. *Solar Energy*, 78:257–267.

Nallusamy, N., Sampath, S., and Velraj, R. (2007). Experimental investigation on a combined sensible and latent heat storage system integrated with constant/varying (solar) heat sources. *Renewable Energy*, 32:1206–1227.

Net-Zero Energy Home Coalition (2007). Website. http://www.netzeroenergyhome.ca/ (Last accessed March 8, 2007).

NRCan (2005). R-2000 Standard. Office of Energy Efficiency. http://oee.nrcan.gc.ca (Last accessed March 23, 2007).

NRCan (2006). *Energy Use Data Handbook, 1990 and 1998 to 2004.* Office of Energy Efficiency. http://oee.nrcan.gc.ca/Publications/statistics/handbook06 (Last accessed March 2, 2007).

NRCan (2008). Website. http://www.nrcan.gc.ca/ (Last accessed September 15, 2008).

Passive Houses in Europe, CEPHEUS (2007). Website. http://www.cepheus.de/ (Last accessed March 5, 2007).

Pierce, M. (2000). Energy saving window treatments. Cornell Cooperative Extension. Department of Design & Environmental Analysis, Cornell University.

Province of Quebec (1992). Regulation respecting energy conservation in new buildings. Publications du Québec, Québec.

RETScreen (2007). NRCan. website. http://www.retscreen.net/ (Last accessed June 29, 2007).

Richards, B. and Watt, M. (2007). Permanently dispelling a myth of photovoltaics via the adoption of a new net energy indicator. *Renewable and Sustainable Energy Reviews*, 11:162–172.

RSMeans (2007). *RSMeans Residential Cost Data 2007*, volume 26. RSMeans Comp., Kingston, MA.

Schnieders, J. and Hermelink, A. (2006). CEPHEUS results: measurements and occupants' satisfaction provide evidence for Passive Houses being an option for sustainable building. *Energy Policy*, 34(2):151–171.

SEL (2007). *TRNSYS 16*. A Transient Simulation Program. University of Wisconsin, Madison, WI.

Shah, L., Andersen, E., and Furbo, S. (2005). Theoretical and experimental investigations of inlet stratifiers for solar storage tanks. *Applied Thermal Engineering*, 25:2086–2099.

Smeds, J. and Wall, M. (2007). Enhanced energy conservation in houses through high performance design. *Energy and Buildings*, 39(3):273–278.

Solar Building Research Network (SBRN) (2007). Website. http://www.solarbuildings.ca (Last accessed March 5, 2007).

Solvis (2007). Website. http://www.solvis.de/ (Last accessed May 23, 2007).

SPF Economy (2008). Website. http://mineco.fgov.be/energy/ (Last accessed March 5, 2007).

SRCC (2008). Directory of SRCC certified solar collector ratings. Technical report, Solar Rating and Certification Corporation. http://www.solar-rating.org/ (Last accessed February 1, 2008).

Statistics Canada (2005). Electric power generation, transmission and distribution. Catalogue no. 57-202-XIE.

Statistics Canada (2008). Website. http://www.statscan.ca/ (Last accessed September 22, 2008).

Streicher, E., Heidemann, W., and Muller-Steinhagen, H. (2004). Energy payback time - A key number for the assessment of thermal solar systems. In *Proceedings of Eurosun 2004, 20-23 June 2004, Freiburg, Germany.*

Technischen Universität Berlin (2007). Website. http://www.tu-berlin.de/ (Last accessed April 5, 2007).

Tepe, R., Bales, C., Bony, J., Pittet, T., and Heimrath, R. (2004). Elements and examples of "Dream Systems" of solar combisystems. Technical report, IEA SHC - Task 26.

TESS (2007). *TESS Library Documentation.* Thermal Energy System Specialists, Madison, WI.

The Building Group, NRCan (2007). Website. http://www.buildingsgroup.nrcan.gc.ca (Last accessed March 6, 2007).

Thevenard, D. and Haddad, K. (2006). Ground reflectivity in the context of building energy simulation. *Energy and Buildings*, 38:972–980.

Thomsen, K. E., Schultz, J. M., and Poel, B. (2005). Measured performance of 12 demonstration projects - IEA Task 13 "Advanced solar low energy buildings". *Energy and Buildings*, 37(2):111–119.

Thür, A. (2007). *Compact Solar Combisystem*. PhD thesis, Danmarks Tekniske Universitet.

UNFCCC (2008). Website. United Nations Framework Convetion on Climate Change. http://unfccc.int/ (Last accessed March 2, 2008).

UNIPHIZ Lab (2007). Findgraph v 1.860. http://www.uniphiz.com/ (Last accessed July 26, 2007).

Van der Veken, J., Peeters, L., and Hens, H. (2005). Comparison of heating system in a residential building. In *Building Simulation 2005, Ninth International IBPSA Conference*. http://www.ibpsa.org/proceedings/BS2005/BS05_1277_1284.pdf (Last accessed October 10, 2007).

van Moeseke, G., Bruyère, I., and De Herde, A. (2007). Impact of control rules on the efficiency of shading devices and free cooling for office buildings. *Building and Environment*, 42:784–793.

Venmar (2007). Website. http://www.venmar.ca/ (Last accessed October 11, 2007).

Viessmann (2008). Website. http://www.viessmann.de/ (Last accessed January 31, 2008).

Wall, M. (2006). Energy-efficient terrace houses in Sweden: Simulations and measurements. *Energy and Buildings*, 38(6):627–634.

Walloon Region Ministry (2008). Website. General Directorate for Technology, Research and Energy. http://www.cepheus.de/ (Last accessed September 26, 2008).

Watt, M. E., Johnson, A. J., Ellis, M., and Outhred, H. R. (1998). Life-cycle air emissions from pv power systems. *Progress in Photovoltaics: Research and Applications*, 6:127–136.

Weiss, W. (2003). *Solar Heating Systems for Houses: A design handbook for solar combisystems*. IEA SHC.

Weiss, W., Bergmann, I., and Faninger, G. (2008). Solar Heat Worldwide - Markets and Contribution to the Energy Supply 2006. Technical report, IEA SHC.

Welfonder, T., Hiller, M., Holst, S., and Knirsch, A. (2003). Improvements on the capabilities of trnsys 15. In *Eighth International IBPSA Conference*, Eindhoven, Netherlands.

Wiedemann, T. (2004). *World in Transition: Towards Sustainable Energy Systems*. Inderscience Publishers.

Wilo (2008). Website. http://www.wilo.com/ (Last accessed March 29, 2008).

Yang, L. (2005). Life cycle analysis of the residential HVAC systems in montreal. Master's thesis, Concordia University.

Zmeureanu, R., Fazio, P., DePani, S., and Calla, R. (1998a). Development of an energy rating system for existing houses. *Energy and Buildings*, 29:107–119.

Zmeureanu, R., Marceau, M. L., Payer, J., and Derome, D. (1998b). Evaluation of energy performance of nine identical row houses in montreal. In *Thermal Performance of the Exterior Envelopes of Buildings VII*, Clearwater Beach, Florida.

Zmeureanu, R. and Wu, X. (2007). Energy and exergy performance of residential heating systems with separate mechanical ventilation. *Energy*, 32:187–195.

Appendices

Appendix A

Technical specifications of the HRV system

Dimensions and Service Clearances: Venmar AVS NOVOFIT 1.5
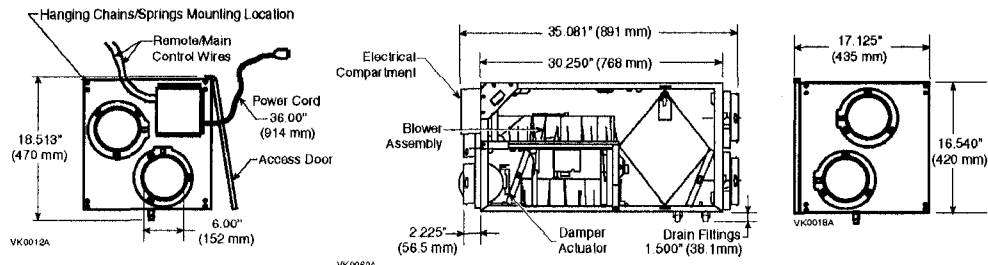
Ventilation Performance

EXT STATIC PRESSURE		NET SUPPLY AIR FLOW			GROSS AIR FLOW					
					SUPPLY			EXHAUST		
Pa	inwg	l/s	cfm	m³/h	l/s	cfm	m³/h	l/s	cfm	m³/h
25	.1	83	175	299	83	176	299	83	175	295
50	.2	79	168	285	80	169	288	78	165	281
75	.3	75	159	270	75	159	270	75	158	270
100	.4	71	150	256	71	151	256	69	146	248
125	.5	64	136	230	64	136	230	60	127	216
150	.6	59	126	214	60	127	216	48	103	173
175	.7	53	113	192	53	113	192	38	80	136
200	.8	43	91	155	43	91	155	21	45	76

CFM (l/s = CFM x 0.4719) (m³/h = l/s x 3.6)
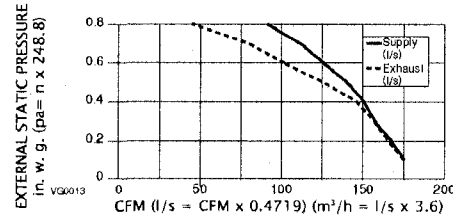
Energy Performance

SUPPLY TEMPERATURE C°	F°	NET AIR FLOW l/s	cfm	m³/h	POWER CONSUMED WATTS	SENSIBLE RECOVERY EFFICIENCY	APPARENT SENSIBLE EFFECTIVENESS	LATENT RECOVERY MOISTURE TRANSFER
HEATING								
0	+32	31	66	112	85	69	81	-0.01
0	+32	56	119	202	124	60	70	-0.01
0	+32	--	--	--	--	--	--	--
-25	-13	37	78	133	114	62	80	0.08
-25	-13	--	--	--	--	--	--	--
COOLING						TOTAL RECOVERY EFFICIENCY		
+35	+95	--	--	--	--	Not tested		
+35	+95	--	--	--	--	--		

Air Flow - l/s (0.47 l/s = 1 CFM)
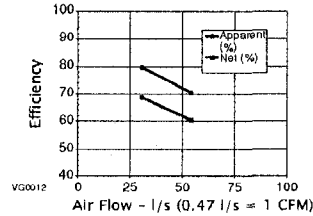
NOTE: All specifications are subject to change without notice.

Specifications and Ratings

- Model: Venmar AVS NOVOFIT 1.5
- Part Number: 43120
- Total Assembled Weight: (Including polypropylene core) 65 lb (29.5 kg)
- Supply and Exhaust Air Duct Connections: 6" (15.24 cm) diameter
- Drains: ½" (1.2 cm) fittings with 10 ft (3 m) PVC drain
- Filters: -15 ppi washable reticulated foam -15.375" x 7.125" x 0.75" (39 x 18 x 1.9 cm)

- Cabinet: 20 ga. pre-painted steel
- Insulation: 1" (2.54 cm) aluminum foil faced fiberglass 0.825" (2.10 cm) expanded polystyrene
- Mounting: suspension by chains and springs
- Supply & Exhaust Blower Motor: 1 motor
  - Protection type: Thermally protected
  - Insulation class: B
  - V (motor marking): 120 V ac, 50/60 Hz, 1.2/1.0 A, 1050/1300/1660 RPM

- Fan Speed Control:
  - Low, increased low & high speed
  - Two speeds available to user
  - Low or increased low speed is selected at the time of installation
- Heat Recovery Core:
  - Heat Exchange Surface Area: 102 ft² (9.54 m²)
  - Type/Material: Crossflow/ Polypropylene
- Unit Electrical Characteristics:

Volts	Freq.	Amps	Watts	IP
120	60 Hz	1.3	150	–

Submitted by:			Date:	Project:
Qty:	Model No.:	Remarks:		Location:
				Architect:
				Engineer:
				Contractor:

Appendix B

Coefficients used to calculate the temperature of cold water from the city line

n^{th} harmonic	c_n	d_n
1	0.18399457	0.09056716
2	-6.7763674	-7.3992997
3	-0.096571472	-0.20339461
4	0.084368625	0.88293357
5	-0.0031887082	-0.037057249
6	-0.09697441	0.1161188
7	0.014070618	-0.022911697
8	-0.33625031	-0.014277327
9	-0.027762869	-0.017975378
10	-0.036247456	-0.13904543
11	-0.013672282	-0.054122503
12	-0.018720731	0.1353561
13	-0.0066015323	-0.020641118
14	-0.089322769	0.084332139
15	-0.04498332	-0.012268606
16	0.17270848	0.068648872
17	0.024281561	0.00080673597

Coefficient a and b are equal to 11.490452 and 0.0086904361, respectively.

Appendix C

Technical specifications of evacuated tube collectors

SOLAR COLLECTOR CERTIFICATION AND RATING	CERTIFIED SOLAR COLLECTOR
SRCC OG-100	SUPPLIER: **Viessmann Manufacturing Company (US) Inc.** 45 Access Road Warwick, RI 02886 USA MODEL: Vitosol 300 Type SP3, 3m2 COLLECTOR TYPE: Tubular CERTIFICATION #: 100-2005-020B

COLLECTOR THERMAL PERFORMANCE RATING

Megajoules Per Panel Per Day				Thousands of Btu Per Panel Per Day			
CATEGORY (Ti-Ta)	CLEAR DAY 23 MJ/m²·d	MILDLY CLOUDY 17 MJ/m²·d	CLOUDY DAY 11 MJ/m²·d	CATEGORY (Ti-Ta)	CLEAR DAY 2000 Btu/ft²·d	MILDLY CLOUDY 1500 Btu/ft²·d	CLOUDY DAY 1000 Btu/ft²·d
A (-5°C)	46	34	23	A (-9°F)	43	33	22
B (5°C)	44	33	22	B (9°F)	42	31	20
C (20°C)	42	30	19	C (36°F)	39	29	18
D (50°C)	37	25	14	D (90°F)	35	24	13
E (80°C)	31	20	10	E (144°F)	29	19	9

A-Pool Heating (Warm Climate) B-Pool Heating (Cool Climate) C-Water Heating (Warm Climate) D-Water Heating (Cool Climate) E-Air Conditioning

Original Certification Date: August 9, 2006

COLLECTOR SPECIFICATIONS

Gross Area:	4.287	m²	46.15	ft²	Net Aperture Area:	3.760	m²	40.47 ft²
Dry Weight:	68	kg	150	lb	Fluid Capacity:	1.8	l	0.5 gal
Test Pressure:	130	kPa	19	psig				

COLLECTOR MATERIALS

Frame:	Aluminum
Cover (Outer):	Glass Vacuum Tube
Cover (Inner):	None
Absorber Material:	Tube - Copper / Plate - Copper fin
Absorber Coating:	Sputtered cermet
Insulation (Side):	Vacuum
Insulation (Back):	Vacuum

PRESSURE DROP

Flow		Δ P	
ml/s	gpm	Pa	in H₂O

TECHNICAL INFORMATION

Efficiency Equation [NOTE: Based on gross area and (P) = Ti-Ta]

							Y Intercept	Slope	
S I Units:	$\eta =$ 0.5079	-0.9156	(P)/I	-0.0030	(P)²/I		0.5093	-1.0948	W/m²·°C
I P Units:	$\eta =$ 0.5079	-0.1614	(P)/I	-0.0003	(P)²/I		0.5093	-0.193	Btu/hr·ft²·°F

Incident Angle Modifier [(S) = 1/cos θ - 1, 0°≤ θ ≤60°]			Model Tested:	Vitosol 300, SP3, 2m2
$K_{\alpha\tau} =$ 1.0	+0.5192 (S)	-0.7428 (S)²	Test Fluid:	Prolylene Glycol & Water
$K_{\alpha\tau} =$ 1.0	-0.26 (S)	(Linear Fit)	Test Flow Rate:	ml/s 0.00 gpm

REMARKS: Collector tested with long axis of tubes oriented north-south. IAM perpendicular to the tubes is listed above. IAM parallel to the tubes = 1.0 - 0.31(S)

Appendix D

Parameters used in the mathematical models of aqueous solutions of polypropylene glycol

Parameter	ρ	C_p	λ	μ
	[kg/m^3]	[kJ/(kg·°C)]	[W/(m·°C)]	[Pa·s]
A_1	508.41109	4.47642	1.18886	-1.02798
A_2	-182.40820	0.60863	-1.49110	-10.03298
A_3	965.76507	-0.71497	-0.69682	-19.93497
A_4	280.29104	-1.93855	1.13633	14.65802
A_5	-472.22510	0.47873	0.06735	14.62050

Source: M. CONDE Engineering (2002).

Appendix E

Technical specifications of flat-plate collectors

SOLAR COLLECTOR CERTIFICATION AND RATING	CERTIFIED SOLAR COLLECTOR
SRCC OG-100	SUPPLIER: **Viessmann Manufacturing Company (US) Inc.** 45 Access Road Warwick, RI 02886 USA MODEL: Vitosol 100 SV1, SH1 COLLECTOR TYPE: Glazed Flat-Plate CERTIFICATION #: 100-2005-019A

COLLECTOR THERMAL PERFORMANCE RATING

Megajoules Per Panel Per Day				Thousands of Btu Per Panel Per Day			
CATEGORY (Ti-Ta)	CLEAR DAY 23 MJ/m²·d	MILDLY CLOUDY 17 MJ/m²·d	CLOUDY DAY 11 MJ/m²·d	CATEGORY (Ti-Ta)	CLEAR DAY 2000 Btu/ft²·d	MILDLY CLOUDY 1500 Btu/ft²·d	CLOUDY DAY 1000 Btu/ft²·d
A (-5°C)	39	30	20	A (-9°F)	37	28	19
B (5°C)	36	27	17	B (9°F)	34	25	16
C (20°C)	31	22	13	C (36°F)	30	21	12
D (50°C)	23	14	5	D (90°F)	22	13	5
E (80°C)	15	6		E (144°F)	14	6	

A-Pool Heating (Warm Climate) B-Pool Heating (Cool Climate) C-Water Heating (Warm Climate) D-Water Heating (Cool Climate) E-Air Conditioning

Original Certification Date: July 31, 2006

COLLECTOR SPECIFICATIONS

Gross Area:	2.523	m²	27.16	ft²	Net Aperture Area:	2.334	m²	25.12	ft²
Dry Weight:	44.2	kg	97	lb	Fluid Capacity:	1.9	l	0.5	gal
Test Pressure:	897	kPa	130	psig					

COLLECTOR MATERIALS

Frame:	Aluminum
Cover (Outer):	Tempered Glass
Cover (Inner):	None
Absorber Material:	Tube - Copper / Plate - Copper Fin
Absorber Coating:	Sputtered cermet
Insulation (Side):	Polyurethane Foam
Insulation (Back):	Mineral Wool

PRESSURE DROP

Flow		ΔP	
ml/s	gpm	Pa	in H₂O
20	0.32	18	0.07
50	0.79	64	0.25
80	1.27	133	0.53

TECHNICAL INFORMATION

Efficiency Equation [NOTE: Based on gross area and (P) = Ti-Ta]

							Y Intercept	Slope	
S I Units:	η = 0.7162	-3.0562 (P)/I	-0.0067 (P)²/I				0.7203	-3.4981	W/m²·°C
I P Units:	η = 0.7162	-0.5386 (P)/I	-0.0007 (P)²/I				0.7203	-0.616	Btu/hr·ft²·°F

Incident Angle Modifier [(S) = 1/cos θ - 1, 0°≤ θ ≤60°]

					Model Tested:	Vitosol 100, SVI
$K_{\alpha\tau}$ ≈	1.0	-0.0707 (S)	-0.1232 (S)²		Test Fluid:	Propylene Glycol & Water
$K_{\alpha\tau}$ ≈	1.0	-0.20 (S)	(Linear Fit)		Test Flow Rate:	50 ml/s 0.79 gpm

REMARKS: Pressure drop shown above is for Model SV1